Materiale-Mekanik (Mat-Mek)

En introduktion til analyser af materialers mekanisk/fysiske adfærd

Nielsen, Lauge Fuglsang

Publication date:
2003

Document Version
Publisher's PDF, also known as Version of record

Lauge Fuglsang Nielsen

Materiale-Mekanik (Mat-Mek)

En introduktion til analyser af materialers mekanisk/fysiske adfærd

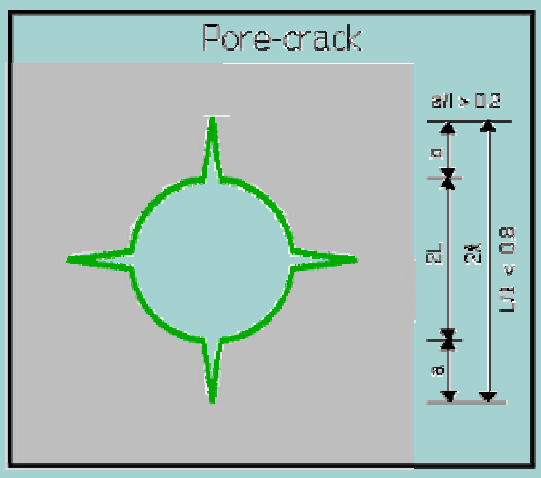

Pore-cracks are spherical or cylindrical voids with concentric cracks crossing at 90°.

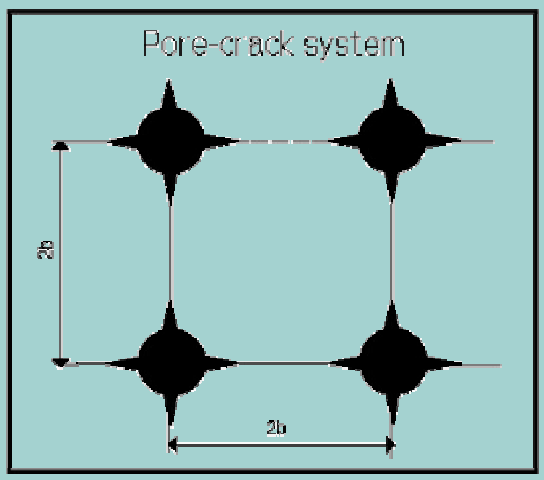

Cubic porous material with pore-cracks. Load is perpendicular to crack plane.

DANMARKS TEKNISKE UNIVERSITET

Rapport
BYG·DTU
R-059
April 2003
ISSN 1601-2917
ISBN 87-7877-121-8

Department of Civil Engineering
Technical University of Denmark
DK-2800 Lyngby
Telephone: 45 251828
Telefax: 45 886753
e-mail: lfn@byg.dtu.dk

FORORD

I den foreliggende rapport, Materialemekanik, gennemgås principperne i de mest grundlæggende fagdiscipliner, der er nødvendige til forklaring/beskrivelse af bygningsmaterialers reelle mekaniske og fysiske adfærd. Det vil sige, Kompositteori, Rheologi og Brudmekanik - samt disse discipliners integrering (Materialemekanik).

Rapporten er tilrettelagt som et undervisningsnotat med en række forelæsningsøvelser, samt regneøvelser. Materialet til disse aktiviteter er inkluderet som specielle afsnit sidst i notatet. Som en udfordring til læseren er regneøvelserne bevidst beskrevet meget løst - nærmest kun ved stikord.

Rapportens skiftende anvendelse af sprogene dansk og engelsk afspejler, at teksten er hentet fra diverse af forfatterens nationale og internationale publikationer.

Som titlen angiver omhandler rapporten en introduktion til de betragtede emneområder. Videregående analyser med anvendelser kan studeres i (1,2) og software, der kan downloades fra *http://www.byg.dtu.dk/publicering/software_d.htm.*

INDLEDNING

Næsten alle bygningsmaterialer har tidsafhængige egenskaber. Man siger, at de kryber. For eksempel har en betonbjælke efter 10 år en udbøjning, der er 2 - 4 gange større end efter 5 minutter. En træbjælke kan under gunstige omstændigheder nøjes med en faktor på 2. Nogle materialer som for eksempel plastbaserede har større faktorer. Andre som for eksempel natursten har mindre.

Så godt som alle bygningsmaterialer er defekte. Dårlig vedhæftning mellem tilslagsmateriale og cementpasta i beton er et hyppigt forekommende eksempel herpå. Ikke alle steder er mursten og gasbeton afhærdet på en sådan måde, at revner er undgået. Træ har uundgåeligt fået revner under nedtørring fra den grønne, nyfældede tilstand, o.s.v.

Næsten alle bygningsmaterialer er sammensatte materialer - såkaldte kompositmaterialer. Beton består for eksempel af cement, vand, sand og sten. Mursten og gasbeton er porøse materialer, d.v.s. at en væsentlig komponent er luft. Spånplader er træ plus lim. Konstruktionstræ er knastfrit træ plus knaster, o.s.v.

Så godt som alle bygningsmaterialer er altså defekte og sammensatte med tidsafhængige egenskaber. Materialemekanik er den disciplin i bygningsmateriallæren, der behandler disse afvigelser fra den klassiske, homogene idealelastiske (Hooke) materialeopfattelse.

Følgende 3 fagdiscipliner kan hver for sig beskrive de nævnte elementer i byg-ningsmaterialers mekaniske adfærd:

- *Rheologi* (græsk: læren om det, som flyder) beskriver materialers tidsafhængige egenskaber.
- *Brudmekanik* beskriver de styrke- og deformationsmæssige konsekvenser af fejl i materialer.
- *Kompositteori* beskriver, hvilke mekaniske egenskaber, der kan forventes opnået ved at blande forskelligartede materialer.

Materialemekanik

I almindelighed kan materialers adfærd ikke forklares alene ved hjælp af en enkelt fagdisciplin. Med hensyn til byggebranhens materialer, for eksempel, kan en tilfredsstillende beskrivelse ofte kun opnås gennem en kombineret anvendelse af rheologi, revnemekanik og kompositteori. Fagområdet, der behandler denne kombination kaldes Materialemekanik.

Contents

1. KOMPOSITMATERIALER

Stivheden (elasticiteten) for et kompositmateriale afhænger ikke blot af fasernes stivheder og volumenmæssige andele - men i meget væsentlig grad også af fasegeometrien. For eksempel ville en teglstens stivhed være 0 såfremt porerne var fordelt lagvist vinkelret på belastningsretningen. Der er en uendelighed af muligheder for forskellige fasegeometrier: I et tofasesystem kan den ene fase være kontinuert (sammenhængende), mens den anden fase består af diskrete (isolerede) partikler, der kan have en geometri som for eksempel fibre, plader, lange bånd eller kompakte korn. Det kan også være modsat. Det vil sige at faserne bytter geometri. I det generelle tilfælde forekommer begge faser i et kompositmateriale med både kontinuert og diskret geometri.

Kun i få tilfælde kan man ad analytisk vej bestemme den eksakte løsning for et kompositmateriales stivhed. Det gælder materialer med simpel fasegeometri som nogle fiberarmerede materialer, lagdelte materialer samt visse typer af materialer, hvor den ene fase forekommer som kugleformede partikler.

Det er imidlertid muligt gennem nogle enkle gennemsnitsbetragtninger over spændinger, tøjninger og geometrier at opstille øvre og nedre grænser for den søgte stivhed. I nogle tilfælde ligger disse grænser så tæt, at en middelværdi vil være et tilstrækkeligt godt praktisk skøn. I andre tilfælde ligger grænserne så langt fra hinanden, at andre metoder til stivhedsbestemmelse må tages i anvendelse.

Dette afsnit omhandler forskellige metoder til udvikling af en række gode tilnærmede (og i nogle tilfælde eksakte) stivhedsløsninger for isotrope kompositmaterialer, der alle tilgodeser kompositgeometriens afgørende indflydelse. De udviklede løsningerne udspænder rummet mellem de førnævnte grænser således at alle tænkelige isotrope geometrier kan "behandles".

1.1 Classification of composites

1.1.1 Volume concentration and stiffness ratio

To classify a composite we must, as a minimum, know about volume concentrations and stiffness of the constituent phases. We will use the definitions and notations introduced in Equation 1.1. The composite is made of phase P and phase S. The volumes of phase P and phase S are V_P and V_S respectively. Corresponding stiffness are E_P and E_S respectively. The composite stiffness is denoted by E. The volume concentration of phase P is c as defined by the first expression in Equation 1. Automatically the volume concentration of phase S then becomes 1 - c. Relative composite stiffness and relative phase stiffness (stiffness ratio) are defined by the latter two expressions in Equation 1.1.

$$c = \frac{V_P}{V_P + V_S} \quad (phase\ P) \quad ; \quad 1 - c = \frac{V_S}{V_p + V_S} \quad (phase\ S)$$
$$e = \frac{E}{E_S} \quad (composite\ stiffness) \quad ; \quad n = \frac{E_P}{E_S} \quad ; \quad (stiffness\ ratio) \qquad (1.1)$$

1.1.2 Composite geometry

As shall be seen subsequently, only simple upper and lower bounds for composite properties can be obtained from these basic composite information (c and n). To get accurate prediction of composite properties we must know about composite geometry. For this purpose we will classify geometries according the schemes presented in this section.

Composites can be classified according to their internal geometry as shown by the matrix in Figure 1.1. A phase with continuous geometry (C) is a phase in which the total composite can be traversed without crossing the other phase. This is not possible in a phase with discrete geometry (D). A mixed geometry (m) is a continuous geometry with some discrete elements. For practice the scheme of geometries may be simplified as shown in Figure 1.2.

Fixed concentration

We introduce the following terminology for the composite geometry at a fixed volume concentration,

- DC means that phase P appears as discrete elements in a continuous phase S.
- MM is a common descriptor for geometries mC, CC, mm, and Cm defined in Figure 1.2. Both phases have mixed geometries and/or continuous geometries. Discrete

elements may dominate in MM geometries. Continuous elements, however, are always present.

- CD means that phase P appears as a continuous phase mixed up with discrete phase S elements.

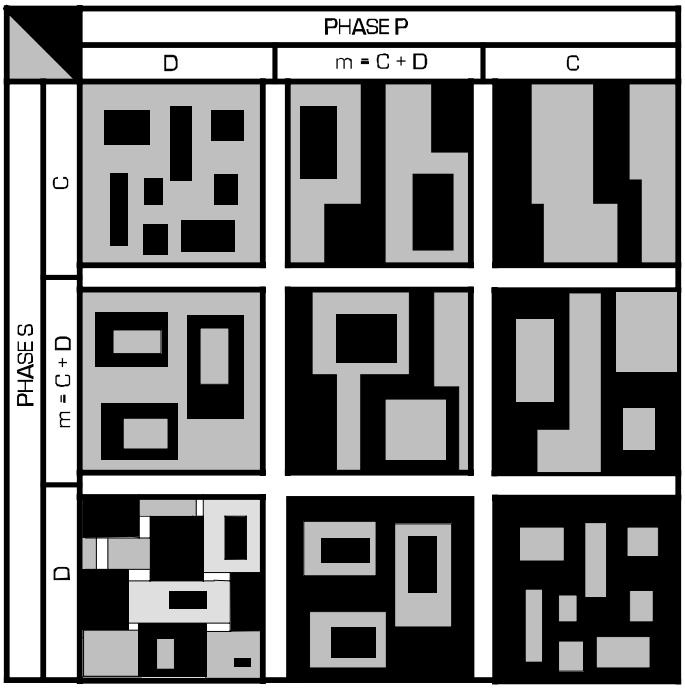

Figure 1.1. *Phase geometries in two-phase materials. C, D and m (= C + D) denotes continuous-, discrete-, and mixed geometries respectively.*

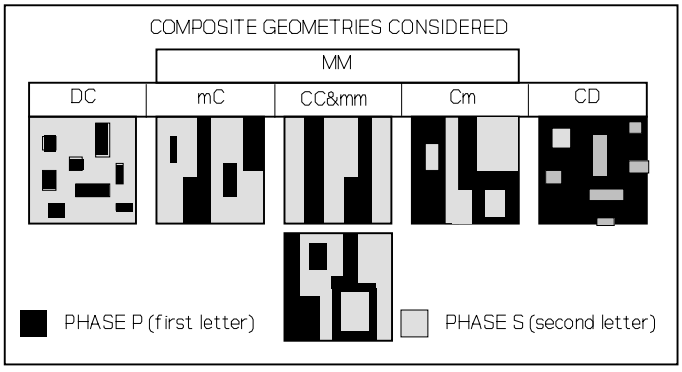

Figure 1.2. *Simplified scheme of geometry classification.*

Variable concentrations

To classify a composite, geometrically, with variable volume concentrations c we introduce the following concept outlined in Equation 1.2: A four letter clas-

sification symbol UV-XY is used. The composite considered has the UV type of geometry at c = 0 and the XY type of geometry at c = 1.

DC–DC (ex CSA_p) *DC–MM* *DC–CD*	*MM–MM* *MM–CD*	*CD–CD (ex CSA_S)*	(1.2)

The way geometries change with respect to volume concentrations is demonstrated in Figures 1.3 and 1.4. The CSA-composites referred to in Equation 1.2 are outlined in subsequent Figures 1.9 and 1.10.

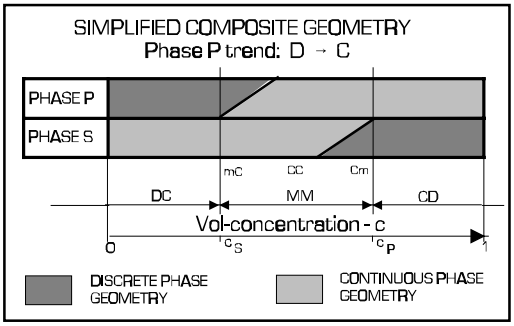

Figure 1.3. *Composite geometry when phase P goes from D to C.*

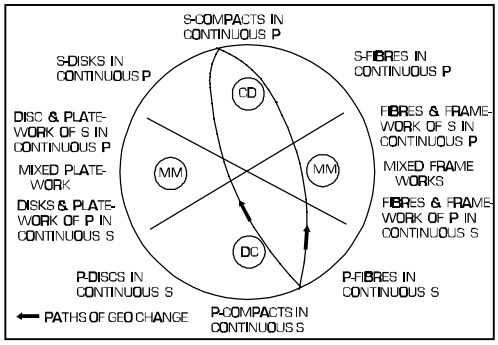

Figure 1.4. *Examples of geometry transformation from compact to anti-compact (shell).*

Critical concentrations - type of composite

The critical "concentrations" c_P and c_S ($<c_P$) introduced in Figure 1.3 indicate geometrical transitions: The geometry of phase S changes from being mixed (as in MM) to being discrete in a fully continuous phase P (as in CD) at c_P. The geometry of phase P changes from being mixed (as in MM) to being discrete in a fully continuous phase S (as in DC) at c_S.

An alternative definition of critical concentrations is: c_P is that concentration at which discrete phase P particles in a DC-composite start growing together (interfering). c_S is that concentration at which phase S becomes dissolved as discrete particles in a fully grown together phase P.

Depending on technologies used to produce composites, critical concentrations can be real (in c = 0-1) or un-real (outside c = 0-1). From Figure 1.5 can be seen that type of composite can be classified by their critical concentrations. Both critical concentrations are un-real (>1) for DC-DC composites (particulate composites) such as the CSA_P-composite outlined in Figure 1.9. The critical concentrations are also un-real for MM-MM composites (lamella composites), with $c_P > 1$ and $c_S <$

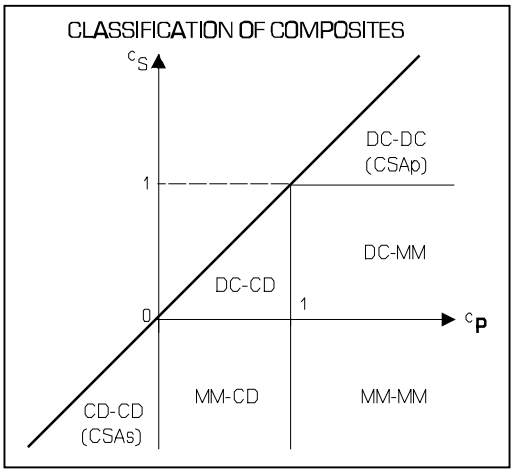

Figure 1.5. *Types of composite geometries as related to critical concentrations, (see Figures 1.9 and 1.10 for CSA_P and CSA_S).*

0, however. DC-CD composites such as materials made of compacted powders have both critical concentrations real.

Obviously the classification of composite geometries presented in this chapter is closely related to the concepts of percolation and connectivity briefly discussed in the subsequent section.

1.1.3 Percolation, permeability, impregnability

Percolation theory considers the connectivity of a phase across a microstructure (3,4). Connectivity was related to the geometrical classification of composites by the author in (5) to explain properties (others than elastic) of composite materials such as permeability and impregnability of porous materials.

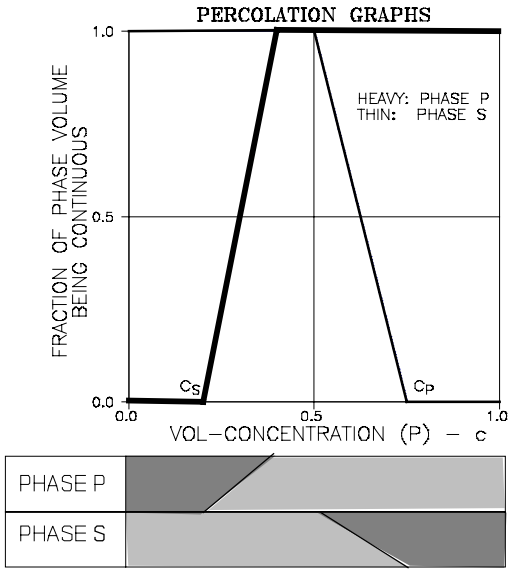

Figure 1.6. *Percolation graphs for phase P and phase S respectively.*

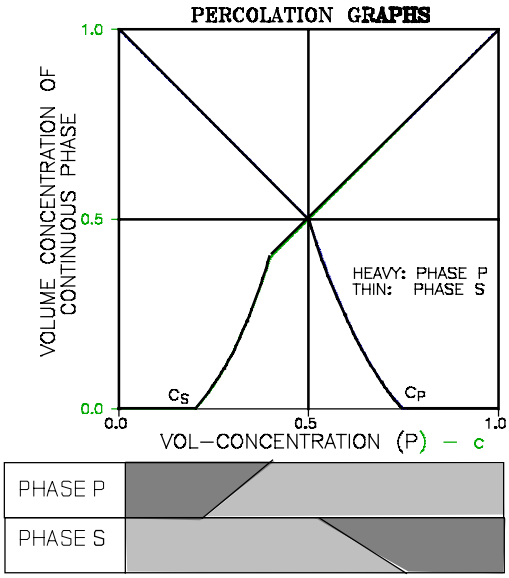

Figure 1.7. *Concentration of continuous parts of phase P and phase S respectively.*

The relation between geometrical classification and connectivity is as outlined in Figures 1.6 and 1.7. A porous material (P-pores) is not impregnable in $c = 0 - c_S$, it is partly impregnable in $c = c_S - c'$ (with $c_S < c' < c_P$), and it is fully impregnable

in c = c' - 1. In c = c_P - 1, however, the porous material is without any coherence. The concept of connectivity has recently been used by Bentz in (6) to relate the microstructure of cement paste to the amount of cement hydrated.

1.2 Stiffness

Hill (7) has shown that the remarkably simple relations presented in Equations 1.3 exist between *averages (by volume) of stresses, strains,* and stiffness of homogeneous (not necessarily isotropic) composite materials consisting of homogeneous and isotropically elastic components.

$$\left.\begin{aligned}\sigma &= (1-c)\,\sigma_S + c\,\sigma_P \\ \varepsilon &= (1-c)\,\varepsilon_S + c\,\varepsilon_P\end{aligned}\right\} \quad \varepsilon_P = \frac{\sigma_P}{E_P} \;;\; \varepsilon_S = \frac{\sigma_S}{E_S} \tag{1.3}$$

The expressions in Equation 1.3 form the basis of the stiffness analysis of composites made in this note. They can (8) be organized as follows which can be used to predict composite stiffness from a known average stress (or strain) in phase P.

$$e = \frac{E}{E_S} = \left[1 + c\frac{1-n}{n}\frac{\sigma_P}{\sigma}\right]^{-1} = 1 + c(n-1)\frac{\varepsilon_P}{\varepsilon} \tag{1.4}$$

It is emphasized that this expression is exact, meaning that accurate composite stiffness is predicted by Equation 1.4 if the exact phase P average stress (or average strain) is known.

1.2.1 Layered materials

Equation 1.4 can be used to determine the stiffness of the very special anisotropic composites shown in Figure 1.8. We only have to introduce homogeneous stress and homogeneous strain states respectively. The results are shown in Equation 1.5.

$$\begin{aligned}&\perp\text{-}layers: \quad \frac{\sigma_P}{\sigma} = 1 \quad \Rightarrow \quad e = \frac{n}{n + c(1-n)} \\ &\parallel\text{-}layers: \quad \frac{\varepsilon_P}{\varepsilon} = 1 \quad \Rightarrow \quad e = 1 + c(n-1)\end{aligned} \tag{1.5}$$

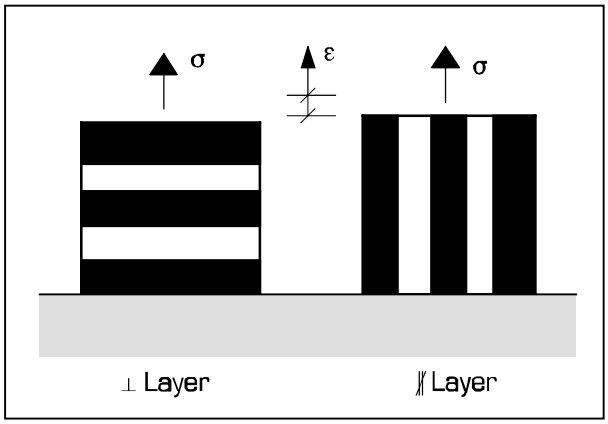

Figure 1.8. *Extreme anisotropic composites.*

Anisotropic stiffness bounds

These solutions are exact because the estimates on stress and strain are exact. As no geometries can be thought to be more anisotropic than the layered materials just considered, it is obvious that lower and upper bounds for anisotropic composite materials are as follows,

$$\frac{n}{n + c(1 - n)} \leq e \leq 1 + c(n - 1) \quad (\textit{anisotropic bounds}) \tag{1.6}$$

These bounds, graphically presented in Figure 1.11, are the so-called P/H-bounds named after their first "inventors": Paul (9) and Hansen (10).

1.2.2 Composite spheres assemblage (CSA)

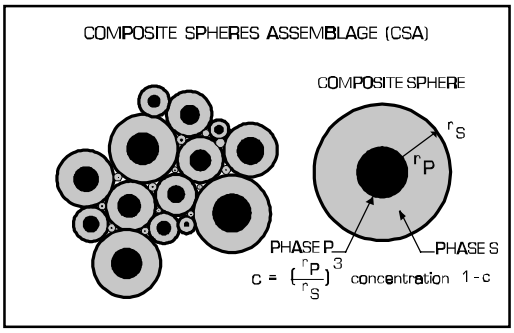

Figure 1.9. *Composite spherical assemblage with phase P particles, CSA_P.*

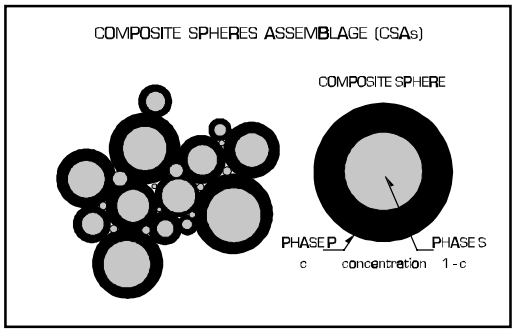

Figure 1.10. *Composite Spheres Assemblage with phase S particles of concentration 1-c (CSA_S).*

The phase P stress in a CSA_P-material can easily be derived from Hashin (11) or from Timoshenko and Goodier (12) for example. The result is presented in Equation 1.7 together with the phase S stress derived from the Equation 1.3. The phase P stress and phase S stress in a CSA_S material (with the same phase P

concentration) are derived from Equation 1.7 by replacing (c,n) with (1-c,1/n). The results are presented in Equation 1.8.

CSA_P geometry:

$$\frac{\sigma_P}{\sigma} = \frac{2n}{n+1+(n-1)c} \quad ; \quad \frac{\sigma_S}{\sigma} = \frac{n+1}{n+1+(n-1)c} \tag{1.7}$$

CSA_S geometry:

$$\frac{\sigma_P}{\sigma} = \frac{1+n}{2+(n-1)c} \quad ; \quad \frac{\sigma_S}{\sigma} = \frac{2}{2+(n-1)c} \tag{1.8}$$

The stiffness of CSA composites are now determined introducing the phase P stresses into Equation 1.4. We get

$$e = \frac{E}{E_S} = \begin{cases} \dfrac{n+1+c(n-1)}{n+1-c(n-1)} & (CSA_P) \\ n\dfrac{2+c(n-1)}{2n-c(n-1)} & (CSA_S) \end{cases} \tag{1.9}$$

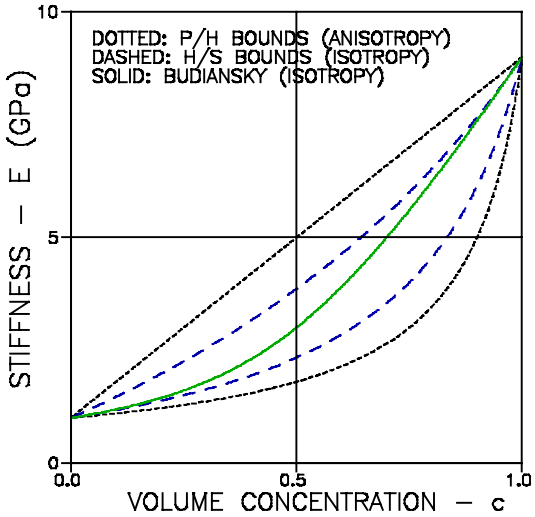

Figure 1.11. *P/H bounds, H/S bounds, and Budiansky's expression.*

Isotropic stiffness bounds

These solutions are the exact stiffness bounds for isotropic composite materials. The geometries of CSA_P and CSA_S are each others extreme opposite isotropic geometries. Any other isotropic composite has a stiffness between these bounds. This means,

$$\frac{n + 1 + c(n - 1)}{n + 1 - c(n - 1)} \leq \frac{E}{E_S} \leq n\,\frac{2 + c(n - 1)}{2n - c(n - 1)} \quad ; \quad n \geq 1 \qquad (1.10)$$

reverse signs when $n < 1$ (*Isotrope stivhedsgrænser*)

These bounds, shown in Figure 1.11, are the the so-called H/S-bounds named after their first "inventors": Hashin and Shtrikman (13).

1.2.3 Powder material (SCS-analysis)

The phase P stress in a particulate composite can be approximated from its dilute suspension solution (single P particle in infinite S matrix) by replacing the matrix property in that solution with its unknown composite property. This method (SCS = Self Consistency Scheme) works as demonstrated in Equation 1.11 to estimate phase P stress in a powder material.

$$\left.\begin{aligned} &\frac{\sigma_P}{\sigma} = \frac{2n}{1 + n} \quad n = \frac{E_P}{E_S} \quad (\sigma_P \textit{ in dilute suspension, Goodier}) \\ &\frac{\sigma_P}{\sigma} \approx \frac{2\bar{n}}{1 + \bar{n}} \quad \textit{with } \bar{n} = \frac{E_P}{E} = \frac{n}{e} \\ &\Rightarrow \frac{\sigma_P}{\sigma} \approx \frac{2n}{e + n} \end{aligned}\right\} \quad \begin{aligned} &\textit{SCS-estimate of } \sigma_P \\ &\textit{in general composite} \end{aligned} \qquad (1.11)$$

With this stress estimate the composite stiffness can now be determined as follows from Equation 1.4,

$$e \approx \frac{1}{2}\left[(1 - n)(1 - 2c) + \sqrt{(1 - n)^2(1 - 2c)^2 + 4n}\right] \qquad (1.12)$$

which is the so-called Budiansky's expression illustrated in Figure 1.11. This expression was first developed (in another way, however) by Budiansky in (14).

1.2.4 Isotropic composites in general

The following way of developing stress and stiffness of composites with arbitrary geometry is a very brief and adapted summary of the authors composite analysis in (8):

It is noticed that the stress expressions presented in Equations 1.7 and 1.8 can be given a common description as shown in Table 1.2 where the parameter $\theta = 1$ when the composite geometry is a CSA_P geometry, and where $\theta = n$ when the composite geometry is a CSA_S geometry.

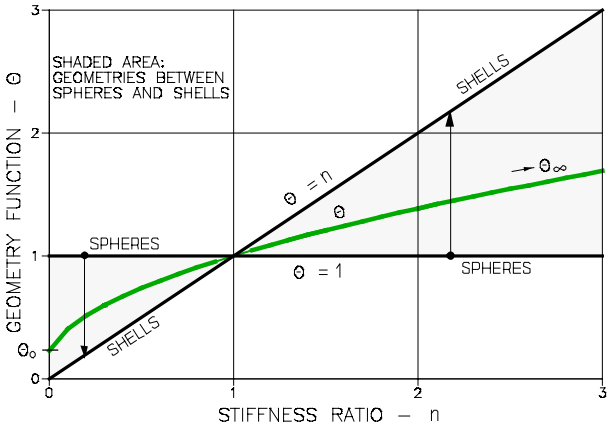

Figure 1.12. *Influence of phase P geometry on geometry function* θ.

In between, when composite geometry changes from phase P being spheres to phase P being spherical shells, composite stresses can still be expressed as shown in Table 1.2 - the parameter θ, however, must now be considered as a *geo-function* which varies with n as shown in Figure 1.12. Obviously the geo-function must also consider composite geometry as previously classified Section 1.1. The θ-expression presented in Table 1.1 has been shown in (8) to consider both n and geometry successfully. It is noticed that the influence of geometry is considered by separate, so-called *shape functions* ($\mu_P(c)$, $\mu_S(c)$) outlined in Figure 1.14 and quantified by Table 1.1 and Figure 1.13.

The quantification, just described, of shape functions to consider specific composite geometries is the result of the author's ongoing research on composite properties versus geometry. Figure 1.13, for example, is a further development of ideas already reported in (5,15,16).

We notice that geometries changing from compacts ($\approx CSA_P$) to shells ($\approx CSA_S$) through "flat" geometries are considered to the left of Figure 1.13. Geometries changing from compacts to shells through "long" geometries are considered to the right. Geometries changing from compacts to shells through a mixture of "flat" and "long" geometries are considered in the "middle".

The terms "flat" and "long" geometries used above refer to the aspect ratio, A = length of element/diameter of element, often used to describe the shapes of fibres. Flat shapes have $A < 1$, long shapes have $A > 1$. Compact shapes have $A \approx 1$.

1.2.5 Analysis of isotropic composites

The stiffness for isotropic composites in general is now obtained from Equation 1.4 introducing the phase P stress presented in Table 1.2. The stiffess result such obtained is also presented in Table 1.2.

GEO-FUNCTION		
$\theta = \frac{1}{2}\left[\mu_P + n\mu_S + \sqrt{(\mu_P + n\mu_S)^2 + 4n(1 - \mu_P - \mu_S)} \right]$		
SHAPE FUNCTIONS		
$\mu_P = \mu_P^o\left(1 - \frac{c}{c_P}\right) \quad \mu_S = \mu_S^o\left(1 - \frac{c}{c_S}\right) \; ; \; if \begin{cases} > 1 \text{ predicted then } = 1 \\ < -1 \text{ predicted then } = -1 \end{cases}$		
Shape factors	μ_P^o	μ_S^o
Critical concentration	c_P	$c_S = -\mu_S^o/\mu_P^o c_P$

Table 1.1. *Geo-function and shape functions based on estimates (shaded area) of shape factors μ_P^o, μ_S^o estimated from Figure 1.13 and critical concentration estimated from Figure 1.14.*

ISOTROPIC COMPOSITES
STRESS
$\frac{\sigma_P}{\sigma} = \frac{n(1 + \theta)}{n + \theta[1 + c(n - 1)]} \; ; \; \frac{\sigma_S}{\sigma} = \frac{n + \theta}{n + \theta[1 + c(n - 1)]}$ *or* $\frac{\sigma_P}{\sigma} = \frac{1/e - 1}{c(1/n - 1)} \; ; \; \frac{\sigma_S}{\sigma} = \frac{1/n - 1/e}{(1 - c)(1/n - 1)}$
STIFFNESS
$e = \frac{E}{E_S} = \frac{n + \theta[1 + c(n - 1)]}{n + \theta - c(n - 1)}$

Table 1.2. *Composite stresses and stiffness. Geo-function (θ) from Table 1.1.*

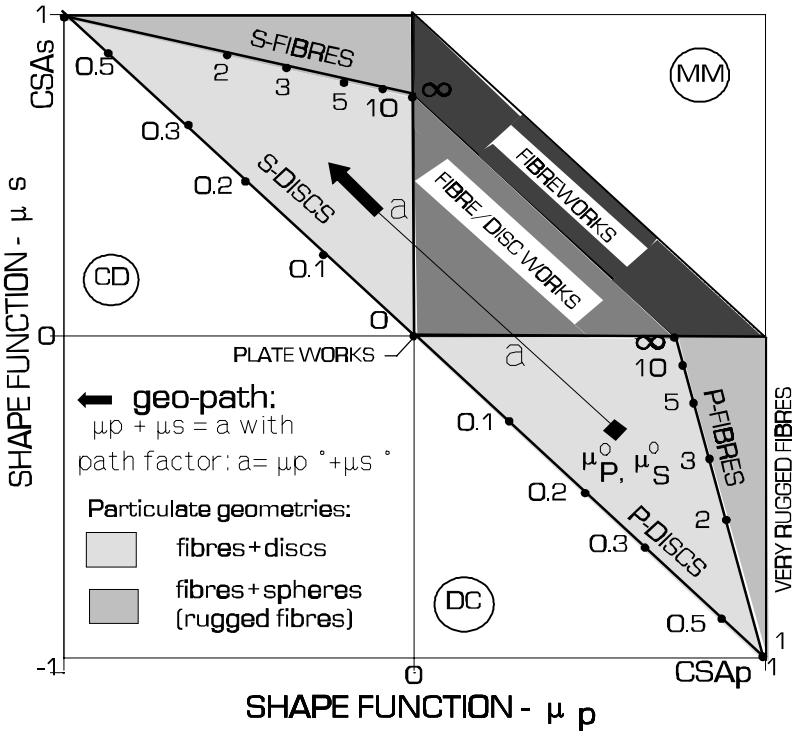

Figure 1.13. *Shape factors. Aspect ratio of phase elements is A = length/thickness. Fibres have A > 1. Discs have A < 1. Compacts have A = 1.*

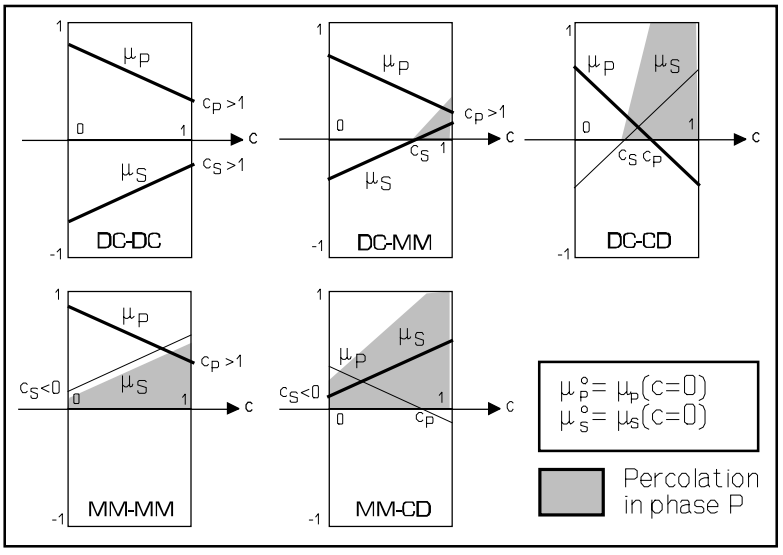

Figure 1.14. Comp-types versus critical concentrations. Former and latter two letters denote comp-geometry at c = 0 and at c = 1 respectively. Shadings indicate phase P percolation.

Remark: The arrow shown in Figure 1.13 is the so-called geo-path which indicates geometries passed when volume concentration c proceeds from 0 to 1.

It is obvious how Tables 1.1 and 1.2 can be used in an algorithm for computer analysis of composite materials: 1) Look at Figure 1.14 to define type of composite and critical concentration c_P from technology (and/or experience) used to produce the material considered. 2) Look at Figure 1.13 to decide shape factors (μ_P^o,μ_S^o) from knowing about composite geometry at low concentrations. 3) Then, go to Table 1.1 to calculate the geofunction - and then 4) go to Table 1.2 for the final stress/stiffness analysis.

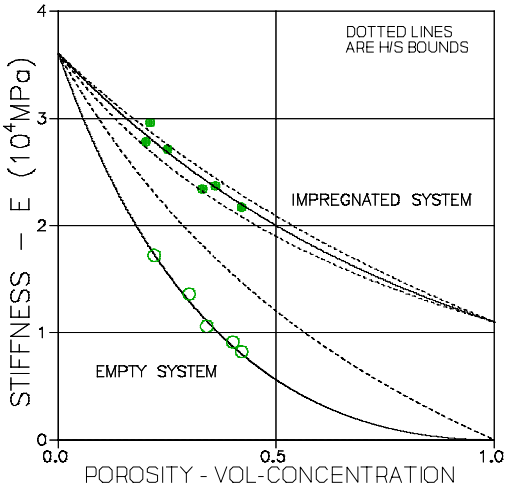

Figure 1.15. *Young's moduli of porous and sulphur impregnated autoclaved Portland cement/silicate systems.*

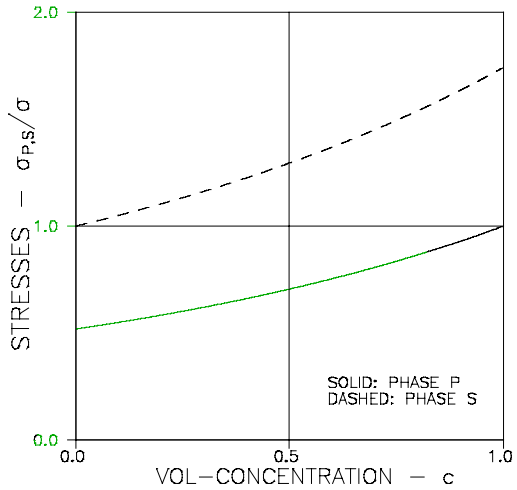

Figure 1.16. *Stresses in sulphur impregnated autoclaved Portland cement/silicate systems.*

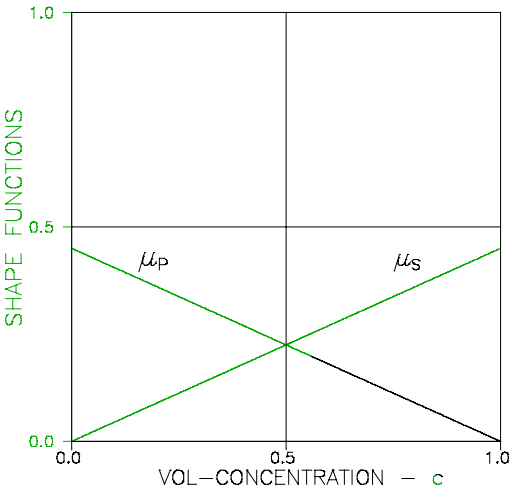

Figure 1.17. *Shape functions for analysis presented in Figures 1.15 and 1.16. (μ_P^o, μ_S^o) = (0.45,0) and c_P = 1.*

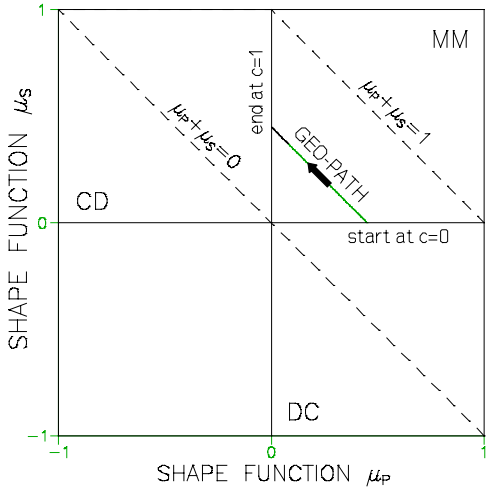

Figure 1.18. *Shape functions for analysis presented in Figures 1.15 and 1.16. (μ_P^o, μ_S^o) = (0.45,0) and c_P = 1.*

Example

The experimental data presented in Figure 1.15 are from tests reported in (17) on porous and sulphur impregnated autoclaved Portland cement/silicate systems. The theoretical stiffness results shown by solid lines in Figure 1.15 are calculated by the present theory. Stress predictions are shown in Figure 1.16. Shape functions applied are as indicated in Figures 1.17 and 1.18.

1.2.6 Porous materials

Porous materials are composites where one phase is an empty pore system. In the present context we consider phase P to be pores. Porosity and stiffness ratio are then given by c and n = 0 respectively from which the following stiffness expression is easily obtained from Table 1.2 with geo-function $\theta = \mu_P$ from Table 1.1. Stiffness is identical 0 whenever negative values are predicted.

$$
\begin{aligned}
&e = \frac{1 - c}{1 + c/\mu_P} \quad with \quad \mu_P = \mu_P^o\left(1 - \frac{c}{c_P}\right) \\
&e \to 1 - \left(1 + \frac{1}{\mu_P^o}\right)c \qquad as \quad c \to 0 \\
&e = \frac{(1 - c)^2}{1 + (1/\mu_P^o - 1)c} \qquad when \quad c_P = 1
\end{aligned}
\tag{1.13}
$$

Examples of stiffness predictions by Equation 1.13 are presented graphically in Figures 1.19 and 1.20. An easy approximation of Equation 1.13 is presented in Equation 1.14 with $e \equiv 0$ when $c > c_P$.

$$
e \approx \left(1 - \frac{c}{c_P}\right)^D \quad with \quad D = c_P\left(1 + \frac{1}{\mu_P^o}\right) \quad ; \quad (c_P \le 1) \tag{1.14}
$$

Theory versus empirical expressions

A variety of empirical stiffness-porosity expressions, critically revieved by Fagerlund in (18), are presented in the literature on porous materials. It is of some interest to discuss briefly Equations 1.13 and 1.14 in relation to the two expressions presented in Equation 1.15 which are (still to day) among the most frequently used to fit data obtained from tests on porous media, the former in (19,20) and the latter in (21,22) for example. F and H are constants to be determined experimentally.

$$\left.\begin{array}{l} e = (1-c)^F \\ e = \exp(-Hc) \end{array}\right\} \rightarrow \begin{cases} 1 - Fc \\ \\ 1 - Hc \end{cases} \quad as \quad c \rightarrow 0 \tag{1.15}$$

Excellent fits are often observed by these expressions at low and moderately low porosities. At higher porosities, however, difficulties may be encountered. The former expression cannot be used when DC-CD and MM-CD composites are considered with $c_P < 1$. The latter expression always predicts a finite stiffness at c = 1. Non of these disadvantages apply to Equations 1.13 and 1.14.

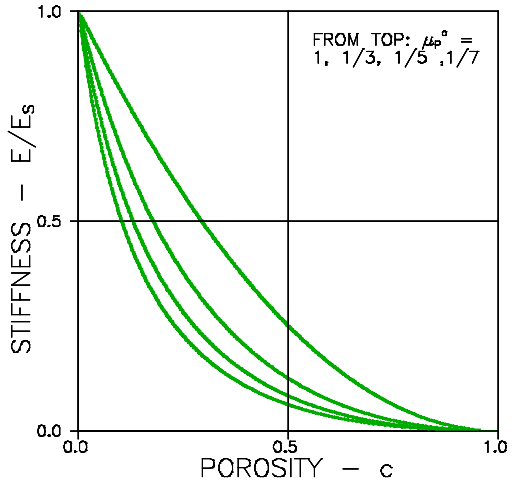

Figure 1.19. *Porous material with shape factors as indicated, and $c_P = 1$.*

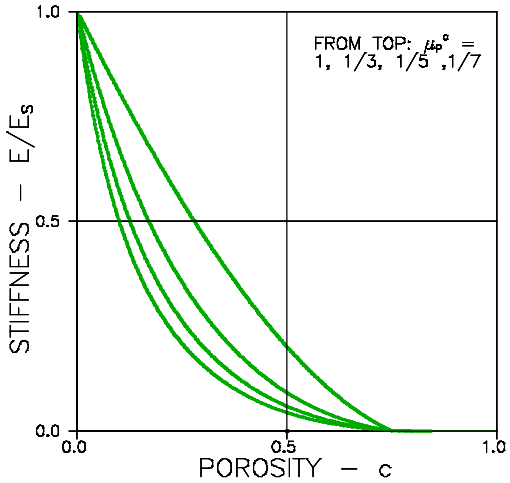

Figure 1.20. *Porous material with shape factors as indicated, and $c_P = 0.75$.*

Deduction of shape parameters from experiments

At low porosities both fit expressions in Equation 1.15 and the results obtained by the present method in Equations 1.13 and 1.14 approach identical stiffnesses when Equation 1.16 applies.

$$F = H = \frac{1}{\mu_P^o} + 1 \qquad \left(i.e.,\ \mu_P^o = \frac{1}{F-1} = \frac{1}{H-1} \right) \tag{1.16}$$

Obviously this observation can be used to deduce shape factors from experimental data - or it can be used to give some geometrical explanation to the empirical factors F and H used in the literature.

More general information, however, on the geometry and stiffness of porous materials can be retrieved from experimental data. We linearize Equation 1.13 (with $e = E/E_S$) as shown in Equation 1.17. Then μ_P°, c_P, and E_S are easily deduced by

linear regression of the manipulated experimental data (X,Y), optimizing the fit quality with respect to c_P.

$$Y = Y_o + \alpha X \quad with \quad X = \frac{c}{1 - c/c_P} \quad and \quad Y = \frac{1 - c}{E} \Rightarrow$$
$$E_S = 1/Y_o \;\; ; \;\; \mu_P^o = Y_o/\alpha \quad from\ intersection\ Y_o\ and\ slope\ \alpha \qquad (1.17)$$

Remark: It is noticed that no other information on pore geometry than μ_P and c_P can be obtained directly from mechanical tests. To get information on μ_S and c_S the pore system considered has to be impregnated - or supplementary studies on percolation (Section 1.1.3) and diffusivity (Section 1.5) have to be made.

Examples

The following data (plotted in Figure 1.22) on stiffness versus capillary porosity are from tests on HCP reported by Helmuth & Turk in (20):

(c,E(GPa) = (0.0175,29.3), (0.0351,28.78), (0.123,20.93), (0.123,20.756), (0.281, 11.686), (0.281,11.512), (0.3947,6.977), (0.4035,6.977).

The solid line in Figure 1.22 are results calculated by the present theory with solid stiffness (E_S) and geo-parameters (μ_P^o and c_P) deduced from experimental data as described in Equation 1.17, see Figure 1.21.

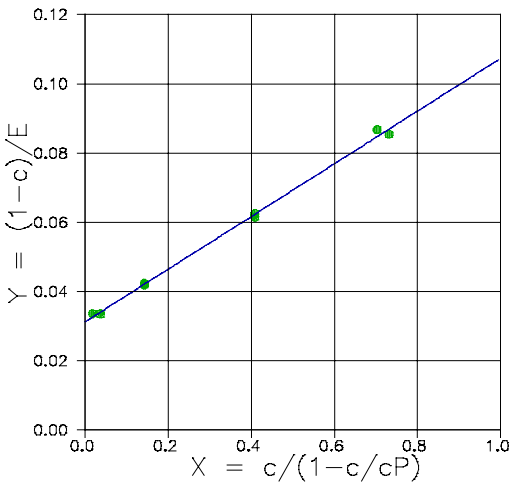

Figure 1.21. *Linear regression of manipulated experimental data. HCP stiffness versus capillary pores.*

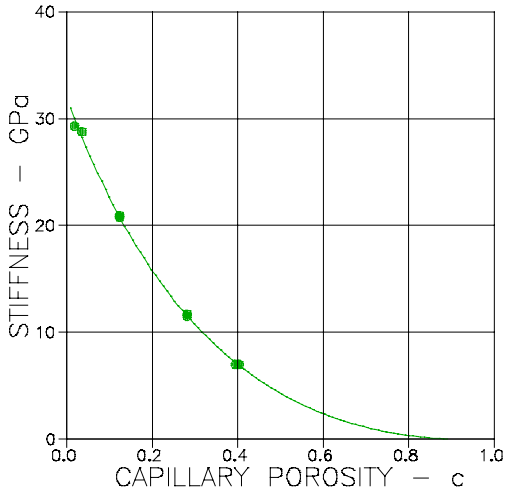

Figure 1.22. *Results of regression: E_S = 32.0 GPa, μ_P^o = 0.41, and c_P = 0.90. Fit quality r^2 = 0.998.*

The data in Figure 1.23, reproduced from (23), illustrates the influence of porosity (evaporable water measurement) on elasticity of nearly fully hydrated hardened portland cement paste (HCP). The experimental data shown by dots in the

figure are from (20) cement 15366). They are related to two pore systems defined in (8). *System I:* Solid phase (S) is made of cement gel solids, the pore phase is the total of cement gel pores and capillary pores. *System II:* Solid phase is cement gel, the pore phase is capillary pores. The theoretical data (solid lines in Figure 1.23) are based on the following information.

Composite:	System I: $(\mu_P^o, c_P) = (0.33, \approx 1)$
	System II: $(\mu_P^o, c_P) = (0.4, \approx 1)$
Phase S:	System I: $E_S = 80000$ MPa
	System II: $E_S = 32000$ MPaP

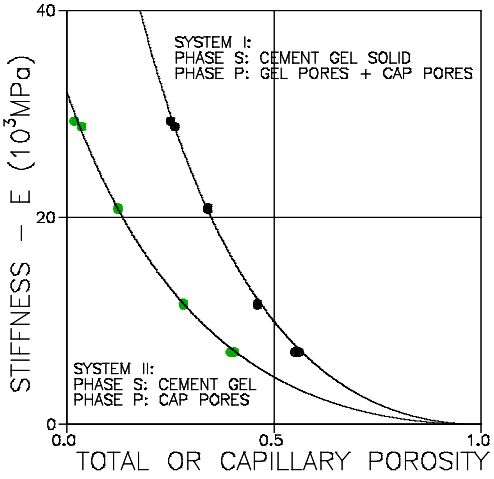

Figure 1.23. *Young's modulus of hardened Portland cement paste.*

1.3 Eigenstrain-stress

It can be shown (24,15) that an analysis of eigenstrain/stress problems in composite of arbitrary geometry can be made in a similar way as stiffness has been determined in this note. The results from (24,15) are reproduced in Table 1.3.

EIGENSTRAIN
$\lambda = \lambda_S + \Delta\lambda \dfrac{1/e - 1}{1/n - 1} \quad ; \quad (\Delta\lambda = \lambda_P - \lambda_S)$
$\dfrac{\lambda}{\lambda_S} = \dfrac{1/n - 1/e}{1/n - 1} = \begin{cases} 1 & \text{for } n = 0 \\ 1 - c & \text{for } n = 1 \\ 1/e_\infty & \text{for } n = \infty \end{cases} \quad ; \quad (\text{if } \lambda_P = 0)$
EIGENSTRESS ($K_S \approx 0.6E_S$)
$\rho_P = -3K_S\Delta\lambda\dfrac{c(1/n - 1) - (1/e - 1)}{c(1/n - 1)^2} \quad ; \quad \rho_S = -\dfrac{c}{1 - c}\rho_P$

Table 1.3. *Eigenstrain/stress of composite material. (λ_P,λ_S) and (ρ_P,ρ_S) are eigenstrain (linear) and eigenstress (hydrostatic) of phase P and phase S respectively. λ is linear composite eigenstrain. K_S is bulk modulus of phase S.*

1.3.1 Analysis

Numerically there are no problems in solving the eigenstrain/stress problem for composites of arbitrary geometry. We only have to use Table 1.3 with the composite stiffness previously determined in Section 1.2.5. Examples of the analysis of eigenstrain/stress problems are presented in Section 1.4.1.

1.3.2 Pore pressure

It also comes from (24,15) that the linear expansion of a porous material (arbitrary pore shapes) subjected to hydrostatic pore pressure can be predicted by the former expression in the following Equation 1.18.

$$\varepsilon = \frac{p}{3K_S}\left(\frac{1}{e} - 1\right) \quad \textit{where} \begin{cases} \varepsilon \textit{ is linear strain} \\ p \textit{ is hydrostatic pore pressure} \\ e \textit{ is relative } E\textit{-modulus of porous mat} \\ K_S \textit{ is bulk modulus of solid material} \end{cases} \qquad (1.18)$$

$$\varepsilon = \frac{p}{3K_S} \qquad \textit{if } p \textit{ is acting all over } (\textit{not only in pores})$$

The latter expression in Equation 1.18 is linear expansion if the hydrostatic pressure acts all over, meaning that the material considered is submerged in water, for example, with hydrostatic pressure p.

Equation 1.18 has been used in (25,15) to study the frost resistancy of porous materials. The expressions are usefull also when the phenomenon of drying shrinkage of porous materials is studied (26,27).

1.4 Complete analysis of particulate composites (CSA)

The composite analysis of stiffness and eigenstrain/stress can be considerably simplified when CSA_P-composites are considered. As previously mentioned, the geo-function for such composites is $\theta \equiv 1$ by which the results hitherto developed are reduced as shown in Table 1.4.

1.4.1 Numerical analysis (CSA)

It is obvious how Table 1.4 can be used as an algorithm for a general computer analysis of CSA-composites. A program based on Table 1.4 works very fast. As an extra it calculates the *matrix stresses close to the aggregates.*

Example

Some results of a complete analysis of a CSA_P-composite are presented in Figures 1.24 - 1.27. Composite stiffness and composite thermal behavior are considered together with internal stresses associated. Phase stiffness are $(E_P,E_S) = (15,1)*10^2$ MPa. Thermal eigenstrains are $(\lambda_P,\lambda_S) = (2*10^{-5},0)/°C$.

PROBLEM	**CSA_P-SOLUTIONS**
Young's modulus	$e = \frac{A+n}{1+An}$; $E = E_S\frac{A+n}{1+An}$ *with* $A = \frac{1-c}{1+c}$
Internal stress caused by external stress σ	$\sigma_P = \sigma\frac{(1+A)n}{A+n}$; $\sigma_S = \frac{\sigma - c\sigma_P}{1-c}$
Eigenstrain/stress caused by particle eigenstrain λ_P and matrix eigenstrain λ_S	$\lambda = \lambda_S + \Delta\lambda\frac{n(1-A)}{A+n}$; $\Delta\lambda = \lambda_P - \lambda_S$ $\rho_P = -3K_P\Delta\lambda\frac{A}{A+n}$; $\rho_S = -\frac{c}{1-c}\rho_P$
Matrix-stress at spheres	$\sigma_{S,RAD} = \rho_P$; $\sigma_{S,TAN} = -\frac{3-A}{4A}\rho_P$

Table 1.4. *Composite analysis of CSA_P-material. In eigenstrain/stress analysis: (λ_P,λ_S) and (ρ_P,ρ_S) are eigenstrain (linear) and eigenstress (hydrostatic) of phase P and phase S respectively. $\sigma_{S,RAD}$ is radial phase S stress at sphere, $\sigma_{S,TAN}$ is tangential phase S stress at sphere.*

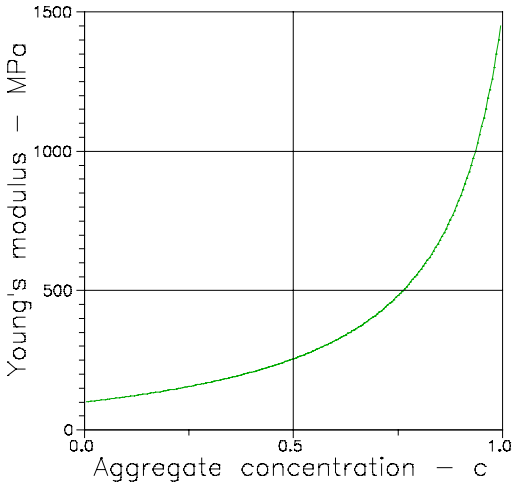

Figure 1.24. *Stiffness of CSA_P-composite. $(E_P,E_S) = (15,1)*10^2$ MPa*

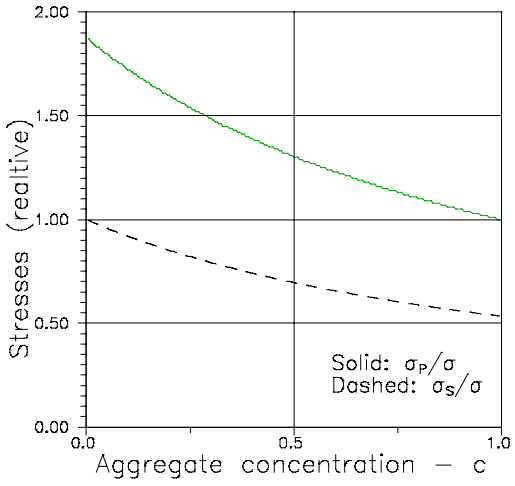

Figure 1.25. *Internal stresses in composite defined in Figure 1.24.*

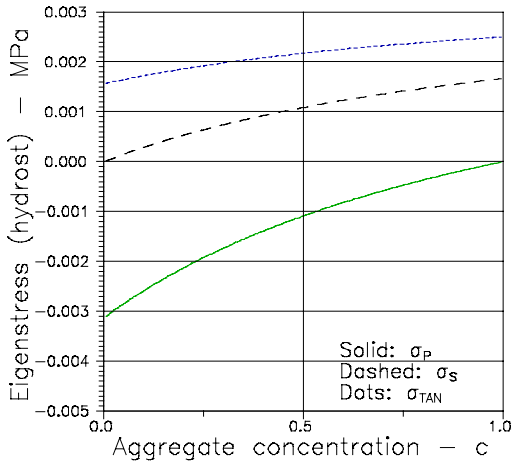

Figure 1.26. *Thermal eigenstreses/°C in composite defined in Figure 1.24. (λ_P, λ_S) = (2*10^{-5},0)/°C.*

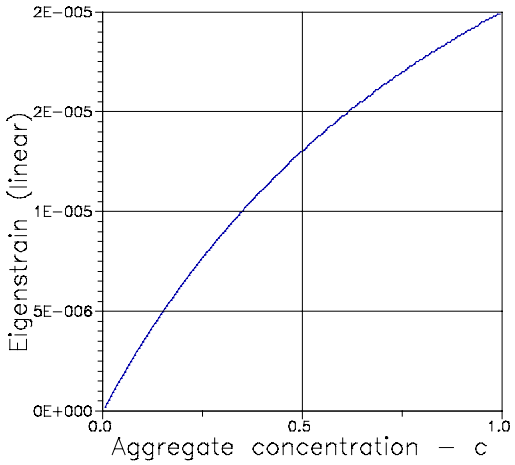

Figure 1.27. *Thermal eigenstrain/°C in composite defined in Figure 1.24. (λ_P,λ_S) = (2*10^{-5},0)/°C.*

1.5 Other physical properties

Many physical properties are proportionality constants between fluxes and potential gradients (just as Young's modulus is proportionality constant between stress and strain), e.g. thermal and electrical conductivities, and diffusion coefficients. Other physical properties are proportionality constants between inductions and force field strengths, e.g. dielectric constants and magnetic permeabilities. A composite materials analysis with respect to any of these properties will, by analogy, follow the same pattern and produce similar solutions. For example, expressions developed to predict the stiffness of composites can also be used to predict thermal conductivity of composites. Of course appropriate substitutions of notations have to be introduced (including proper transformation of vector field phenomenons (stiffness) to scalar field phenomenons (like thermal conductivity). The efficiency of the analogy can be observed comparing the works on dielectric properties by Hashin (28) and Hashin and Shtrikman (29) on CSA materials with the same authors analysis (13,11) previously referred to on stiffness of such materials.

The stiffness expressions presented in this paper for composites of arbitrary geometry are generalized by the author in (8) to include other physical properties only by *doubling the geometry function* θ. For example, when Q is the physical scalar field property considered we use Table 1.1 + Table 1.2 with symbols E replaced by symbols Q, and θ replaced with 2θ. The analogy is demonstrated in the following Equation 1.19 which reduces as shown in Equation 1.20 when porous materials are considered

$$q = \frac{Q}{Q_S} = \frac{n + \theta[1 + c\,(n - 1)]}{n + \theta - c(n - 1)} \quad ; \quad \left(n = \frac{Q_P}{Q_S}\right) \quad \textit{with} \qquad (1.19)$$

$$\theta = \mu_P + n\mu_S + \sqrt{(\mu_P + n\mu_S)^2 + 4n(1 - \mu_P - \mu_S)}$$

$$\frac{Q}{Q_S} = \frac{1 - c}{1 + c/(2\mu_P)} \quad ; \quad \textit{porous materials} \qquad (1.20)$$

Conductivity bounds corresponding to the H/S stiffness bounds previously referred to are obtained introducing $\theta \equiv 2$ and $\theta \equiv 2n$ respectively into the stiffness expression in Table 1.2. We get

$$\frac{n + 2[1 + c\,(n - 1)]}{n + 2 - c(n - 1)} \le q \le n\frac{3 + 2c\,(n - 1)}{3n - c(n - 1)} \qquad (1.21)$$

valid for $n \ge 1$; *reverse signs when* $n < 1$

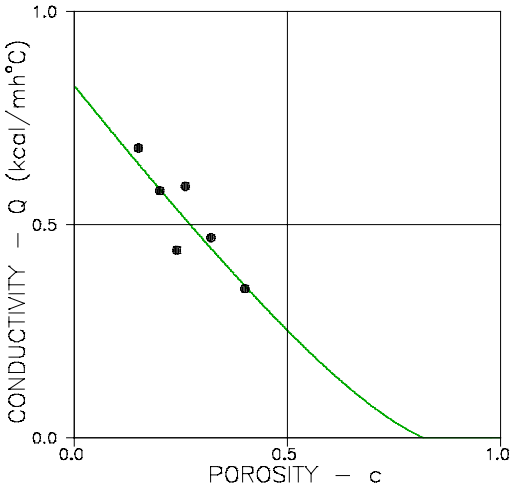

Figure 1.28. *Thermal conductivity of fire-brick. Geometry:* $(\mu_P^o, \mu_S^o, c_P) = (1, 0, 0.82)$

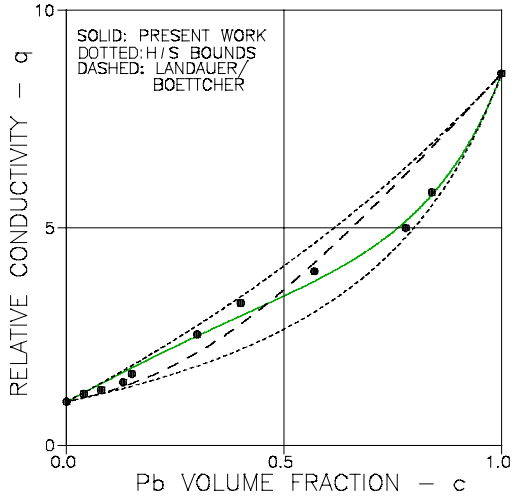

Figure 1.29. *Electrical conductivity of* Mg_2Pb*-Pb.* $(\mu_P^o, \mu_S^o, c_P) = (-1,1,1/2)$.

1.5.1 Numerical analysis

The above analogy can easily be programmed. The algorithms hitherto developed can be re-used with only small modifications.

Examples (a.o. Cloride diffusion in HCP)

Some results of an analysis are presented in Figures 1.28 and 1.29 with experimental data from (30) and (31) respectively.

The experimental data shown in Figure 1.30 are from studies on chloride diffusion in hardened cement paste made by Mejlhede in (32). The diffusion coefficient in gel (c = 0) and in free water (c = 1) has been estimated by Mejlhede to be $Q_S \approx 10^{-13}$ m^2/sec and $Q_P \approx 10^{-8}$ m^2/sec respectively.

The theoretical date shown in Figure 1.30 are the results of an analysis made, assuming a MM-MM composite with shape functions defined by (μ_P^o, μ_S^o,c_P) ≡ (1.e-10,1.e-10,>1). From Figures 1.13 and 1.14 is concluded that such shape functions define a platework geometry (crumbled foils). For these special shape functions the following analytical solution can be derived (with $\mu_P = \mu_S \equiv 0$).

$$q = \frac{Q}{Q_S} = \frac{n + 2\sqrt{n}[1 + c(n - 1)]}{n + 2\sqrt{n} - c(n - 1)} \quad ; \quad (\theta \equiv 2\sqrt{n}) \tag{1.22}$$

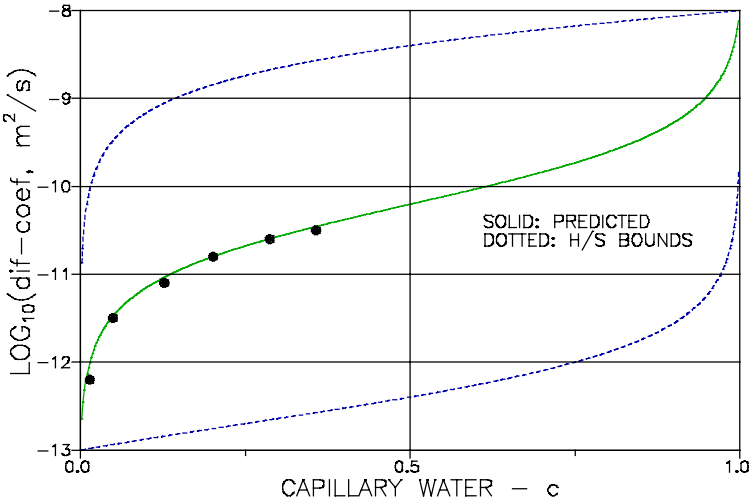

Figure 1.30. *Chloride diffusion in hardened cement paste as a function of capillary water content.*

Remark: The simple analytical expression presented in Equation 1.22 compares positively with a numerical diffusivity analysis reported in (33,34) which is based on a computer simulated HCP-microstructure. The basic geometrical concepts of the composite analysis presented in this note are justified considerably by this observation.

2. VISCOELASTIC MATERIALS

In principles any relation previously developed on composite geometry influencing stiffness, stress, strain, and eigenstress/strain of composites made of elastic components apply also when viscoelastic composite materials are considered. Powerful analogies exist in the theory of viscoelasticity by which elastic composite solutions can be generalized to include solutions to composites made of viscoelastic components. In the present context this means, for example, that creep of a viscoelastic composite can be deduced from the elastic flexibility (reciprocal Young's modulus) solution of the elastic composite (same geometry same phase contents). These comments indicate the topics dealt with in Chapter 3.

The present Chapter 2 is meant for readers who are not too familiar with viscoelastic materials and the theory of viscoelasticity.

Læren om viskoelastiske materialer betegnes ofte som rheologi. Dette udtryk er græsk og betyder læren om det, som flyder. Som sådan rummer begrebet enhver tænkelig materialerelation mellem kraft (spænding) og deformation (tøjning) samt tid. Rheologisk set er mange bygningsmaterialer som for eksempel træ vist at kunne klassificeres som såkaldte lineær viskoelastiske materialer, såfremt belastningen er lavere end cirka 50 % af den, der fremkalder brud. Det vil sige, at de fleste brugstilstande er tilgodeset i denne relativt simple materialeopfattelse, der skal forklares nærmere i de følgende afsnit.

2.1 Lineær viskoelasticitet

Et viscoelastic materiale er et materiale, hvis spændings-tøjningsrelation kan beskrives ved en ligning af typen

$$\sum_{k=0}^{N} p_k \frac{d^k \sigma}{dt_k} = \sum_{k=0}^{N} q_k \frac{d^k \varepsilon}{dt^k} \qquad (2.1)$$

hvor p_k og q_k er materialekonstanter. Spænding og tøjning er betegnet ved σ henholdsvis ε.

Benævnelsen, "lineær viskoelastisk", anvendes fordi 1) sammenhængen mellem spænding og tøjning er lineær (ligning 2.1 er en lineær differentialligning), fordi 2) tiden er indblandet (flydning, viskositet) og fordi 3) almindelig elasticitet også er involveret. Det sidste indses ved at lade alle p_k og q_k, undtagen p_0 og q_0, blive 0. Herved reduceres Ligning 2.1 til Hooke's lov, $\sigma = E\varepsilon$, hvor $E = q_0/p_0$ er Young modulen.

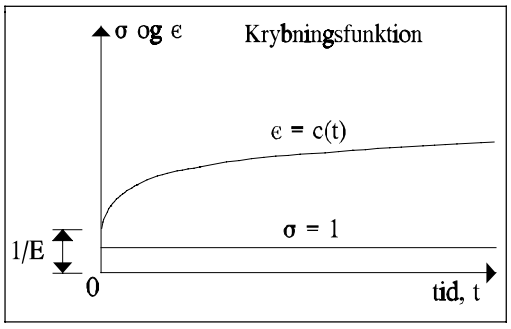

Figure 2.1. *Krybningsfunktionen er tøjningen under spændingen 1.*

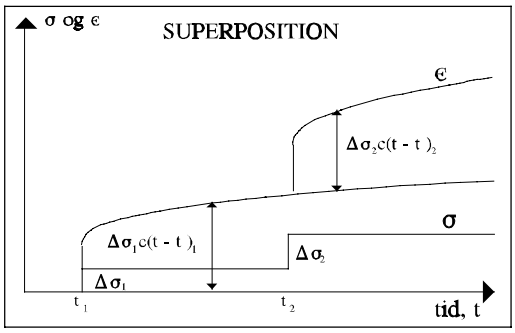

Figure 2.2. *Superpositionslovens anvendelse i forbindelse med stepformet spændingsvariation.*

Et vigtigt kendetegn for viskoelastiske materialer er den såkaldte krybningsfunktionen, C(t), der angiver den tøjning, der fremkaldes, når materialet belastes til tidspunkt t = 0 med den konstante spænding, $\sigma = 1$. Krybningsfunktionen forløber typisk som vist i Figur 2.1. Begyndelsesværdien er C(0) = 1/E.

Krybningsforløbet kan ved superposition, som vist i Figur 2.2, anvendes til opbygning af tøjningsløsningen for et stepvarierende spændingsforløb. Vi får

$$\varepsilon(t) = \Delta\sigma_1 C(t - t_1) + \Delta\sigma_2 C(t - t_2) + ... = \sum_{n=1}^{N} \Delta\sigma_n C(t - t_n) \qquad (2.2)$$

hvor $\Delta\sigma_n = \Delta\sigma(t_n)$ betyder en springvis spændingsforøgelse til tidspunkt t_n. Ved overgang til et vilkårligt, kontinuert spændingsforløb erstattes i Ligning 2.2 t_n med θ, spændingsspringene med $\Delta\sigma(\theta) = (d\sigma/d\theta)d\theta$ og summationstegnet med et integral. Vi får herefter

$$\varepsilon(t) = \int_{-\infty}^{t} C(t - \theta)\frac{d\sigma}{d\theta}d\theta \qquad (2.3)$$

Løsning af Ligning 2.1 kan også ske under anvendelse af den såkaldte relaxationsfunktion, R(t). Denne funktion er defineret som den spænding, der induceres i materialet, når dette påvirkes med en konstant tøjning, $\varepsilon = 1$ virkende fra t = 0. En relaxationsfunktion forløber typisk som vist i Figur 2.3.

På ganske tilsvarende måde, som krybningsfunktionen fører frem til tøjningsløsningen i Ligning 2.3, fører relaxationsfunktionen frem til spændingsløsningen

$$\sigma(t) = \int_{-\infty}^{t} R(t - \theta)\frac{d\varepsilon}{d\theta}d\theta \qquad (2.4)$$

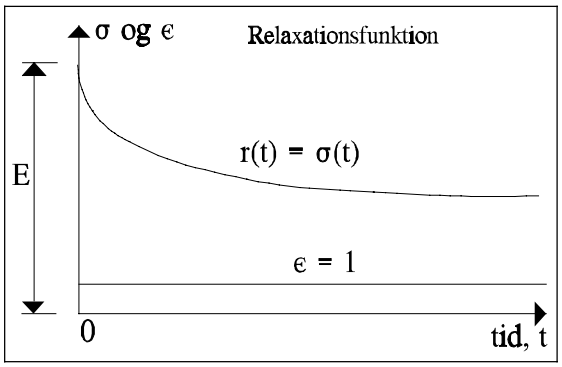

Figur 2.3. *Relaxationsfunktionen er spændingen fremkaldt af en konstant tøjning.*

Det er vigtigt at gøre sig klart, at spændings-tøjnings-relationerne som udtrykt ved Ligningerne, 2.1, 2.3 og 2.4, er ensbetydende. Et af udtrykkene definerer entydigt et materiales viskoelastiske opførsel.

Med hensyn til anvendelser kan der imidlertidig være meget store forskelle i den matematiske kompleksitet. Normalt vil det være således, at integralrepresentationen udtrykt ved Ligning 2.3 vil være at foretrække ved løsning af problemer med foreskreven last, mens Ligning 2.4 er mere hensigtsmæssig at anvende, når deformationen er givet.

2.2 Viscoelastic models

A complete analogy exist between viscoelastic stress-strain relations and force-deflection relations for mechanical systems composed of springs (Hooke elements with $\varepsilon = \sigma/E$) and dash pots (Newton elements with $d\varepsilon/dt = \sigma/\eta$) where E and η denote spring constant and viscosity respectively. Examples are presented in Equations 2.5 - 2.7 demonstrating how mechanical models can be developed to represent viscoelastic materials. An infinite number of viscoelastic materials (models) can be defined in this way. In this note, however, we will limit our interest to the so-called simple models of viscoelastic materials considered in Section 2.2.1 and the special models considered in Section 2.2.2.

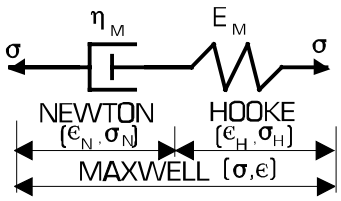

$$\sigma = \sigma_H = \sigma_N \qquad (\textit{Equilibrium})$$
$$\varepsilon = \varepsilon_H + \varepsilon_N \qquad (\textit{Geometry})$$
$$\varepsilon_H = \frac{\sigma_H}{E_M} \;;\; \frac{d\varepsilon_N}{dt} = \frac{\sigma_N}{\eta_M} \qquad (\textit{Physics}) \qquad (2.5)$$
$$\textbf{\textit{MAXWELL:}} \quad \frac{d\sigma}{dt} + \frac{E_M}{\eta_M}\sigma = E_M\frac{d\varepsilon}{dt}$$

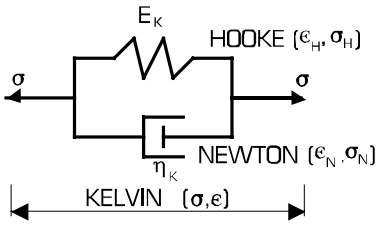

$$\sigma = \sigma_H + \sigma_N \qquad (\textit{Equilibrium})$$
$$\varepsilon = \varepsilon_H = \varepsilon_N \qquad (\textit{Geometry})$$
$$\varepsilon_H = \frac{\sigma_H}{E_K} \;;\; \frac{d\varepsilon_N}{dt} = \frac{\sigma_N}{\eta_K} \qquad (\textit{Physics}) \quad (2.6)$$
$$\textbf{\textit{KELVIN}:}\quad \sigma = \eta_K \frac{d\varepsilon}{dt} + E_K \varepsilon$$

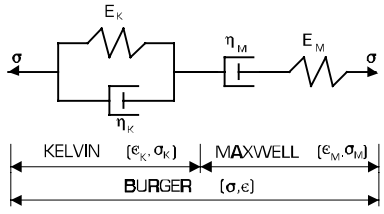

$$\sigma = \sigma_M = \sigma_K \quad ; \; \textit{Equilibrium}$$
$$\varepsilon = \varepsilon_M + \varepsilon_K \quad ; \; \textit{Geometry}$$
$$\left.\begin{aligned} \frac{d\sigma_M}{dt} + \frac{E_M}{\eta_M}\sigma_M &= E_M \frac{d\varepsilon_M}{dt} \\ \sigma_K &= \eta_K \frac{d\varepsilon_K}{dt} + E_K \varepsilon_K \end{aligned}\right\} \textit{Physics} \qquad (2.7)$$

$$\textbf{\textit{BURGER}:}\quad \frac{d^2\sigma}{dt^2} + \left(\frac{E_K}{\eta_K} + \frac{E_M}{\eta_K} + \frac{E_M}{\eta_M}\right)\frac{d\sigma}{dt} + \frac{E_M E_K}{\eta_M \eta_K}\sigma = E_M\left(\frac{d^2\varepsilon}{dt^2} + \frac{E_K}{\eta_K}\frac{d\varepsilon}{dt}\right)$$

2.2.1 Simple models

The procedure just demonstrated in Equations 2.5 - 2.7 to develop stress-strain relations has been made on a number of simple viscoelastic materials. Closed analytical expressions for stress-strain relations, analogy Young's moduli, creep- and relaxation functions are summarized in Tables 2.1 and 2.2 reproduced from (35). Very convenient abbreviations of groups of material parameters are defined in Table 2.1.

MODELS	**MATERIAL PARAMETERS**
HOOKE, NEWTON, MAXWELL, KELVIN, THOMSON, LETHERSICH, BURGER	$\tau = \frac{\eta}{E} \;;\; \tau_K = \frac{\eta_K}{E_K}$ *Relaxation times* $\alpha = \frac{E}{E_K} \;;\; m_T = 1 + \alpha \;;\; m_L = \frac{1}{1 + \eta/\eta_K}$ $m_{B1}, m_{B2} = \frac{1}{2}\left(1 + \alpha + \frac{\tau_K}{\tau} \pm \sqrt{\left(1 + \alpha + \frac{\tau_K}{\tau}\right)^2 - 4\frac{\tau_K}{\tau}}\right)$ $m_{B1} m_{B2} = \frac{\tau_K}{\tau} \;;\; m_{B1} + m_{B2} = 1 + \alpha + \frac{\tau_K}{\tau}$

Table 2.1. Simple models of viscoelastic materials. Hooke and Newton are the basic models. Reproduced from (35).

MODEL	STRESS-STRAIN RELATION
Hooke	$\sigma = E\varepsilon$
Newton	$\sigma = \eta\dot{\varepsilon}$
Maxwell	$\dot{\sigma} + \sigma/\tau = E\dot{\varepsilon}$
Kelvin	$\sigma = E_K(\tau_K\dot{\varepsilon} + \varepsilon)$
Thomson	$\tau_K\dot{\sigma} + m_T\sigma = E(\tau_K\dot{\varepsilon} + \varepsilon)$
Lethersich	$\tau_K\dot{\sigma} + m_L\sigma = m_L\eta(\tau_K\ddot{\varepsilon} + \dot{\varepsilon})$
Burger	$\tau_K^2\ddot{\sigma} + (m_{B1} + m_{B2})\tau_K\dot{\sigma} + m_{B1}m_{B2}\sigma = E(\tau_K^2\ddot{\varepsilon} + \tau_K\dot{\varepsilon})$

Table 2.2. Stress-strain relations of simple viscoelastic models.

MODEL	**CREEP FUNCTION**	**RELAXATION FUNCTION**
Hooke	$1/E$	E
Newton	t/η	$\eta\delta(t)$; *Dirac's delta function* $\delta(t)$
Maxwell	$\frac{1}{E}\left(1 + \frac{t}{\tau}\right)$	$E\exp\left(-\frac{t}{\tau}\right)$
Kelvin	$\frac{1}{E_K}\left(1 - \exp\left(-\frac{t}{\tau_K}\right)\right)$	$E_K(1 + \tau_K\delta(t))$
Thomson	$\frac{1}{E}\left(1 + \alpha\left[1 - \exp\left(-m_T\frac{t}{\tau_K}\right)\right]\right)$	$E\left(1 - \frac{\alpha}{1+\alpha}\left[1 - \exp\left(m_T\frac{t}{\tau_K}\right)\right]\right)$
Lethersich	$\frac{t}{\eta} + \frac{1}{E_K}\left(1 - \exp\left(-\frac{t}{\tau_K}\right)\right)$	$m_L\eta\left(\delta(t) + \frac{1+m_L}{\tau_K}\exp\left(-m_L\frac{t}{\tau_K}\right)\right)$
Burger	$\frac{1}{E}\left(1 + \frac{t}{\tau} + \alpha\left[1 - \exp\left(-\frac{t}{\tau_K}\right)\right]\right)$	$\frac{E}{m_{B1} - m_{B2}}\left[(m_{B1} - 1)\exp\left(-m_{B1}\frac{t}{\tau_K}\right) - (m_{B2} - 1)\exp\left(-m_{B2}\frac{t}{\tau_K}\right)\right]$

Table 2.3. *Creep functions and relaxation functions of simple viscoelastic models.*

2.2.2 Special materials

Time modified Maxwell material

Some viscoelastic materials like Portland cement paste and concrete are so-called aging viscoelastic materials (36) with time dependent material properties

meaning that the creep functions, relaxation functions, and the material parameters p and q in Equation 1 become dependent of time.

Some aging materials, however, can be considered by the theory of non-aging materials hitherto considered if we assume that the "spring constants" (E) in the mechanical models are constants (in practice almost constants) and that viscosities (η) change in the same way with time. Then the aging phenomenon can be removed by introducing a modified time as subsequently demonstrated in Equation 2.8 on a Maxwell material with time dependent viscosity ($\eta(t)$ or time dependent relaxation time $\tau(t) = \eta(t)/E$). The modified time concept was suggested by the author in (36,37) and subsequently further developed in a number of papers (38,39) on the rheology of hardened portland cement paste and Portland cement based materials like hardened concrete older than 2-3 weeks.

$$\begin{aligned}
&\textit{Aging Maxwell:} && \frac{d\sigma}{dt} + \frac{\sigma}{\tau(t)} = E\frac{d\varepsilon}{dt} && \Rightarrow \\
&\textit{differentiation through } \phi: && \frac{d\sigma}{d\phi}\frac{d\phi}{dt} + \frac{\sigma}{\tau(t)} = \frac{d\varepsilon}{d\phi}\frac{d\phi}{dt} && \Rightarrow \\
& && \frac{d\sigma}{d\phi} + \frac{\sigma}{\tau(t)d\phi/dt} = E\frac{d\varepsilon}{d\phi} && \Rightarrow \\
&\underline{\textit{Non-aging Maxwell}} \textit{ with} \\
&\tau = 1 \textit{ and modified time } \phi && \underline{\frac{d\sigma}{d\phi} + \sigma = E\frac{d\varepsilon}{d\phi}}
\end{aligned} \qquad (2.8)$$

The modified time is related to real time by $\tau(t)d\phi/dt = \tau = 1$, meaning

$$\phi = \phi(t) = \int_{t_o}^{t-t_o} \frac{1}{\tau(t)}dt \quad (\textit{time } t \textit{ is measured from age of reference } t_o) \qquad (2.9)$$

Conclusion: Thus, a Maxwell material with aging viscosity can be considered as a non-aging Maxwell material when time t is replaced with modified time ϕ (also named "creep parameter)", and relaxation time $\tau(t)$ is replaced with modified relaxation time $\tau = 1$. Then from Table 2.3 creep functions and relaxation functions become,

$$C(\phi) = \frac{1}{E}(1 + \phi) \quad ; \quad R(\phi) = E\exp(-\phi)) \qquad (2.10)$$

Remark: In general the relaxation time τ is sensitive to climate such that it becomes lower with increasing levels of temperature and humidity. This means that climates different from a certain reference climate (where τ is replaced with

1) can in principle be considered replacing τ with a quantity different from 1 which will influence modified time as expressed by Equation 2.9.

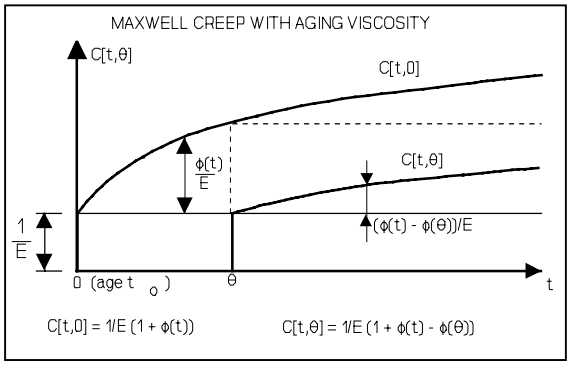

Figure 2.4. *Real creep functions C[t,θ] as related to modified time φ (creep parameter).*

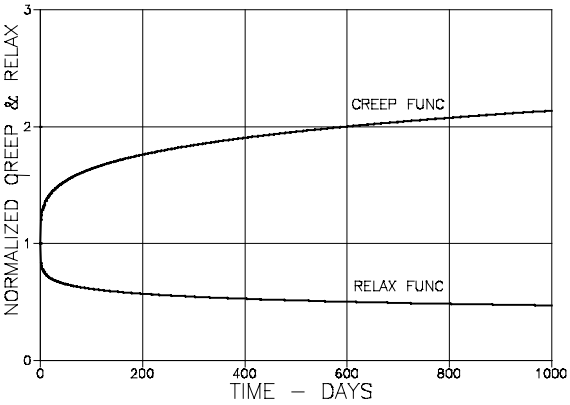

Figure 2.5. *Normalized Power law creep function EC(t), and normalized relax function R(t)/E (b = 0.25, τ = 600 days).*

2.2.3 Hardened cement paste (HCP)

When HCP especially is considered Young's modulus and creep parameter (modified time) can be introduced as presented in Equation 2.11 approximated from (38). Time at first load application is t_o (> 2-3 weeks). Water/Cement ratio is W/C ≥ 0.4. A_W is a compactness factor which depends on water-cement ratio.

$$C_{HCP}(\phi) = \frac{1}{E_{HCP}}(1 + \phi) \quad with \ \phi = \phi^{1000}\frac{\log_E\left(\frac{t + t_o}{t_o}\right)}{\log_E\left(\frac{1000 + t_o}{t_o}\right)} \ ; \ (\phi^{1000} \approx 5-8) \qquad (2.11)$$

$$E_{HCP} = 3.2 * 10^4 A_W \ MPa \quad with \quad A_W = \left(\frac{0{,}4}{W/C}\right)^{1.5}$$

The basic ideas of considering aging cement based materials as time modified viscoelastic materials have been used in international code considerations (40). They have been generalized by the author in (41) such that also younger concretes (with some stiffness aging) can be considered by this simple method.

2.2.4 Power Law creep (Wood, polymers, ceramics)

The *Power Law model* (42) explained in Table 2.4 is of special interest in this note. The principal rheological properties predicted by this model "cover" a wide range of materials only by changing a few parameters, the relaxation time τ (creep doubling time, $C(\tau) = 2C(0)$), and the dimensionless creep power b. It has often been demonstrated in the literature on creep of materials (ex. 43) that many materials (such as wood, polymers, and ceramic materials) behave viscoelastically with creep functions which can be fitted very well by power law type of expressions. An example of associated creep and relaxation is presented graphically in Figure 2.4. As for HCP the relaxation time is very sensitive to climate. It is lowered at increasing levels of temperature and humidity.

POWER LAW MODEL	
CREEP FUNCTION C(t)	**RELAX FUNCTION R(t)**
$\frac{1}{E}\left(1 + \left(\frac{t}{\tau}\right)^b\right)$	$E \sum_{k=0}^{\infty} \frac{(-Z(t))^k}{\Gamma(1 + kb)} \approx \frac{1}{C(t)}$ *if* $b < \frac{1}{3}$

Table 2.4. *Power law creep.* $Z(x) = \Gamma(1+b)(x/\tau)^b$ *where* $\Gamma(1+b) = b!$ *(faculty b) is gamma function of b.*

For træ er relaxationstiden τ og dens afhængighed af orthotropi og ligevægtsfugt angivet i nedenstående Ligninger 2.12 og 2.13. En krybningseksponent på $b \approx 0.25$ kan fastholdes under alle omstændigheder. Elasticitetsmodulen, E, er den fugtkorrigerede modul med $E_{15}\| \approx 12000$ MPa, $E_{15}\perp \approx 1000$ MPa. Under ikke-stabile klimaforhold bliver relaxationstiden formindsket. En faktor på 0.1 eller mindre er ikke ualmindelig.

$$\tau = \tau_{15} * 10^{\frac{15 - U}{10}} \quad ; \quad E \approx E_{15}\left(1 + \frac{15 - U}{150}\right) \quad ; \quad (U > 30 = 30) \tag{2.12}$$

$$\tau_{15}(døgn) \approx \begin{cases} 10^4 - 10^5 & træk, tryk, bøjning \| med fibre \ (\tau\|) \\ 30 - 300 & forskydning \| med fibre \ (\tau\rightleftharpoons) \\ 3 - 30 & træk \perp på fibre \ (\tau\perp) \end{cases} \tag{2.13}$$

Bestemmelse af krybningsparametre

Udfra en række målte krybningsdata er det ret enkelt at bestemme krybningsparametrene τ og b. Vi benytter, at krybningsfunktionen i Tabel 2.4 kan lineariseres ved logaritmisering, hvorefter

$$Y = Y_o + \alpha X \quad med \quad Y = \log_{10}(Ec(t) - 1) \quad ; \quad X = \log_{10}(t)$$
$$\Rightarrow \quad b = \alpha = -\frac{Y_o}{X_o} \quad ; \quad \tau = 10^{-Y_o/\alpha} = 10^{X_o} \tag{2.14}$$

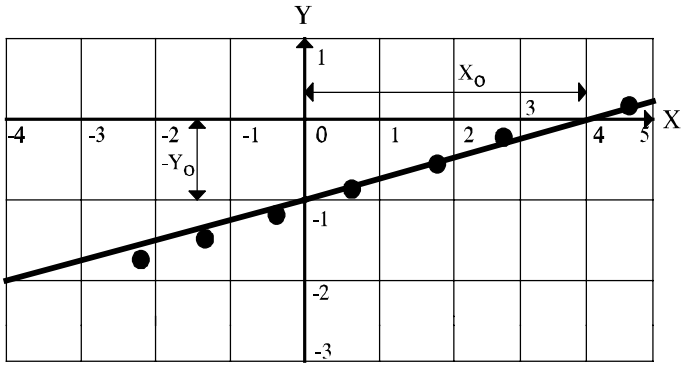

***Figur 2.6**. Bestemmelse af træs rheologiske parametre udfra experimentelt bestemte krybningsdata, se Ligning 2.14.*

2.3 Spændings-tøjnings-analyse

2.3.1 Viskoelastiske operatorer

De to ligeværdige integraludtryk i Ligningerne 2.3 og 2.4 kan skrives på operatorformen vist i Ligning 2.15. Operatorerne kaldes ofte analogioperatorer på grund af den slående lighed til elasticitetsmodulen E i de tilsvarende elasticitetsudtryk ($\varepsilon = \sigma/E$ og $\sigma = E\varepsilon$).

$$\varepsilon = \overline{E}^{-1}[\sigma] \quad ; \quad \overline{E}^{-1}[\ ] = \int_{-\infty}^{t} C(t-\theta)\frac{d[\ ]}{d\theta}d\theta$$
$$\sigma = \overline{E}[\varepsilon] \quad ; \quad \overline{E}[\ ] = \int_{-\infty}^{t} R(t-\theta)\frac{d[\ ]}{d\theta}d\theta \tag{2.15}$$

2.3.2 Elastisk-viskoelastisk analogi

Det kan vises, at løsningen til et lineær-viskoelastisk problem kan opnås ved at erstatte elasticitetskoefficienten i løsningen for det tilsvarende lineær-elastiske

problem med den tilsvarende viskoelastiske operator defineret i Ligning 2.15. E-v-analogien er den forkortede betegnelse for denne analogi.

E-v-analogien medfører at viskoelastiske løsninger til problemer, hvis elastiske løsninger er $\varepsilon = \sigma(t)/E$ eller $\sigma = \varepsilon(t)E$, kan udtrykkes som anført i Ligning 2.16. Spænding og tøjning kan her opfattes i generaliseret betydning. Spændingen kan være kraften på en konstruktion, mens tøjningen er konstruktionens udbøjning.

$$\varepsilon_{VISK} = \int_{-\infty}^{t} C(t-\theta)\frac{d(E\varepsilon_{EL})}{d\theta}d\theta \quad eller \quad \sigma_{VISK} = \int_{-\infty}^{t} R(t-\theta)\frac{d(\sigma_{EL}/E)}{d\theta}d\theta \qquad (2.16)$$

E-v-analogien er et meget nyttigt matematisk værktøj, når nøjagtige analyser skal foretages - især når den anvendes i forbindelse med Laplace transformation (44,45,46,36,35). Men den involverede matematik kan i mange tilfælde antage et omfang, der ikke rigtigt står i forhold til den nøjagtighed, hvormed materiale-egenskaber kendes i praksis - og den nøjagtighed, hvormed analyseresultatet egentlig ønskes.

2.3.3 Approximate e-v-analogy (Effective Young's modulus)

I det foreliggende notat er det valgt at gennemføre viskoelastiske analyser på grundlag af nedenstående stærkt forenklede udgave af analogien. Intet principielt går tabt herved. I nogle tilfælde er analyseresultaterne tæt ved at være nøjagtige. Oftest ligger nøjagtighed imidlertid på niveauet "gode estimater".

The following very simple approximation of the e-v-analogy exist (47) when stress or strain varies monotonically in materials which have creep functions and relaxations functions which are approximately each others reciprocals such as for many materials exhibiting Power Law creep ($b < 1/3$).

***Approximate e-v-analogy*:**
$\Delta_{VISC}(t) \approx F[E^{EFF}, P(t)]$ *Viscelastis solution comes from*
$\Delta_{ELAST}(t) = F[E, P(t)]$ *Elastic solution with E replaced with*
$E^{EFF} = R(t) \approx 1/C(t)$ *Effecttive Young's modulus* (2.17)

Example: Udtørring af træ

Lad os som et eksempel på en viskoelastisk spændingsanalyse beregne den svind-fremkaldte spænding i et stykke ligevægtsfugtigt træ, hvis længde fastholdes fra tiden, $t = 0$, hvorefter fugtindholdet i træet ændres homogent over tværsnittet.

Det svind, der fremkaldes i træet, såfremt det ikke er indspændt, er det såkaldte frie svind, der kan udtrykkes ved

$$\varepsilon_{SV,I} = s_I * [u(0) - u(t)] \quad ; \quad (I = T, R, L) \tag{2.18}$$

hvor s_I er svindkoefficienten og fugtindholdet, u (i rent tal, 0.1 kg/kg fex), er vægt af indeholdt vand i forhold til tørvægten af det betragtede træemne. Fugtændringen u(0)-u(t) giver positivt svind ved udtørring. Index I på ε_{SV} og svindkoefficienten, s, angiver retning således, at T, R, og L refererer til træets tangentielle (T), radiære (R) henholdsvis axiale retning (L). Disse symboler er almindeligt anvendte som retningsgivende i træteknologien; f.eks. betegner E_R træets elasticitetkoefficient i radiær retning o.s.v. Svindkoefficientens størrelsesorden er givet i Ligning 2.19.

$$s_T \approx 0.4, \quad s_R \approx 0.2, \quad s_L \approx 0.01 \tag{2.19}$$

Den elastiske spænding i vort eksempel kan beregnes som anført i Ligning 2.20 (se Figur 2.7). Den nøjagtige viskoelastisk spænding fås herefter ved hjælp af e-v-analogien (Ligning 2.15) som angivet i Ligning 2.21.

$$\sigma_{EL} = E * s * [u(0) - u(t)] \tag{2.20}$$

$$\sigma_{VISK} = s * \int_0^t R(t - \theta) \frac{d[u(0) - u(\theta)]}{d\theta} d\theta \quad (\textit{accurate solution}) \tag{2.21}$$

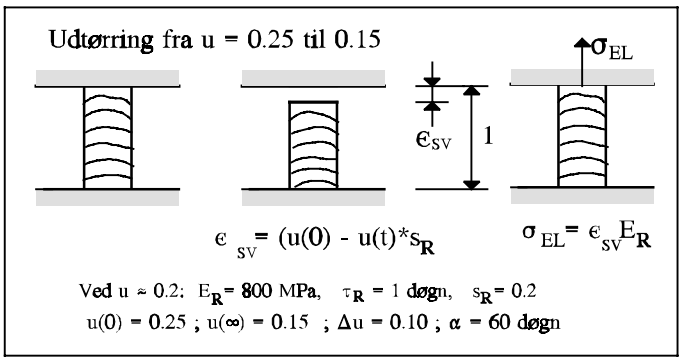

Figur 2.7. *Udtørring af fastholdt bræt. Elastisk spænding.*

Vi forudsætter nu i eksemplet at udtørringen sker exponentielt som angivet i Ligning 2.22, hvor "relaxationstiden" for udtørring α kontrollerer udtørringshastigheden (mindre α, hurtigere udtørring). Ligning 2.21 reduceres nu til løsningen i Ligning 2.23, hvor relaxationsfunktionen er introduceret fra Tabel 2.4.

$$u(0) - u(t) = \Delta u\left(1 - EXP\left(-\frac{t}{\alpha}\right)\right) \quad ; \quad (\Delta u = u(0) - u(\infty)) \tag{2.22}$$

$$\sigma_{VISC} \approx \frac{Es\Delta u}{\alpha}\int_0^t \frac{\exp(-\theta/\alpha)}{1 + [(t-\theta)/\tau]^b}d\theta \quad accurate\ solution \tag{2.23}$$

En tilnærmet løsning på problemet kan fås ved at anvende den forenklede e-v-analogi i afsnit 2.3.3 på det elastiske spændingsudtryk i Ligning 2.20: E erstattes med R(t) ≈ 1/C(t). Resultatet er givet i Ligning 2.24.

$$\sigma_{VISK} \approx Es\Delta u\frac{1 - \exp(-t/\alpha)}{1 + (t/\tau)^b} \quad (approximate\ solution) \tag{2.24}$$

Tilnærmelsen kan forventes at være nogenlunde god, idet dens forudsætning vedrørende monotont varierende spænding eller tøjning er overholdt. Det bemærkes, at udtørringsspændingen som udtrykt i både Ligning 2.23 og Ligning 2.24 forøges med aftagende α (hurtigere udtørring).

Taleksempel: De ovenfor anførte resultater er behandlet numerisk for det i Figur 2.7 viste radiært indspændte bræt med udtørring fra u = 0.25 til 0.15. De for beregningerne nødvendige parametre er angivet i figuren. Young's modul E_R og relaxationstiden τ_R er skønnede ved en "gennemsnitsfugtighed" på u = 0.2. Krybningsexponenten er b = 0.25.

Resultaterne er vist i Figur 2.8 sammen med den elastiske løsning fra Ligning 2.20. Bemærk, at træets krybning i betydelig grad reducerer risikoen for skadelige udtørringsrevners opståen. Yderligere bemærkes, at svindspændingerne er stadigt aftagende fra t ≈ 120 dage. Til belysning af udtørringshastighedens betydning viser Figur 2.9 supplerende resultater fra en analyse med α = 10 døgn (hurtigere udtørring).

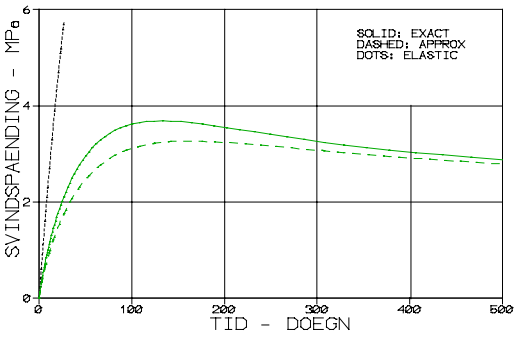

Figure 2.8. *Svindspænding ved udtørring af fastholdt bræt.* α *= 60 døgn.*

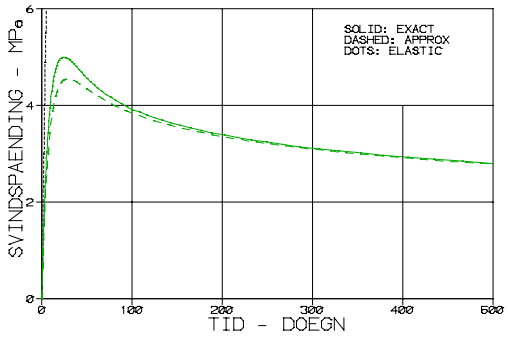

Figure 2.9. *Svindspænding ved udtørring af fastholdt bræt.* α *= 10 døgn.*

3. VISCOELASTIC COMPOSITES

The elastic-viscoelastic analogy explained in Chapter 2 is now utilized to generalize the elastic results presented in Chapter 1 on composite materials such that viscoelastic composites can also be considered. This means that creep functions, relaxation functions, internal stresses, and eigenstress/strain phenomenons of composite materials with various geometrical configurations can be predicted from known viscoelastic properties of the constituent phases.

3.1 Accurate analysis

Den tidligere nævnte e-v-analogi for homogene viskoelastiske materialer kan også anvendes i analyser af viskoelastiske kompositmaterialers adfærd. Omfanget af matematik er mere end fordoblet, idet der nu er to fasers E-moduler, der skal erstattes med tilsvarende viskoelastiske operatorer (46,35) - også i geo-funktionen (θ), der med shape functions (μ_P,μ_S) tilgodeser geometrien i det betragtede kompositmateriale.

Vi vælger at gennemføre kompositanalyserne på grundlag af den simple e-v-analogi beskrevet i Afsnit 2.3.3. Som før tabes der ikke noget principelt herved. Resultaternes nøjagtighed skal vurderes som for den simple e-v-analogis anvendelse på homogene materialer: "Gode estimater".

3.2 Approximate analysis

An approximate stress/strain analysis of viscoelastic materials can be made by the well-known E^{EFF}-method (47) previously considered which tells that a solution to a viscoelastic problem can be obtained from the corresponding elastic solution only by replacing Young's modulus with an effective Young's modulus expressed by the reciprocal creep function, $E^{EFF} = 1/C(t)$. It has been discussed that the E^{EFF}-method is best if $1/C(t) \approx R(t)$ applies for the material considered (as for "Power Law materials" with creep powers $b < 1/3$) - and if stress increases monotonically like the creep function or decreases monotonically like the relaxation function. In composite analysis similar conditions must be required. Then

3.2.1 Creep and relaxation of composite

$$C(t) \approx \frac{1}{R(t)} \approx \left[E\left(c,\theta^{EFF}E_P^{EFF},E_S^{EFF}\right)\right]^{-1} \quad with \tag{3.1}$$

$$E = E(c,\theta,E_P,E_S) \quad (Tables\ 1.1\ and\ 1.2)$$

Important: It is important to remember that the Young's moduli in the geo-function must also be replaced by their effective quantities, such that θ becomes θ^{EFF}.

3.2.2 Internal stresses from external load

$$\textit{Viscoelastic } \sigma_I \approx \sigma_I\left(c,\theta^{EFF},load,E_P^{EFF},E_S^{EFF}\right) \quad (I = P,S) \quad \textit{with}$$
$$\textit{elastic } \sigma_I = \sigma_I(c,\theta,load,E_P,E_S) \quad (\textit{Tables } 1.1 \textit{ and } 1.2) \tag{3.2}$$

3.2.3 Eigenstress/strain

$$\textit{Viscoelastic } \lambda \approx \lambda\left(c,\theta^{EFF},\lambda_P,\lambda_S,E_P^{EFF},E_S^{EFF}\right) \quad \textit{with}$$
$$\textit{elastic } \lambda = \lambda(c,\theta,\lambda_P,\lambda_S,E_P,E_S) \quad (\textit{Tables } 1.1,\ 1.2, \textit{ and } 1.3) \tag{3.3}$$

$$\textit{Viscoelastic } \rho_I = \rho_I\left(c,\theta^{EFF},\lambda_P,\lambda_S,E_P^{EFF},E_S^{EFF}\right) \quad (I = P,S) \quad \textit{with}$$
$$\textit{elastic } \rho_I = \rho_I(c,\theta,\lambda_P,\lambda_S,E_P,E_S) \quad (\textit{Tables } 1.1,\ 1.2, \textit{ and } 1.3) \tag{3.4}$$

3.2.4 Examples

Some applications are presented in this section which demonstrate the analysis of viscoelastic composites by means of the approximate e-v-analogy.

Hardened cement concrete

A mature concrete (W/C = 0.4, c = 0.7, E_S = 32000 MPa, E_P = 55000 MPa) is considered. How does this material creep, and how does it shrink when it is subjected to drying which causes the HCP to shrink according to the following expression with λ_S^{1000} = -2.6 o/oo.

$$\lambda_S = \frac{\phi}{\phi^{1000}}\lambda_S^{1000} \qquad \textit{shrinkage of HCP} \tag{3.5}$$

We assume that the aggregate phase does not creep or shrink. HCP creeps according to Equation 2.11 with ϕ^{1000} = 5. The problems are solved as indicated in Equations 3.1-3.4 using the elastic solutions from Table 1.4 with the following effective Young's modulus and effective stiffness ratio.

$$E_S^{EFF} \approx \frac{E_S}{1 + \phi} \;;\quad n^{EFF} = n(1 + \phi) \tag{3.6}$$

The results of the analysis are shown in Figures 3.1 - 3.3.

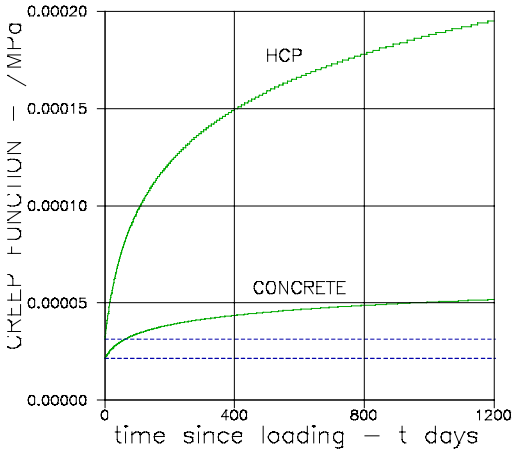

Figure 3.1. *Creep of HCP and concrete loaded at t_o = 28 days.*

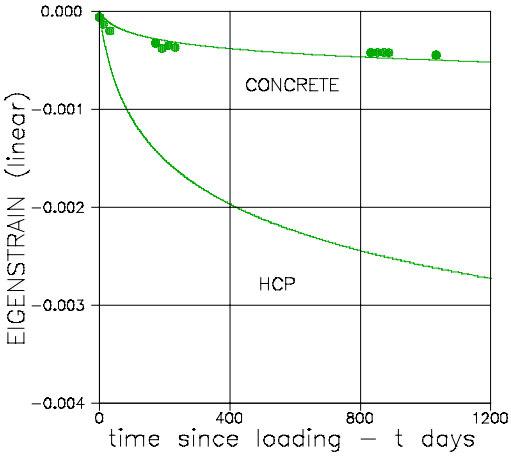

Figure 3.2. *Shrinkage of HCP and concrete from the age of t_o = 28 days.*

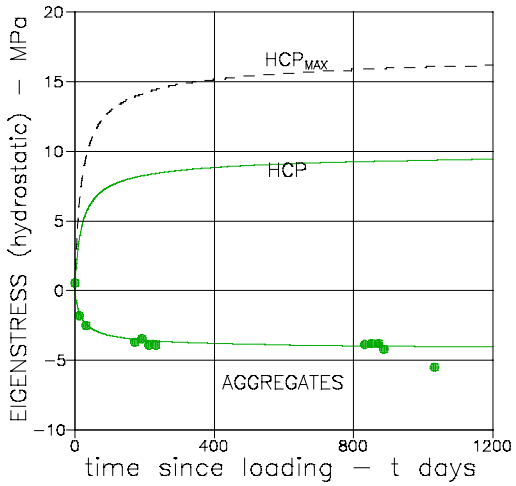

Figure 3.3. *Stresses in concrete caused by shrinkage from the age of t_o = 28 days.*

Shrinkage of concrete versus stress in aggregates were studied experimentaly in (48). The concrete used and the test conditions applied were similar to those considered in this example. The experimental results obtained are shown by dots in Figures 3.2 and 3.3. A very satisfactory agreement is observed between theoretically and experimentally obtained data.

It is of special interest to notice from Figure 3.3 that a tangential tensile stress of ≈ 16 MPa developes in the HCP close to the aggregates. Whether or not this stress will cause cracking of the HCP calls for a special strength analysis, see Section 5.5.

Remark: It is recalled from Section 2.2.3(HCP) that the underlying viscoelastic model for cement pastes considered in this section is valid for ages > 2-3 weeks. This time limit of validity applies of course also for the concrete results presented. Quite recently a complete composite computer-analysis of aging concretes at any composition, at any age of loading > 10 hours, and at any degree of hydration is presented in (49,50).

Rheology of polymer composites versus geometry

Two viscoelastic composites are considered. They are identical except for geometry. One composite (A) is a particulate (TROC) composite made of discrete, almost spherical phase P particles in a continuous phase S, see Figure 3.4. The other composite (B) is a so-called CROSS-material made of a continuous regular phase P frame work in a continuous phase S, see Figure 3.5.

The geometries are quantified as follows,

Composite A: DC-DC (TROC) with $(\mu_P^o, \mu_S^o, c_P) = (1, -1, \infty)$, $c = 0.5$
Composite B: CC-CC (CROSS) with $(\mu_P^o, \mu_S^o, c_P) = (0.75, 0.25, 1.5)$, $c = 0.5$

Both phases are Power Law viscoelastic with the following parameters,

Phase S: $E_S = 30000$ MPa, $\tau_S = 15$ days, $b_S = 0.3$
Phase P: $E_P = 70000$ MPa, $\tau_P = 10^{10}$ days, $b_P = 0.3$

The questions are, how does composite geometry influence creep, relaxation, and internal stresses of composites made of polymer P mixed with polymer S.

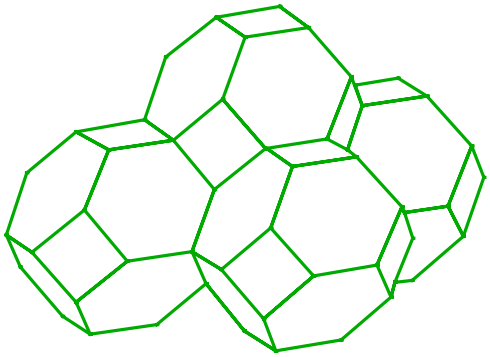

Figure 3.4. *TROC-composite. Stacked TROC composite elements with centrally placed particles of similar shapes.*

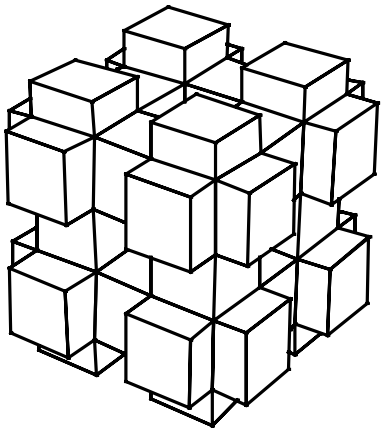

Figure 3.5. *CROSS-composite. 3D-grids of continuous P and S phases. As illustrated, c = 0.5.*

We notice that both phases P and S exibit Power law creep with b_S and $b_P < 1/3$. This means that the approximate e-v-analogy is fully justified to be used to solve the problems. The solid and dashed line solutions in Figure 3.6 show creep and relaxation functions obtained in this way. It is noticed that the results are very close to the exact solutions (otherwise calculated) indicated by dots.

We may now proceed determining the internal stress state of the composite by the simple analogy. The results presented in Figure 3.7 are internal stresses caused by a constant external load σ.

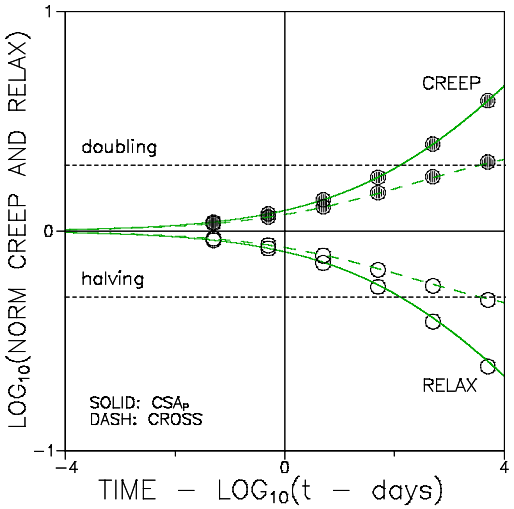

Figure 3.6. *Influence of phase geometry on creep and relaxation for composites defined in text. Open and closed circles indicate accurate analysis.*

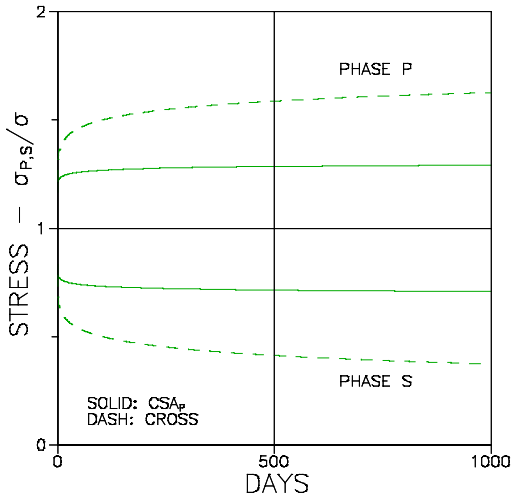

Figure 3.7. *Influence of phase geometry on internal creep stresses in composites described in text.*

Important: It is noticed that the viscoelastic behavior of composites is very much influenced by composite geometry. In round figures the following consequences are observed of changing the geometry of phase P from being spherical to become a continuous network:

- normalized creep function (E*C(t)) decreases with 60%
- normalized relaxation function (R(T)/E) increases with 150%
- phase P stress increases with 30%
- phase S stress reduces with 60%

4. STYRKE

Perfekte, homogene materialer, d.v.s. materialer, der er ensartet og fejlfrit opbyggede ned i den mindste mikrostrukturelle detalje, har meget store styrker. Disse såkaldte teoretiske styrker kan ofte beregnes udfra kendskab til struktur og interatomare kræfter i materialet. Et simpelt eksempel på, hvordan den teoretiske styrke af krystallinske materialer kan forudsiges, vil blive givet i afsnit 4.1.

Det er vigtigt at understrege, at den teoretiske styrke kun kan opnås i meget perfekte (ideale) materialer, der er homogene helt nede fra det atomare niveau. Reproduktionen af egenskaber til mere realistiske materialer, som f.eks. træ, må bestemmes ad anden vej. Det vil sige, under anvendelse af kontinuum-fysiske metoder, der kan kvantificere den - ofte betydelige egenskabsmodifikation, der skyldes tilstedeværelse af medfødte defekter eller tilførte fejl som for eksempel knaster henholdsvis svindrevner i træ. Det vises i afsnit 4.2, hvordan relativt enkle energibetragtninger kan give værdifulde oplysninger om styrkereduktionen i revnede materialer. Knaster i træ kan analogiseres til revner med en længde lig knastens diameter.

I Afsnit 4.3 diskuteres nogle styrkebestemmende materialekonstanter. I Afsnit 4.4 behandles styrken af porøse materialer i relation til stivheden af sådanne materialer.

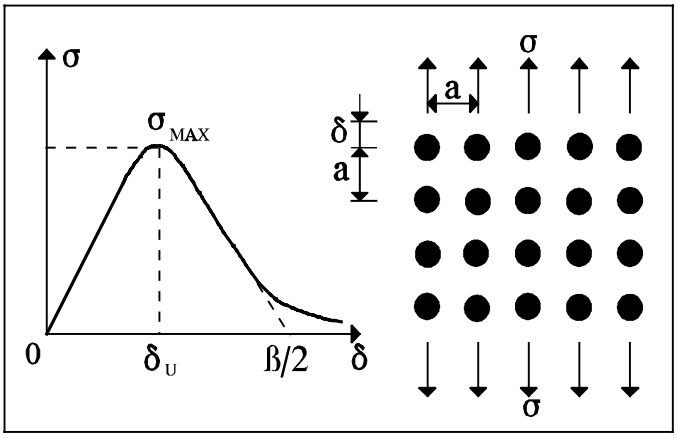

Figur 4.1. *Relation mellem spænding og deformation ved adskillelse af naboatomplaner i krystallinsk materialer.*

4.1 Teoretisk Styrke

Figur 4.1 viser relationen mellem spænding og deformation af atomafstanden, a, i et perfekt krystallinsk materiale. Analytisk kan den viste sammenhæng gives følgende tilnærmede beskrivelse,

$$\sigma \approx \sigma_{MAX} \sin\left(\frac{2\pi\delta}{\beta}\right) = \sigma_{MAX} \sin\left(\frac{2\pi a}{\beta}\varepsilon\right) \tag{4.1}$$

hvor tøjningen $\varepsilon = \delta/a$ og β er en "bølgelængde", der bestemmes ved at udtrykke, at den energi, der medgår til at skabe to nye overflader ved brud er lig 2 gange overfladeenergien, Ω, og lig arealet under arbejdslinien. Vi får

$$2\Omega = \int_0^{\beta/2} \sigma_{MAX} \sin\left(\frac{2\pi\delta}{\beta}\right) d\delta \quad \Rightarrow \quad \beta = \frac{2\pi\Omega}{\sigma_{MAX}} \tag{4.2}$$

Et udtryk for den maximale spænding, den teoretiske brudspænding, kan opstilles ved at udnytte, at arbejdsliniens begyndelsestangent definerer materialets elasticitetskoefficient, E (Young's modul); det vil sige,

$$E = \frac{d\sigma}{d\varepsilon}[\varepsilon = 0] = \sigma_{MAX}\frac{2\pi a}{\beta} \quad \Rightarrow \quad \sigma_{MAX} = \frac{E\beta}{2\pi a} \tag{4.3}$$

Ligningerne 4.2 og 4.3 medfører følgende udtryk for materialets teoretiske styrke,

$$\sigma_{MAX} = \sqrt{\frac{E\Omega}{a}} \tag{4.4}$$

Størrelsesordenen af den teoretiske styrke, σ_{MAX}, og overfladeenergien, Ω, kan udledes af ovenstående udtryk ved at nyttiggøre (andres teoretiske undersøgelser), at max spænding forekommer ved $\delta = \delta_U \approx 0.25a$. Det vil sige, at $\beta \approx a$. Vi får herefter

$$\sigma_{MAX} \approx \frac{E}{2\pi} \approx \frac{E}{10} \quad ; \quad \Omega \approx \frac{Ea}{4\pi^2} \approx \frac{Ea}{50} \tag{4.5}$$

Den teoretiske styrke som udtrykt ved Ligning 4.5 anvendes normalt som et første skøn af materialers (også ikke-krystallinske materialers) assymptotiske styrke, der kun kan opnås på meget tynde materialeenheder, fabrikerede og anvendte under ekstremt velkontrollerede forhold. I Tabel 4.1 er givet nogle eksempler på maksimale styrker, der i dag er opnået på "rene" materialer. Ofte er det således, at jo nærmere et materiales styrke kan drives til den teoretiske værdi, desto skørere er det. Det vil sige, at brud indtræder med aftagende, varslende plastiske deformationer. Der er dog undtagelser herfra, bl.a. en del plastmaterialer.

I reelle materialer (større enheder, grovere produktion, ikke så veldefinerede produktionsomstændigheder) bliver styrken ofte reduceret med en faktor 5 - 100 i

forhold til den teoretiske styrke. En forklaring herfor gives gennem brudmekanikken i det følgende afsnit.

	E/σ_{MAX}
Stål (pianotråd)	70
Jernwiskers	25
Kulfibre	100
Glasfibre	30
Mineraluld	100
Asbestfibre	70
Sisal	40
Bomuld	10
Polypropylenfibre	10
Silicafibre	4
NaCl-whiskers	40

Tabel 4.1. *Eksempler på Young's modul i forhold til styrke*

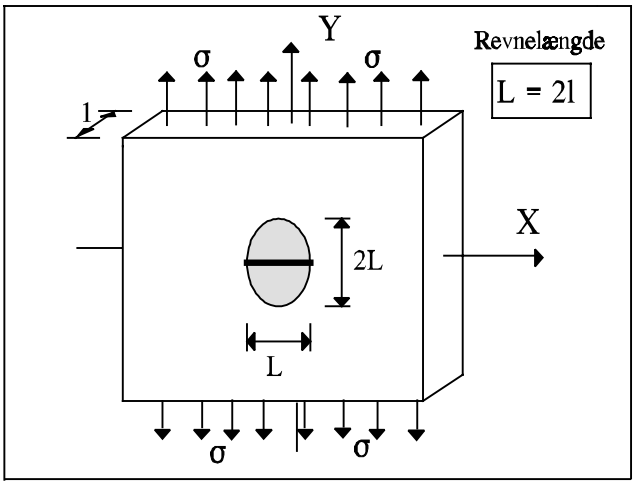

Figure 4.2. *Tunnelrevne i midten af en uendelig stor skive, belastet i det fjerne med en jævnt fordelt spænding vinkelret på den plan, hvori revnen ligger.*

4.2 Reel styrke - brudmekanik

Vi ønsker at bestemme styrken af et revnet materiale. Til dette formål betragter vi først den i Figur 4.2 beskrevne model af et elastisk materiale forsynet med en centralt placeret enkeltrevne. I afsnit 4.2.2 vises, hvordan styrkeløsningen til enkeltrevnesystemet lader sig generalisere til også at gælde multi-revnede materialer.

Energitætheden w (tøjningsenergi per volumenenhed) i materialemodellen i Figur 4.2 kan før revnen placeres udtrykkes som anført i følgende ligning.

$$w = \frac{1}{2}\frac{\sigma^2}{E} \tag{4.6}$$

Ved skæring af en revne i skiven frigøres en tøjningsenergi, svarende til det areal revnen afskygger. Vi skønner gennem "strømlinie" betragtninger, at dette areal vil være ellipseformet som vist skraveret i Figur 4.2. Den frigjorte tøjningsenergi er arealet gange den lige angivne energitæthed

$$W = \frac{1}{2}\frac{\sigma^2}{E}\frac{\pi L^2}{2} \quad \Rightarrow \quad \Gamma = \frac{dW}{dL} = \frac{\pi L\sigma^2}{2E} = \pi l\,\frac{\sigma^2}{E} \tag{4.7}$$

hvor L = 2l er revnens totallængde. Det sidste led giver tillæg af frigjort tøjningsenergi, dW, ved en udvidelse, dL, af revnen - med andre ord, frigjort energi per fladeenhedsudvidelse af revnen (skiven har tykkelsen 1). Denne størrelse, Γ, kaldes tøjningsenergihastighed (eng. strain energy release rate). Ligning 4.7 kan omskrives som vist i Ligning 4.8, der samtidigt definerer den alternative revneparameter K kaldet spændingsintensitetsfaktoren (eng. stress intensity factor). Spændingsintensitetsfaktoren kan vises at bestemme materialespændingen vinkelret på revneplanen ved $\sigma_Y = K/\sqrt{(\pi r)}$ gældende for små afstande r fra revnespidsen.

$$K = \sqrt{E\Gamma} = \sigma \sqrt{\pi l} \tag{4.8}$$

4.2.1 Griffith-styrken (enkelt revne)

Brud indtræder (revnen bliver ustabil), når tøjningsenergihastigheden (under vores udvidelse af revnen) opnår en værdi, der lige netop svarer til 2 gange materialets overfladeenergi Ω, svarende til en kritisk tøjningsenergihastighed på $\Gamma_{CR} = 2\Omega$. Denne energi er nemlig den der skal forbruges til at adskille to atomplaner, således at to nye overfladeenheder kan dannes, se afsnittet om teoretisk styrke. Med andre ord, brud indtræder når frigjort tøjningsenergi netop overskrider den energi, der kan forbruges til dannelsen af de nye overflader. Dette brudkriterium og Ligning 4.8 giver nu den reelle brudstyrke σ_{CR} som følger

$$\sigma_{CR} = \frac{K_{CR}}{\sqrt{\pi l}} \quad ; \quad (K_{CR} = \sqrt{E\Gamma_{CR}}) \tag{4.9}$$

hvor K_{CR} er den såkaldte kritiske spændingsintensitetsfaktor, der ligesom Ω og Γ_{CR} er en materialekonstant. Eksempler på kritiske spændingsintensitetsfaktorer er givet i Tabel 4.2.

Efter sin første "opfinder", Griffith (51)(1920), benævnes udtrykket i Ligning 4.9 ofte Griffith-relationen. Udtrykket forudsiger $\sigma_{CR} \rightarrow \infty$ når $l \rightarrow 0$. Dette kan naturligvis ikke være korrekt. Den reelle styrke kan ikke overskride den teoretiske styrke, σ_{MAX}. Det kan imidlertid vises, at Ligning 4.9 er den korrekte grænseværdi for $\sigma_{CR} \rightarrow 0$, og at udtrykket allerede for $\sigma_{CR}/\sigma_{MAX} \leq 0.4$ er en meget fin tilnærmelse til den såkaldte Dugdale-styrke, Dugdale (52)(1960), der bygger på en ret virkelighedstro modelopfattelse af revnede materialer. Dugdale's model forudsiger, at revnespidsspændingen er endelig og lig den teoretiske styrke σ_{MAX}. Et nærmere studium af Dugdale løsningen (53) viser, at denne som en meget fin tilnærmelse kan formuleres ved det første udtryk i Ligning 4.10, der danner grundlaget for den i Figur 4.3 illustrerede relation mellem de to bæreevner.

K_{CR} [kPa√m] for revneåbning	
Træ (⊥ fibre)	350
Stål (alm. blødt)	100000
Stål (højværdigt)	200000
Granit	3000
Nylon	3000
Mørtel og beton	200
Is	150
Epoxy	400
Glas	800
Porcelæn	1100

Table 4.2. *Eksempler på kritiske spændingsintensitetsfaktorer (størrelsesordner).*

Bemærk at Ligning 4.10 i Figur 4.3 er repræsenteret ved det såkaldte styrkeniveau FL = σ_{CR}/σ_{MAX}, der er et mål for materialekvaliteten. Den introducerede parameter d er en såkaldt karakteristisk mikrostrukturel dimension (54,55). For træ er er d i (55) skønnet ved den logaritmiske middel af en fibers dimensioner: d ≈ $(3*0.03)^{0.5}$ = 0.3 mm.

$$\sigma_{CR} \approx \sigma_L \sqrt{1 - \exp\left(-\frac{d}{l}\right)} \rightarrow \textit{Griffith: } \sigma_L \sqrt{\frac{d}{l}} = \frac{K_{CR}}{\sqrt{\pi l}} \textit{ as } l \rightarrow \infty \qquad (4.10)$$

$$\left.\begin{array}{l}\textit{characteristic micro-}\\ \textit{structural dimension}\end{array}\right\} \quad d = \frac{1}{\pi}\left(\frac{K_{CR}}{\sigma_L}\right)^2$$

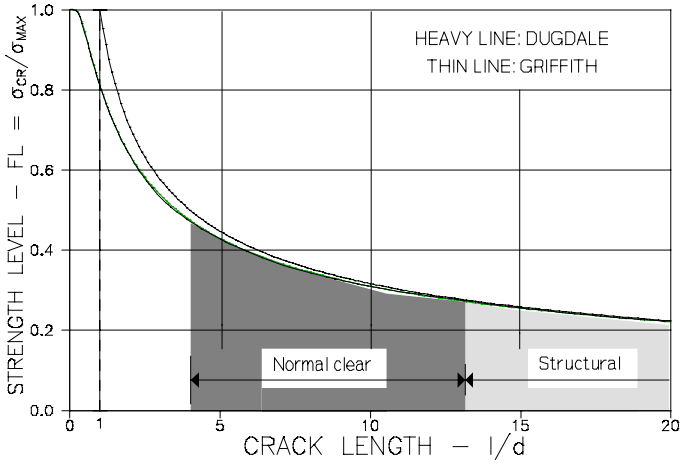

Figur 4.3*. Styrkeniveau (eller materialekvalitet) FL =* σ_{CR}/σ_{MAX} *som funktion af den halve revnelængde l og den karakteristiske mikrostrukturelle dimension d. For træ er d ≈ 0.3 mm. Knastfrit træ og konstruktionstræ ligger i de markerede områder.*

Som tidligere nævnt gælder Griffith bæreevnen egentlig kun for lineært elastiske, skøre materialer. Det kan imidlertid vises, at den meget simple styrkeformel kan anvendes med god tilnærmelse også for mange seje materialer (materialer med flydning). Her skal den kritiske energihastighed, Γ_{CR}, blot inkludere den plastiske energidissipation, der sker omkring revnespidsen ved dannelsen af nye overflader. Samtidig skal σ_{MAX} opfattes som en flydespænding. Vi kan forestille os en effektiv

kritisk energihastighed $\Gamma_{CR,EFF} = 2\Omega + \sigma_{MAX}\delta_{CR}$, hvor δ_{CR} er materialets brudforlængelse ved revnefronten.

Eksempel: Udtørring af træ (fortsat)

Lad os vende tilbage til træeksemplet i afsnit 2.3.3, hvor vi betragtede et træbræt indspændt på tværs af fibrene udsat for udtørring fra u = 0.25 til 0.15. Før udtørringen har vi konstateret enkelte revner af længden 3 mm (l = 1.5 mm = 0.0015 m) i brættet.

Med Ligning 4.9 og K_{CR} = 350 kPa$\sqrt{m}$ fra Tabel 4.2 bestemmes styrken til ≈ 5000 kPa = 5 MPa, hvilket, jævnfør Figur 2.9, netop er tilstrækkeligt til at brættet kan tåle at blive udtørret med en hastighed svarende til α = 10 døgn (se Ligning 2.22). Træet kan altså overleve udtørringsprocessen med sin oprindelige struktur i behold - takket være krybning.

Ved en hurtigere udtørring vil revnen udvide sig, og i værste fald ødelægge træet. En mulighed for overlevelse kan dog findes i det forhold, at revnen, sammen med andre revner, udvider sig til en længde, der reducerer træets stivhed og dermed svindspændingerne til et holdbart niveau. Men overlevelsen sker da på bekostning af stivhed og styrke. Eksemplet belyser problematikken omkring udtørring af træ. Har vi tid (råd) til at udtørre langsomt kan vi få højværdigt træ. I modsat fald må vi affinde os med lavere kvaliteter.

4.2.2 Reel styrke versus teoretisk styrke

I forhold til den teoretiske styrke (Ligning 4.4) kan den reele styrke (Ligning 4.9 med $\Gamma_{CR} = 2\Omega$) skrives som anført i Ligning 4.11. Igen er a og L = 2l atomafstand henholdsvis total revnelængde.

$$\frac{\sigma_{CR}}{\sigma_{MAX}} = \sqrt{\frac{2a}{\pi l}} \approx \sqrt{\frac{a}{L}} \qquad (4.11)$$

Eksempel: Et materiale har en, for det nøgne øje, usynlig revne af længden 2l = $5*10^{-4}$ cm. Atomafstanden er a ≈ $5*10^{-8}$ cm. Hvad er styrken af det revnede materiale i forhold til den maksimalt opnåelige styrke. Ligning 4.11 giver svaret: Den reelle styrke er reduceret til en hundrededel af den teoretiske.

4.2.3 Multi- og kantrevner

Spændingsintensitetsfaktoren fra Ligning 4.8 for et enkeltrevnesystem under simpel belastning kan i mange tilfælde generaliseres til multirevnesystemer som vist i Ligning 4.12. Intensitetsfaktoren modificeres under anvendelse af en såkaldt

interaktionsfaktor F, der tager hensyn til revners indbyrdes placering, afstand til materialekanter samt andre belastningsformer. Brud indtræder ved $\sigma = \sigma_{CR}$, når den modificerede intensitetsfaktor har opnået den kritiske værdi, der gælder for det betragtede materiale.

$$K = \sigma\sqrt{\pi l} * F \quad \Rightarrow \quad \sigma_{CR} = \frac{K_{CR}}{\sqrt{\pi l}} * \frac{1}{F} \tag{4.12}$$

For de simple revnesystemer vist i Figur 4.4 kan faktoren i Ligning 4.13 anvendes med god tilnærmelse. Den resulterende styrke er angivet i samme ligning. Det bemærkes specielt, at en kantrevne af længden l svækker en skive ligeså meget som en central revne af længden 2l.

$$F \approx \left(1 - \left(\frac{l}{b}\right)^2\right)^{-1/2} \quad \Rightarrow \quad \sigma_{CR} = \frac{K_{CR}}{\sqrt{\pi l}} \sqrt{1 - \left(\frac{l}{b}\right)^2} \tag{4.13}$$

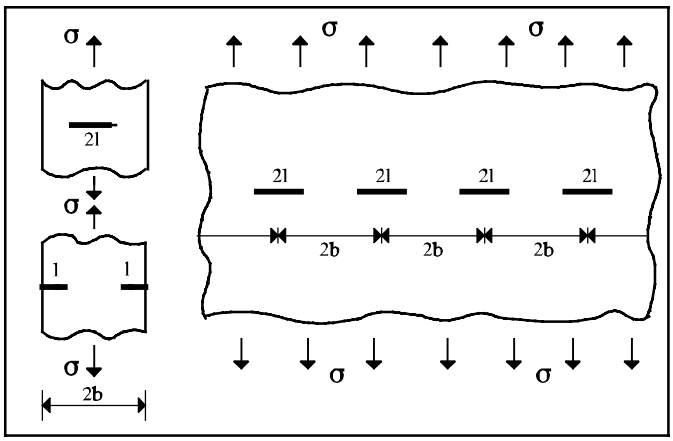

Figure 4.4. *Multirevne- og bæltemodeller. Der kan være flere "revnelag" - blot afstanden mellem dem er > 2b.*

4.2.4 Andre revnesystemer - og prøvning

Der findes en mængde tabelværker (56,57,58,59), hvor spændingsitensitetsfaktorer er bestemt for andre og mere komplicerede revnekonfigurationer end de simple systemer, vi hidtil har betragtet. Et par eksempler på revnekonfigurationer, der ofte anvendes i forbindelse med eksperimentel K-bestemmelse, er vist i Figur 4.5. De tilhørende intensitetsfaktorer er anført i Ligningerne 4.14-4.16.

$$K = 1.12\sigma\sqrt{\pi l}\ f(l/H) \qquad \textit{Bjælkebøjning}$$
$$\sigma = \frac{6M}{H^2} \quad ; \quad f(l/H) \approx \frac{1 - 0.1\ (l/H)^{1/5}}{[1 - (l/H)^2]^{3/2}} \qquad (4.14)$$

$$K = \frac{P}{b}\sqrt{a}\ f(a/b) \qquad \textit{ASTM-prøvning}$$
$$f(a/b) \approx 29.6 - 185.5\frac{a}{b} + 655.7\left(\frac{a}{b}\right)^2 - 1017.0\left(\frac{a}{b}\right)^3 + 638.9\left(\frac{a}{b}\right)^4 \qquad (4.15)$$

$$K = \frac{Eh}{\sqrt{2\pi a}} \qquad \textit{Kiledannet revne} \qquad (4.16)$$

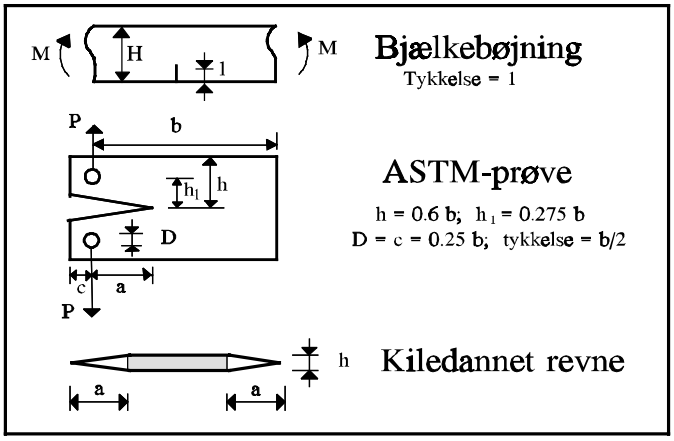

Figur 4.5. *Nogle udvalgte revnekonfigurationer for hvilke spændingsintensitetsfaktorerne er givet i Ligningerne 4.14 - 4.16.*

Compliance calibration equation

En mulighed for eksperimentel bestemmelse af tøjningsenergihastighed og spændingsintensitetsfaktor for revnesystemer i almindelighed findes i den såkaldte 'Compliance calibration equation' (CCE) (ex. 58) vist i Ligning 4.17: Med konstant kraft er energiforskellen mellem et revnet system og det tilsvarende urevnede system den, der skyldes at revnen dannes. Figurerne 4.6 illustrer dette forhold. Figur 4.7 illustrerer hvilke forsøg, der skal udføres forud for CCE's anvendelsen til bestemmelse af spændingsintensistetsfaktorer.

Metoden er noget vanskelig at anvende i reelle (praktiske) eksperimenter, da den kræver meget nøjagtige målinger. Den er til gengæld meget brugbar i computereksperimenter.

$$\frac{1}{2}\frac{P^2}{S} - \frac{1}{2}\frac{P^2}{S_S} = \int_A \Gamma dA \qquad (\textit{Compliance calibration equation})$$

$$\Rightarrow \qquad \Gamma = \frac{1}{2}P^2\frac{d(1/S)}{dA} \qquad or \qquad K = P\sqrt{\frac{E_S}{2}}\sqrt{\frac{d(1/S)}{dA}} \tag{4.17}$$

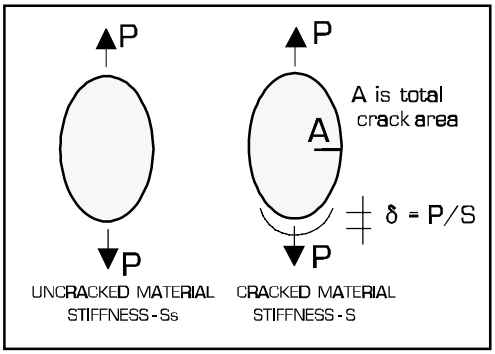

Figure 4.6. *Illustration til belysning af "forsøg", der fører til 'Compliance calibration equation' i Ligning 4.17.*

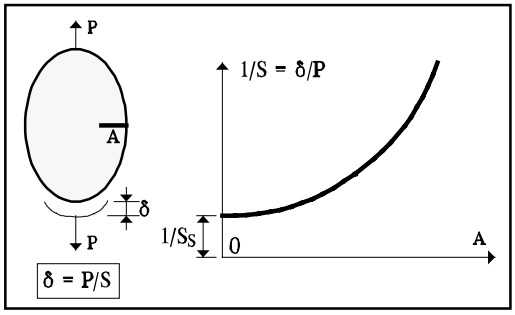

Figure 4.7. *Eksperimentelt underlag til bestemmelse af Γ og K ved hjælp af 'Compliance calibration equation' som beskrevet i Ligning 4.17.*

4.3 Styrkeparametrene som materialekonstanter

Styrkeparametre er en fællesbetegnelse for de to alternative parametre, den kritiske spændingsintensitetsfaktor, K_{CR}, og den kritiske tøjningsenergihastighed, Γ_{CR}, der bestemmer et materiales revnefølsomhed. Styrkeparametrene er materialekonstanter på lige fod med for eksempel Young's modul E. De to parametre er relaterede gennem, $K_{CR} = \sqrt{(E\Gamma_{CR})}$. Brud indtræder, når tilstanden, spændingsintensitet K (eller tøjningsenergihastighed Γ), når sin kritiske værdi gennem forøget belastning.

K_{CR} kan bestemmes ved forsøg på store emner med kendt længde af en centralt placeret enkelt-revne. Den målte styrke og revnelængden samt Griffith's bæreevneformel bestemmer den søgte parameter. Denne metode er meget materialeforbrugene (da revnen skal være lille i forhold til forsøgsemnets dimensioner). Alternativt kan bestemmelsen K_{CR} og Γ_{CR} ske med ASTM's standardopstilling vist i Figur 4.5. K_{CR} angives mest hensigtsmæssigt i dimensionen kPa$\sqrt{}$m eller MPa$\sqrt{}$m. Den alternative parameter, Γ_{CR}, angives normalt i N/m = J/m^2 eller kN/m = kJ/m^2.

4.4 Strength of cracked (and porous) material

The "pore-cracked" material defined in Figures 4.8 and 4.9 has been considered by the author in (60,61). It was found that stiffness and strength of such materials are practically independent of void ratio. The analysis of a porous material with spherical pore-cracks proceeds as follows. We consider a material containing a number of penny cracks of diameters 2l oriented with crack planes perpendicular to load. The cracks are distributed in space such that their centres form a simple cubic lattice with an edge length of 2b.

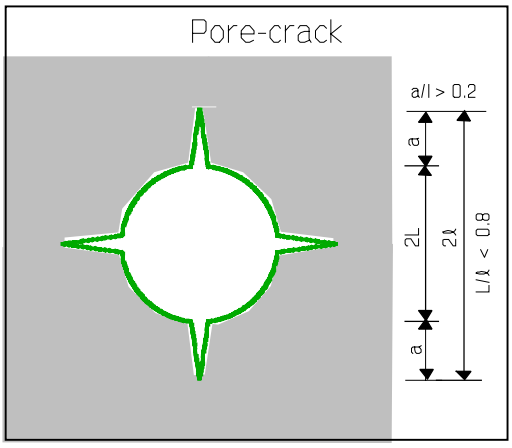

Figure 4.8*. Pore-cracks are spherical or cylindrical voids with concentric cracks crossing at 90°.*

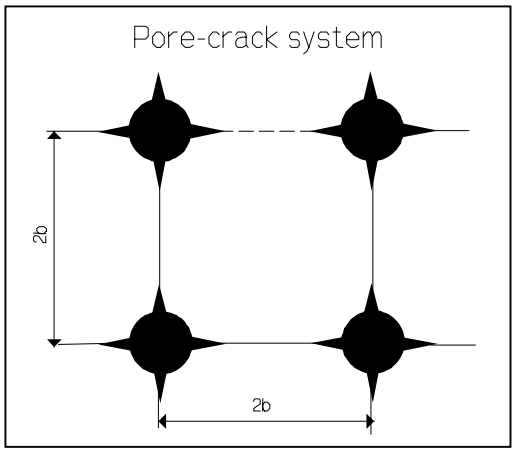

Figure 4.9. *Cubic porous material with pore-cracks. Load is perpendicular to crack plane.*

The stiffness of the pore-crack system can be determined by the following expression developed in (60) from the well-known "compliance calibration equation" explained in Section 4.2.4, and reformulated as shown in Figure 4.10. The abbreviations B, σ, and K mean the total crack area per unit volume, the stress, and the stress intensity factor (not bulk modulus), respectively.

$$\frac{1}{2}\frac{\sigma^2}{E} - \frac{1}{2}\frac{\sigma^2}{E_S} = \int_A \Gamma dA \quad with \quad \Gamma = \frac{K^2}{E_S} \Rightarrow$$

$$\frac{E}{E_S} = \left[1 + 2\int_B \left(\frac{K}{\sigma}\right)^2 dB\right]^{-1} \tag{4.18}$$

When penny cracks especially are considered of density p (number of cracks per vol-unit) we have the following crack area and stress intensity factor. The interaction factor F is estimated by the author from information given in (56,57,58) on a central penny crack in an cylindrical bar.

$$\left.\begin{aligned} K &= \frac{2}{\pi}\sigma\sqrt{\pi l}*F \quad with \quad F = \frac{1}{\sqrt{1-8pl^3}} \\ B &= p\pi l^2 \quad with\ crack\ density \quad p = \frac{1}{8b^3} \end{aligned}\right\} \ Penny\ cracks \qquad (4.19)$$

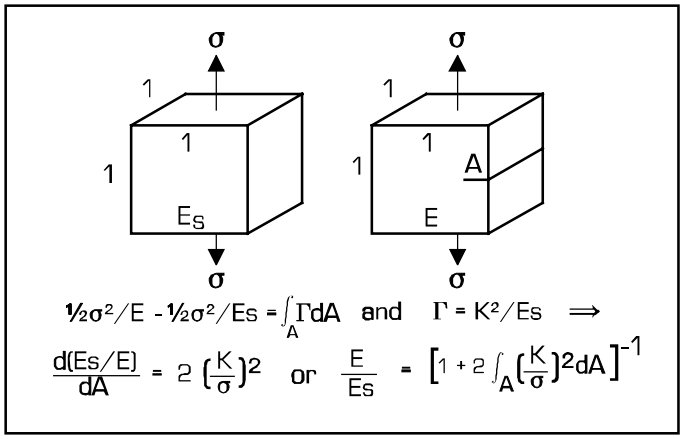

Figure 4.10. *"Compliance calibration equation": Revnet materiales Young's modul som funktion af spændingsintensitetsfaktor K og samlet revneareal A.*

Equation 4.18 can be reduced as shown in Equation 4.20 (former expression) when stress intensity factor is introduced from Equation 4.19. Thus, a relation is established between stiffness of a pore-cracked material and interaction between crack-pores. The strength relation in Equation 4.20 which also involves interaction between crack-pores is obtained as follows: General strength $S = (\pi/2)K_{CR}/ (F\sqrt{(\pi l)}$ comes from Equation 4.12 (latter expression). Reference strength $S_o = (\pi/2)K_{CR}/\sqrt{(\pi l_o)}$ is defined for widely distributed cracks (F = 1) of diameters $2l_o$ at vanishing porosity.

$$\frac{E}{E_S} = \frac{1}{1 + (4/3)\log(F)} \quad ; \quad \frac{S}{S_o} = \frac{\sqrt{l_o/l}}{F} \qquad (4.20)$$

It is *emphasized* that strength S_o at 0 porosity is strength of solid with initial cracks. It is not the strength of a completely clean solid, free of defects.

4.4.1 MOE-MOR

The MOE-MOR relation (modulus of elasticity - modulus of rupture) of the pore-cracked material is obtained by eliminating the interaction factor between stiffness

and strength in Equation 4.20. The result is presented in Equation 4.21 and illustrated in Figure 4.11.

$$\frac{S}{S_o} = \sqrt{\frac{l_o}{l}}\, EXP\left[-\frac{3}{4}\left(\frac{E_S}{E} - 1\right)\right] \quad ; \quad (MOE\text{-}MOR) \tag{4.21}$$

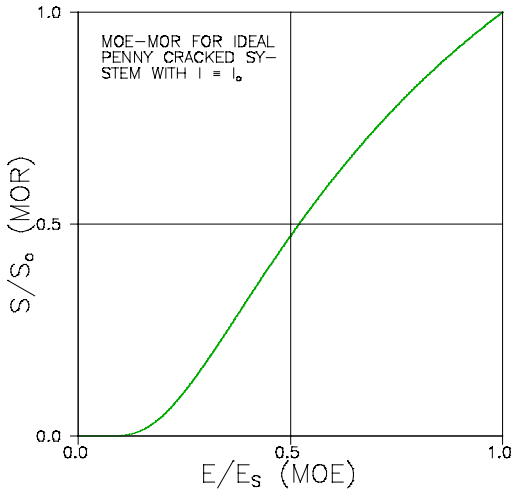

Figure 4.11. *MOE-MOR for system with pore-cracks with* $l \equiv l_o$.

It is emphasized that this equation does include porous systems although it has been developed by crack mechanics. The reason, why has been explained in the introductory remarks to this Section 4.1.

4.4.2 Strength versus porosity

Equation 4.21 is open to use as the basis for relating strength and stiffness of porous materials (61). Approximate strength-porosity relations can be developed by introducing stiffness as predicted in Chapter 1 of this note, meaning

$$\frac{S}{S_o} \approx \sqrt{\frac{l_o}{l}}\, EXP\left[-\frac{3}{4}\left(\frac{1 + c/\mu_P}{1 - c} - 1\right)\right] \quad or$$

$$\frac{S}{S_o} \approx \alpha * EXP\left[-\frac{3}{4}\frac{(1 + 1/\mu_p)c}{1 - c}\right] \quad with \quad \alpha = \alpha(c) = \sqrt{\frac{l_o}{l}} \tag{4.22}$$

It has been shown in (60,61) that this equation is closely related to

$$\frac{S}{S_o} \approx \left(1 - \frac{c}{c_P}\right)^D \tag{4.23}$$

which, formally, is the same expression which predicts stiffness of porous materials, Equation 1.14. It is stated in (61) that Equation 4.23 can be used independently of loading mode (tension, compression, bending). As in Equation 1.14 c_P is critical pore concentration and D is a geometry dependent factor. The influence of geometry on the D factor for stiffness (Equation 1.14) is well documented. It is not that well documented for the strength expression, although serious efforts have been made in (60,61) to do so. For practice the author's guess is that the two D^s have the same orders of magnitudes.

It is very satisfying that Equation 4.23 agrees very positively with the wellknow empirical expressions presented in Equation 4.24 which are based on a huge amount of experimental data compiled in the literature on porous materials (ex. 18). The expressions are suggested by Balshin (62), Hasselman (63), and Ryshkewitch (64,65) with constant parameters A, c_o, and B.

$$\frac{S}{S_o} \simeq \begin{cases} (1 - c)^A & \textit{Balshin} \\ 1 - c/c_o & \textit{Hasselman (strength lost at } c = c_o) \\ EXP(-Bc) \approx 1 - Bc & \textit{Ryskewitch (moderate porosities)} \end{cases} \tag{4.24}$$

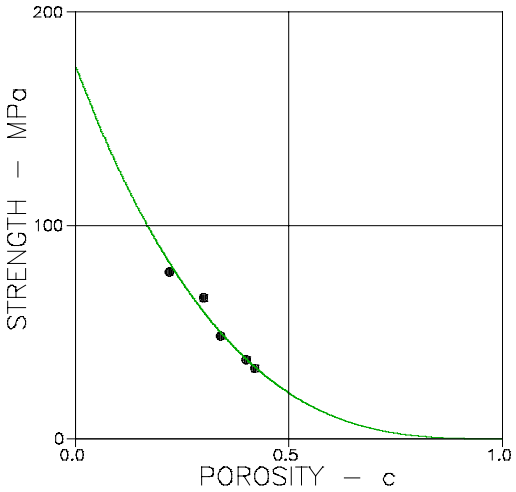

Figure 4.12. *Compressive strength of autoclaved calcium silicate system (66,67). Simple pore system with $c_P = 1 \Rightarrow S_o = 175$ MPa and D = 3.03.*

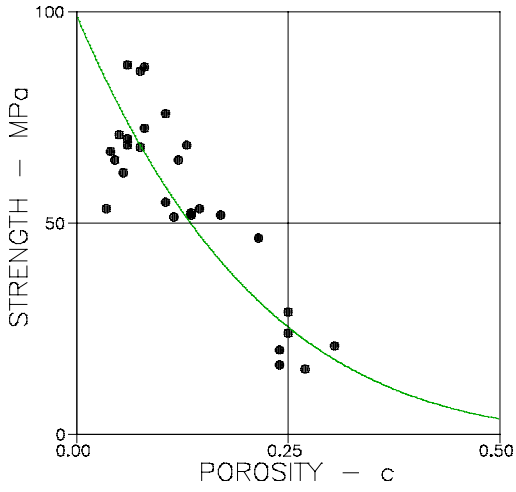

Figure 4.13. *Compression strength of compacted HCP (68). Simple pore system with $c_P = 1 \Rightarrow S_o = 99$ MPa and D = 4.74.*

Equation 4.23 is very easy to handle in practice. The parameters D and the critical concentration c_p can be determined by linear regression of manipulated experimental data as shown in Equation 4.25, optimizing the fit-quality with respect to the critical porosity c_P (which, incidentally, must be close to the same critical porosity as obtained by parallel regression of stiffness data).

$$Y = \log_E(S) \quad ; \quad X = \log_E\left(1 - \frac{c}{c_P}\right) \Rightarrow S_o = EXP(Y_o) \quad ; \quad D = \alpha \qquad (4.25)$$

where Y_o and α are Y−intersection and slope of regression line

Examples

In Figures 4.12 amd 4.13 Equation 4.23 is successfully tested against a number of experimentally obtained strength data reported in (66,67,68). The zero-porosity strengt S_o, the critical concentration c_P and the strength power D have been determined by the linear regression technique explained in Equation 4.25. Another example of establishing strength-porosity descriptions is shown in Figure 4.14. The underlying experimental data presented in Table 4.3 are from tests on tile reported in (69).

c	σ_{CR}(MPa)
0.432	24.5
0.436	22.8
0.435	21.4
0.415	20.1
0.414	25.5
0.418	27.4
0.409	24.9
0.375	26.2
0.381	35.7
0.365	35.6

TABLE 4.3 *Strength of tile.*

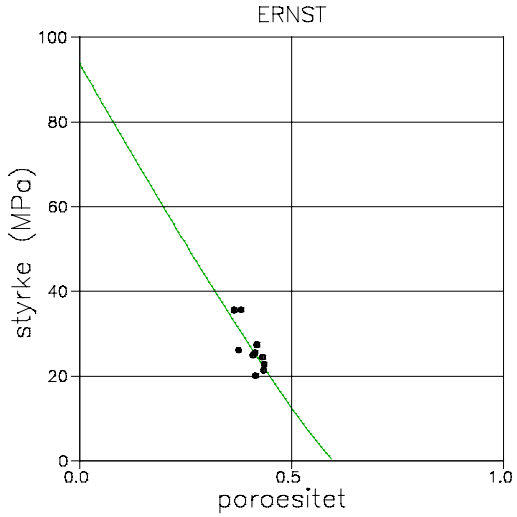

Figure 4.14. *Strength of tile. Regression of the data presented in Table 4.3 gave: $c_P \approx 0.6$, $S_o = 94$ MPa, $D = 1.12$, $r^2 = 0.585$.*

5. MATERIALEMEKANIK - EKSEMPLER

Vi gentager fra indledningen: I almindelighed kan materialers adfærd ikke forklares alene ved hjælp af en enkelt fagdisciplin. Med hensyn til byggebranhens materialer, for eksempel, kan en tilfredsstillende beskrivelse ofte kun opnås gennem en kombineret anvendelse af rheologi, revnemekanik og kompositteori. I dette kapitel gennemgås et par eksempler på, hvordan denne kombination af fagdiscipliner (Materiale Mekanik) kan være nyttig til belysning/beskrivelse af materialers mekanisk/fysiske adfærd.

5.1 Frost i hærdnet cement pasta (HCP)

Vi betragter den samme HCP (Figur 1.15: Empty autoclaved Portland cement/silicate system), som vi anvendte som eksempel i Afsnit 1.2.5. Vi antager, at kapillarporerne er delvist fyldt med vand, der fryser til is. Vi har således et system, hvor fase S er HCP-faststof (gel) og hvor fase P er porøs is.

Geometrien af HCPen er af typen MM-MM som beskrevet ved formfunktionerne $\mu_P = 0.45(1\text{-}c)$ og $\mu_S = 0.45c$, se Figur 1.17, hvormed kompositstivheden er bestemt ved Tabellerne 1.1 og 1.2. Før anvendelse af disse tabeller skal vi imidlertid modificere fase P egenskaberne under hensyntagen til, at kapillarporerene ikke er vandfyldte. Vi modificerer efter Ligning 5.1, hvis informationer er hentet fra (15). (Højre-sidens materialeegenskaber i udtrykkene er faststofegenskaber).

Impregneringsgraden β *er volumen af impregnering i forhold til* det *volumen, der maximalt kan være i poresystemet*.
Porøsiteten i impregneringen, betragtet som udfyldende hele porefasen, bliver $c_i = 1 - \beta$. *Det vil sige, at imptegneringen stivhedsmæssigt kan regnes at virke med*

$$E_P \approx \frac{1 - c_i}{1 + c_i} E_P = \frac{\beta}{2 - \beta} E_P \qquad \text{modificeret stivhed} \tag{5.1}$$

Egentøjningen i "porøse", impregnerende materialer vil også afhænge af β, *således at*

$$\lambda_P \approx \frac{\beta}{5 - 4\beta} \lambda_P \qquad \text{modificeret egentøjning}$$

Vi vil undersøge, hvordan den betragtede HCP opfører sig, når den udsættes for frost med følgende tidsforløb for isens eigenstrain

$$\lambda_P(t) = \lambda_P \frac{t}{t + t_F} \qquad \begin{cases} t \text{ in days since frost initiation at age } t_o \\ t_F \text{ represents rate of frost action} \end{cases} \tag{5.2}$$

Den mekaniske opførsel af HCPen beregnes efter Tabel 1.3 og Afsnit 3.2.3 under hensyntagen til, at materialet kryber efter Ligning 2.11.

Resultaterne, illustreret i Figurerne 5.1 og 5.2, forudsætter: HCP har E_S = 32000 MPa og krybning ϕ^{1000} = 3. Kapillarporøsiteten er c = 0.2. Impregneringsgraden er ß = 0.5. Fast is har E_P = 10000 MPa og lineær egentøjning λ_P = 0.03. Frostbegyndelse er t_o = 28 døgn. Frysehastighed er t_F = 10 dage.

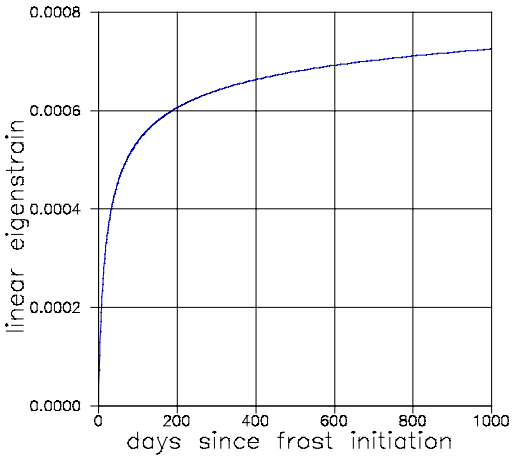

Figure 5.1. *Udvidelse under isdannelse af den betragtede HCP.*

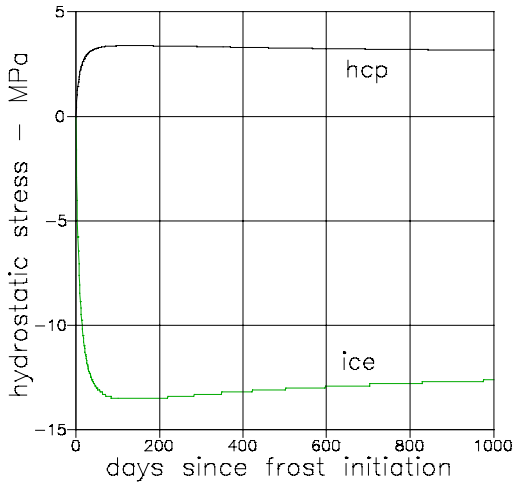

Figure 5.2. *Indre spændinger i den betragtede, frostpåvirkede HCP.*

5.2 Materialers levetid - simpel analyse

En analyse af den mekaniske levetid for et viskoelastisk materiale kræver en kombination af rheologi og brudmekanik. Materialemodellen, der anvendes i nedenstående beregninger svarer til den i Figur 4.2 viste, hvor revnen L = $2l_o$ er en typisk dominerende fejl i materialet. Viskoelastisk regnes materialet at krybe som træ, polymerer og keramiske materialer (Power law creep). Levetiden er naturligt opdelt i to faser. Den første fase omhandler tiden t_S (start) til begyndende revneudvidelse (materialet begynder at knage). Revnelængden i denne fase, og dermed styrken, er konstant mens revnefronten på grund af krybning åbner sig mod en kritisk værdi. Den anden fase omhandler tiden fra t_S til t_{CAT}, hvor det endelige (katastrofale) brud indtræder. Revnen ekspanderer med fastholdt (kritisk) revnefront mod en kritisk længde, der netop nås til t = t_{CAT}.

Det vises efterfølgende hvordan den første fase kan analyseres på simpel måde ved hælp af resultater tidligere fremført i rapporten. Beregningerne i forbindelse med den anden fase er for komplicerede til at de kan retfærdiggøres inden for dette kursus målsætninger. Der henvises til (70).

Vi anvender den simple e-v-analogi som den er fremført i Afsnit 2.3.3. Det vil sige, opskriv først den elastiske løsning på det betragtede problem. Det vil her sige styrken som bestemt i Afsnit 4.2.1,

$$\sigma_{CR} = \frac{K_{CR}}{\sqrt{\pi l}} = \sqrt{\frac{E\Gamma_{CR}}{\pi l}} \tag{5.3}$$

Erstat Young-modulen (E) i denne løsning med den effektive Young's modul $E^{EFF} = R(t)$. Herved fås

$$\sigma_{CR}(t) = \sqrt{\frac{E^{EFF}\Gamma_{CR}}{\pi l}} = \sqrt{\frac{E}{1 + (t/\tau)^b}\,\frac{\Gamma_{CR}}{\pi l}} \tag{5.4}$$

der efter normering med hensyn til korttidsstyrken (Ligning 5.4 med t = 0) kan udtrykkes ved

$$\frac{\sigma_{CR}(t)}{\sigma_{CR}} = \frac{1}{\sqrt{1 + (t/\tau)^b}} \tag{5.5}$$

Tiden i dette udtryk er tiden til begyndende revneudbredelse t_S, under den konstante belastning $\sigma_{CR}(t_S)$, kaldet langtidsstyrken. Den søgte "levetid" til begyndende nedbrydning af materialet er nu bestemt ved

$$\frac{t_S}{\tau} = \left(\frac{1}{SL^2} - 1\right)^{1/b} \quad hvor \quad SL = \frac{\sigma_{CR}(t_S)}{\sigma_{CR}} \quad er\ lastniveauet \tag{5.6}$$

For træ skal relaxationstiden i ovenstående udtryk indsættes svarende til at revneudvidelse sker som en kombination af forskydning og åbning mellem fibre. Den relevante relaxationstid bliver af størrelsesordenen $\tau \approx 1/1000$ af værdien gældende for bjælkebøjning.

Et eksempel på en levetidsanalyse af et viskoelastisk bygningsmateriale (ikke træ) er vist i Figur 5.3. Materialet kryber efter eksponentialudtrykket i Tabel 2.4 med krybningseksponenten b = 1/6. Den analyserelevante relaxationstid er 100 døgn i tør tilstand og 3 døgn i våd tilstand. Resultater vist med stiplede linier er tiden til begyndende brud (Ligning 5.6). Resultater vist med fuldt optrukne linier er tiden til endeligt brud som beregnet efter (70).

Resultaterne fra en fuldstændig levetidsanalyse (til katastrofebrud) efter (70) af knastfrit træ er vist i Figur 5.4. De viste eksperimentelle resultater er fra Madison (71) og fra Krebs (72).

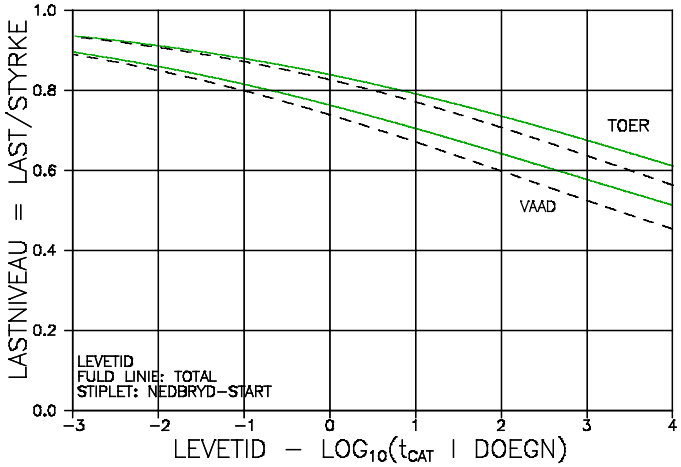

Figur 5.3 *Levetidsanalyse af et bygningsmateriale i tør og våd tilstand. Den stiplede linie er t_S efter dette afsnit. Den totale levetid t_{CAT} er bestemt som angivet i (70).*

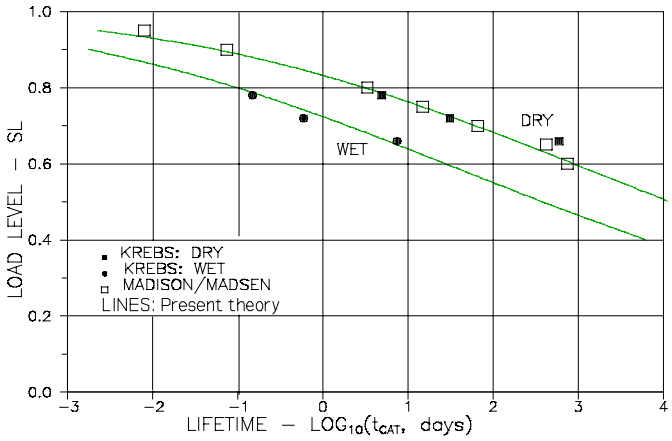

Figur 5.4. *Knastfrit træ - Eksperimentelle levetidsdata fra Krebs: tør (12 %) og våd (> 30 %). Madison: (≈ 10 %). Theoretisk beskrivelse som angivet i (70).*

5.3 Stiffness and thermal conductivity of tile

The following data are from stiffness experiments on bricks (50x50x50 mm), reported in (69),

a) Deduce stiffness (E_S) at 0 porosity, and the geo-parameters (c_P,μ_P^o) from these data. Present graphically, composite stiffness versus porosity.

b) The thermal conductivity of solid tile (at 0 porosity) is Q_S = 0.8 kcal/mh°C. We assume that the voids have Q_P = 0. Present graphically, composite thermal conductivity versus porosity.

The answers to these questions are presented in Figures 5.5 and 5.6a with data predicted by Sections 1.2.6 and 1.5. There are no experimental conductivity results determined in (69). We may, however, compare the theory with such results presented in Figure 5.6b as reported in (73) with Q_S = 0.825 kcal/mh°C. When

the uncertainty on c_P-determination is considered a reasonable agreement is observed between theory and practice.

Porosity (c)	E (GPa)
0.432	6.5
0.436	6.5
0.435	4.9
0.415	6.3
0.414	7.5
0.418	6.0
0.409	9.5
0.375	11.6
0.381	9.2
0.362	8.5
0.365	11.4

***TABLE 5.1**. Stiffness of tile.*

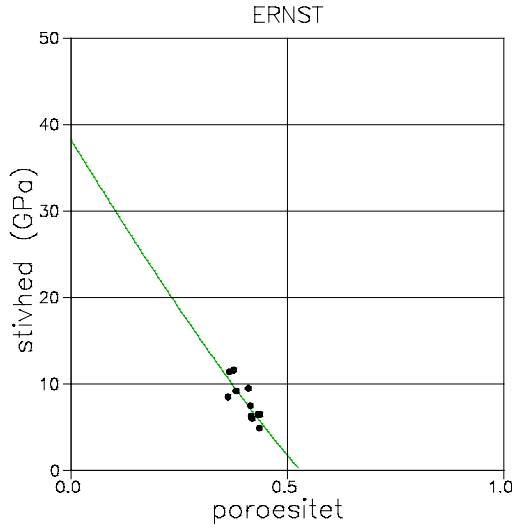

***Figure 5.5.** Stiffness of tile. E_S = 38 GPa, (μ_P^o, c_P) = (0.9, 0.53), r^2 = 0.600.*

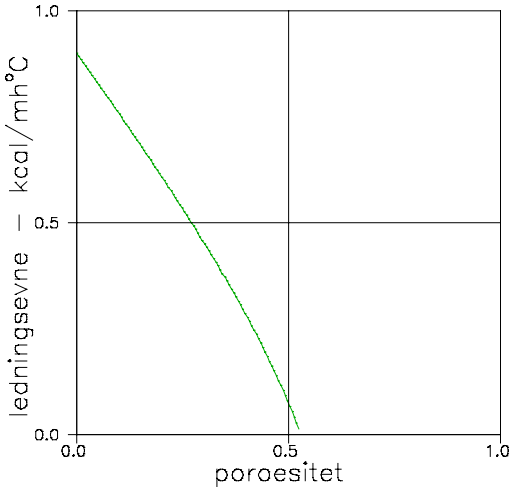

***Figure 5.6a.** Thermal conductivity of the tile considered in this example with geometry (μ_P^o, c_P) = (0.9, 0.53),*

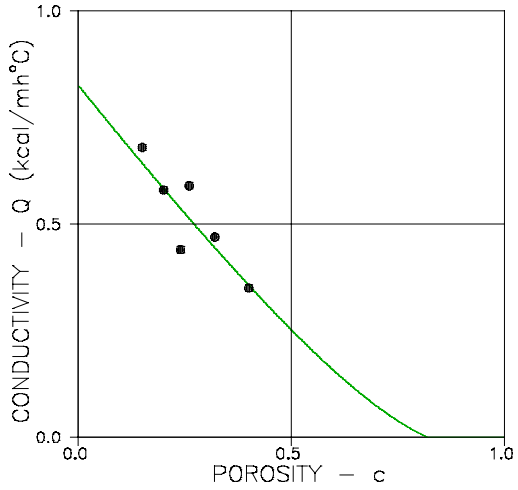

***Figure 5.6b.** Thermal conductivity of firebrick. Geometry: (μ_P^o, c_P) = (1,0.82)*

5.4 Thermal expansion of salt infected tile

The above exercise proceeds as follows

c) The tile becomes salt infected. Salt has a stiffness of E_P = 2220 MPa and a specific thermal expansion coefficient of λ_P = 38e-6/°C. Tile has a solid phase stiffness (E_S) as previously deduced. The critical concentration (c_P) previously deduced is supplemented with a critical concentration of c_S = 0, estimated from Figure 1.14, assuming that pore connectivity (percolation of phase P) starts just at 0-porosity. Its solid

phase specific thermal expansion coefficient is λ_S = 6e-6/°C. Present graphically, specific composite expansion, stress in tile, and stress in salt.

Remark: The symbol ß in Figures 5.7 and 5.8 means degree of impregnation (volume solid salt/pore volume). According to (15) an analysis of impregnated materials can be made introducing an effective phase P stiffness which is E_P = stiffness of solid impregnant multiplied by ß/(2-ß). The experiments referred to in Figures 5.7 and 5.8 are from tests reported in (74) with ß = 0.15-0.25. The stiffness of solid rock salt is 20000 MPa which produces the average E_P = 2220 MPa previously presented as the phase P stiffness. The theoretical data in Figures 5.7 and 5.8 are predicted as explained in Section 1.3.

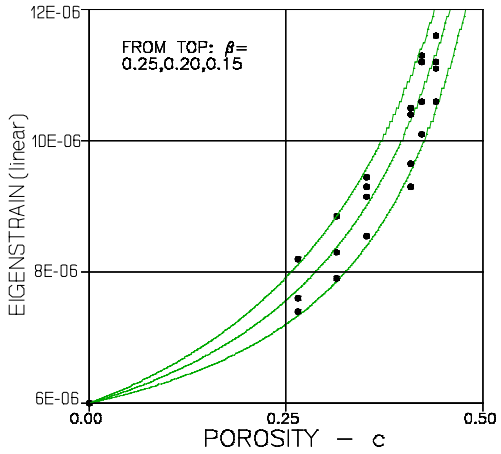

Figure 5.7. *Predicted thermal expansion/C° of salt infected tile. Dots are experimental data.*

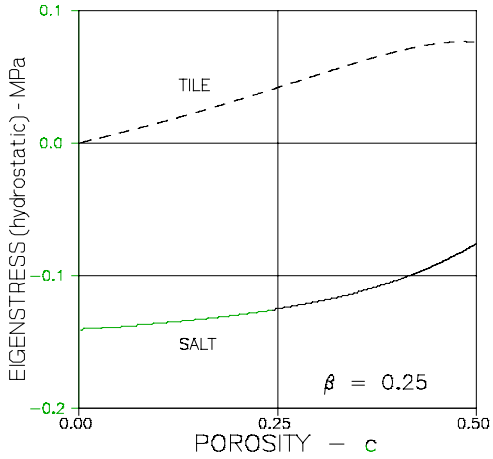

Figure 5.8. *Predicted thermal eigenstresses (/°C) in salt infected brick.*

5.5 Stiffness of concrete and HCP, and strength of HCP

as related to degree of hydration

Composition of HCP and concrete

The volume concentrations presented in Equation 5.7 are of relevance in composite studies of concrete. They are calculated, see (75,76), according to the principles developed by Powers and Brownyard in (77,78). Aggregate, cement, and water are denoted by A, C, and W respectively. W/C is water/cement ratio by weight and A/C is aggregate/cement ratio by weight. The amount of cement hydrated at a certain age (t) relative to the total amount of cement is denoted by the degree of hydration g(t). The description of g(t) presented in Equation 5.7 is suggested by Freiesleben in (79) with characteristic hydration parameters τ and ß.

$$
\begin{aligned}
c &= \frac{38A/C}{100W/C + 38A/C + 32} && \text{aggregate concentration in concrete} \\
c_{TOT} &= \frac{100W/C - 18g(t)}{100W/C + 32} && \text{total porosity of HCP} \\
c_{CAP} &= \frac{100W/C - 38g(t)}{100W/C + 32} && \text{capillary porosity of HCP} \\
g(t) &= \exp\left[-\left(\frac{\tau}{t}\right)^{\beta}\right] && \text{degree of hydration}
\end{aligned}
\qquad W/C \geq 0.38 \qquad (5.7)
$$

Concrete stiffness versus degree of hydration

The stiffness of concrete with W/C > 0.38 can be calculated by Table 1.4 assuming that concrete is a CSA_P composite with an aggregate concentration (phase P) as calculated in Equation 5.7. Young's modulus of HCP (phase S) is age dependent and must be introduced from Equation 5.8 which is based on the author's work in (75) on stiffness and creep of concrete.

$$
\begin{aligned}
E_{BAS} &= 0.85 * 3.2e4 * g(t)\ MPa && \text{static stiffness of basic paste} \\
c_{VOID} &= \frac{W/C - 0.38}{W/C + 0.32} && \text{vol-con of voids in basic paste} \\
E_S &= E_{BAS}\frac{1 - c_{VOID}}{1 + c_{VOID}} && \text{static stiffness of HCP}
\end{aligned}
\qquad (5.8)
$$

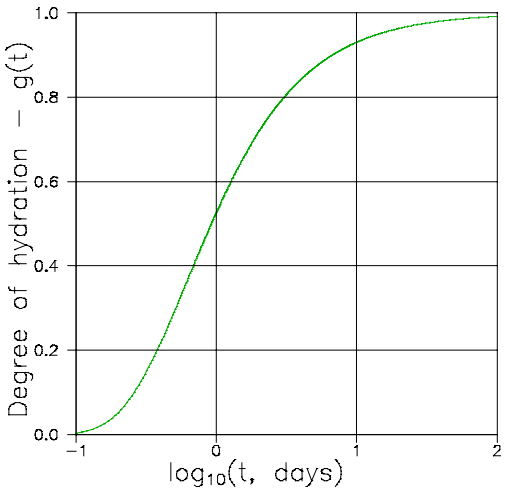

Figure 5.9. *Degree of hydration, g(t), defined by (τ,ß) = (0.625 days,0.95).*

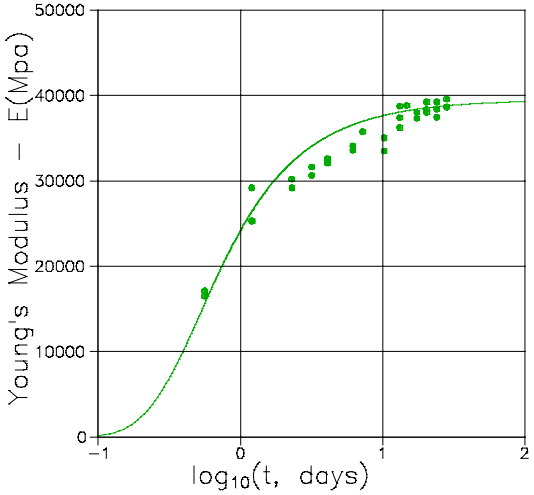

Figure 5.10. *Concrete with (W/C, P/C) = (0.45,5.21), E_P = 50000 MPa, and degree of hydration from Figure 5.9.*

Basic paste (BAS) is defined in (75) as that part of the water-cement system which will hydrate completely. The void concentration, c_{VOID}, in Equation 5.8 is c_{CAP} from

Equation 5.7 with g(t) = 1. Theoretically predicted Young's moduli and experimentally determined moduli from (80) are compared in Figure 5.10. The degree of hydration shown in Figure 5.9 is fitted by Equation 5.7 from experimental data presented in (80).

HCP strength versus degree of hydration

For the sake of curiosity: Based on a number of experimental data it has been shown in (76) that the compressive strength (S) of HCP with W/C > 0.38 can be predicted by the following expression

$$S = \begin{cases} 450(1 - c_{TOT})^{B} \; MPa & at \; c_{TOT} \le 0.78 \\ 0 & at \; c_{TOT} > 0.78 \end{cases} \quad with \; B = \frac{2.35}{[g(t) - 0.19]^{0.45}} \qquad (5.9)$$

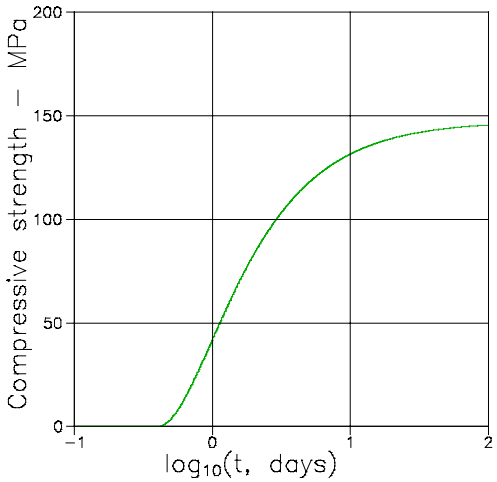

Figure 5.11. *Compressive strength of a HCP with W/C = 0.45 and degree of hydration from Figure C1.*

with total porosity and degree of hydration introduced from Equation 5.7. An example of predicted compressive strength is presented in Figure 5.11. It is interesting to note that the S-expression in Equation 5.9 is exactly as suggested empirically by Balshin in his work (62) on porous materials in general. In Balshin's work, however, there is no restrictions on c_{TOT}, and the exponent B is a constant which has to be determined by experiments. In the present note the exponent B depends on the degree of hydration as indicated in Equation 5.9. This depency can be read as the result of a changing pore geometry. It is noticed that the "Balshin" strength expression in Equation 4.24 is truncated at $c_{TOT} = 0.78$ which tells that the HCP microstructure is unable to carry a finite load at greater porosities. This means that the critical concentration c_p of HCP is close to 0.78.

Remarks: We re-call that ordinary (naturally grown) HCP^s have implicitly been considered in this section with W/C > 0.38. Stiffness and strength expressions, however, are also presented in (75) and (76) respectively which apply for W/C < 0.38. Densified (compacted) HCP systems have been studied by the author in (61). Tensile strength of HCP can be estimated to be ≈ 1/10 of the compressive strength. Ordinary HCP has also been studied by Bentz in (6) using a special com-

puter simulation technique. Concrete is studied by Lokhorst & Breugel (81) using a layered composite model.

Note: Some interesting exercises can be made from this Section 5.5. Examples: Stiffness of concrete and mortar as a function of composition, time, and degree of hydration. Is the assumption acceptable (made by many authors) that stiffness develops proportional to degree of hydration ?. The following rewriting of the former expression in Equation 5.7 might be useful in such analysis.

$$A/C = \frac{c(100W/C + 32)}{38(1 - c)} \quad \begin{cases} \textit{Mortar has } c \approx 0.5 \\ \textit{Concrete has } c \approx 0.75 \end{cases} \tag{5.10}$$

5.6 On swelling and drying of porous material

The feature of interest in this example is: Which orders of magnitudes can be expected for deformation of porous materials subjected to condensation of water from an ambient vapor pressure ϕ. In another formulation: What shrinkage can be expected of the material changing its ambient vapor pressure from ϕ to 0.

It is emphasized that only the aspects of material mechanics are demonstrated. A full shrinkage analysis requires a number of additional information the acchievent of which lays outside the scopes of this note. For example: Amount and distribtion of pore water and pore size distributions. For a complete shrinkage analysis the reader is referred to (26) from which the following "mini analysis" is adapted.

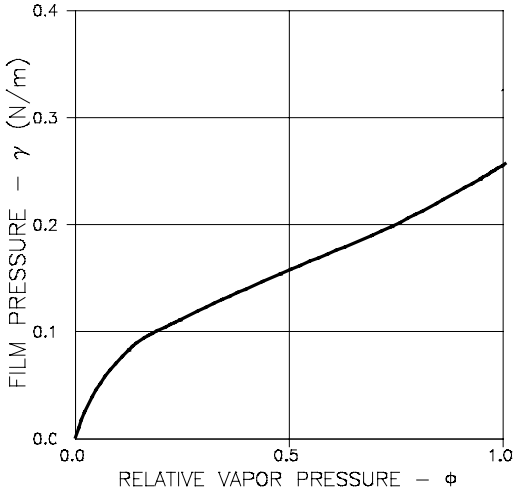

Figure 5.12. *Film pressure on surfaces due to adsorbed water.*

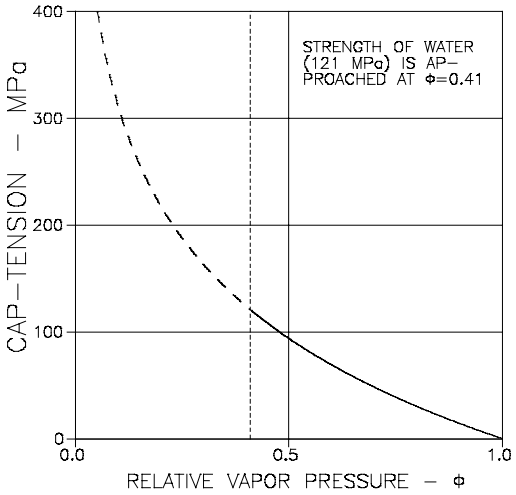

Figure 5.13. *Tension due to capillary condensed water.*

A specific porous material is considered. The material is stored in an ambient vapor pressure of ϕ. Water is condensed as a thin adsorbed film layer on the pore surface and as capillary water in the pore volume. The film pressure shown in Figure 5.12 and the capillary tension shown in Figure 5.13 are the results of a sorption analysis by (26).

The question of interest can be solved by the following expresions adapted from Equation 1.18 in Section 1.3.2. The stiffness expression added is from Equation 1.14 with a constant stiffness power D.

$$\varepsilon = \frac{p}{3K_S}\left(\frac{1}{e} - 1\right) \quad (\textit{shrinkage due to cap-water with pore tension } p)$$
$$\varepsilon = \frac{p}{3K_S} \quad (\textit{swelling due to adsorbed water with pressure } p \textit{ transformed from film pressure } \gamma) \qquad (5.11)$$
$$e = (1 - c)^D \quad \textit{relative stiffness of porous material}$$

Calculationally a film pressure, γ, acting on the pore surface of a porous material can be "transformed" to a hydrostatic pore pressure, p, by the following expression developed from Flood (82).

$$p = \frac{2}{3}\frac{\gamma}{R_{HYD}} \quad \textit{with } R_{HYD} = \textit{hydraulic radius of solid in porous material} \qquad (5.12)$$

In principle this conversion of loading mode is quite familiar with the following well-known phenomenon: Look at a bar with a streched rubber band around it. If the bar has a circular cross section of radius r and the rubber band tension is S, then a pressure of σ = S/r will act on the bar - see Figures 5.14 and 5.15.

The solid phase hydraulic radius can be calculated by the following expression looking at 1 m^3 of the porous material. The solid density is d_S. The pore surface is S_{BET} which is the so-called BET-surface (m^2/kg) experimentally determined.

$$R_{HYD} = \frac{V_S}{S_S} = \frac{1}{d_S S_{BET}} \quad \textit{because}$$
$$V_S = 1 - c = \textit{solid volume}/m^3 \qquad (5.13)$$
$$S_S = (1 - c)d_S S_{BET} = \textit{solid surface}/m^3$$

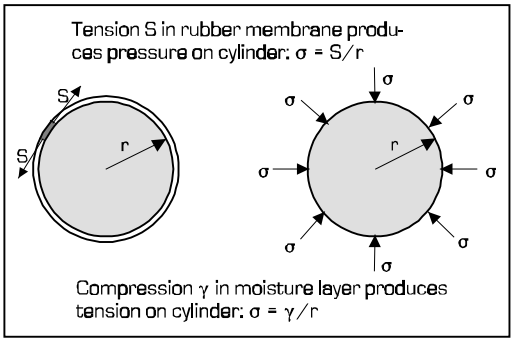

Figure 5.14. *Analogy between pressure on cylinder, caused by stressed rubber membrane and tension on cylinder, caused by film pressure in adsorbed moisture.*

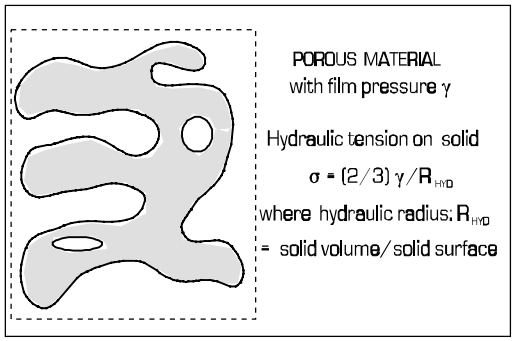

Figure 5.15. *Expansion of porous material due to film pressure on solid surface. Notice that R_{HYD} is hydraulic radius of solid.*

Now the following easy expression will convert a known film pressure to a pore pressure in the porous system considered.

$$p = \frac{2}{3}\gamma d_S S_{BET} \tag{5.14}$$

Example: At a vapor pressure of $\phi \approx 0.5$ a linear swelling of ≈0.2 ‰ is the result of a film pressure of $\gamma = 0.17$ N/m. A linear shrinkage of .1 ‰ is the result of a capillary tension of p = 0.1e6 Pa (a very small amount of capillary water is present at a vapor pressure around 0.5). The material properties applied to obtain these qantities are the following: c = 0.8, D = 2, S_{BET} = 34000 m^2/kg, d_S = 2650 kg/m^3, E_S = 32e9 Pa.

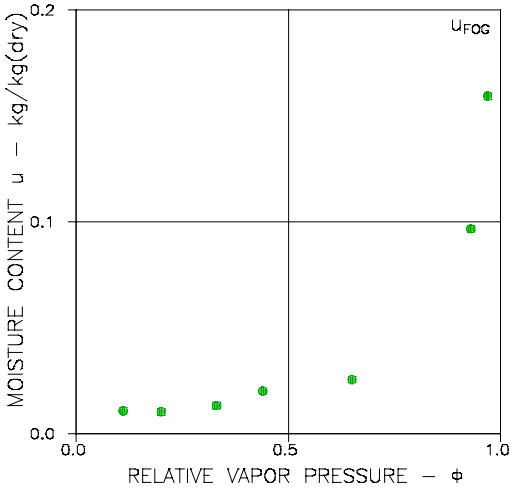

Figure 5.16. *Data from sorption tests on a cellular concrete.*

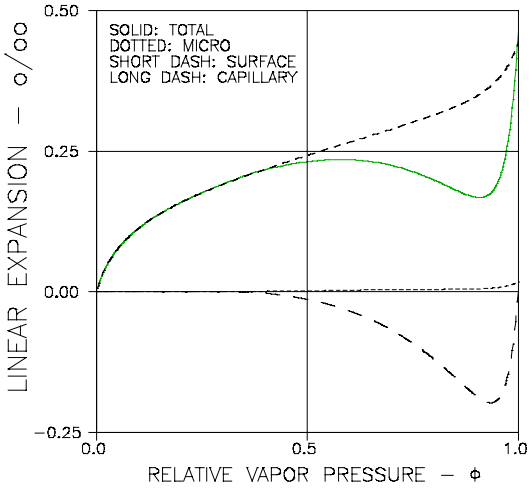

Figure 5.17. *Predicted swelling/shrinkage of the cellular concrete considered in Figure 5.16.*

Remark: We re-call that the analysis just made only demonstrates the principles of a complete drying shrinkage analysis such as the one presented in (26). The results presented in Figure 5.17 are from a complete (26)-analysis of a cellular concrete with experimental sorption data as shown in Figure 5.16.

6. NOTATIONS

The notations most frequently used in this note are listed below. A few symbols have been allowed to have two meanings - only, however, where the proper meaning is obvious from the text associated. The list does not include local symbols used only in intermediate results.

	Sub/supscripts
P, S	Phase P and phase S respectively
no sub/supscript	Composite material
	Volume
V	Phase volumes
$c = V_P/(V_S + V_P)$	Volume concentration of phase P
1 - c	Volume concentration of phase S
$A = (1-c)/(1+c)$	Volume parameter
	Geometry
c_P, c_S	Critical concentrations
$\mu = \mu(c)$	Shape function
$\mu^o = \mu(0)$, $\mu^1 = \mu(1)$	Shape factors
$\theta = \theta(\mu,n)$	Geometry function (n = stiffness ratio, see 'stiffness')
A	Fiber aspect ratio (length/diameter)
	Stress/strain
σ	Stress
ε	Strain
	Eigenstrain/stress
λ	Linear eigenstrain
ρ	Stress (hydrostatic)
	Stiffness - Conductivity
E	Young's modulus
Q	Physical property such as conductivity
$n = E_P/E_S$	Stiffness ratio
$n = Q_P/Q_S$	Conductivity ratio (f.ex)
$e = E/E_S$	Relative stiffness of composite
$q = Q/Q_S$	Relative conductivity (f.ex)
	Viscoelasticity
t	time
C(t)	Creep function
R(t)	Relaxation function
τ	Relaxation time (doubling time)
b	Creep power
$E^{EFF} = E^{EFF}(t)$	Effective Young's modulus ($\approx R(t) \approx 1/C(t)$)
	Fracture
l	Half length of crack
l_{CR}	Critical half length of crack

F	Interaction factor
K	Stress intensity factor
K_{CR}	Critical stress intensity factor
Γ	Strain energy release rate
Γ_{CR}	Critical strain energy release rate
σ_{MAX}, σ_L	Theoretical strength in general
σ_{CR}	Real strength in general
$d = (K_{CR}/\sigma_L)^2/\pi$	Characteristic microstructural dimension
$S = S(c)$	Strength of porous material (Porosity c)
$S_o = S(0)$	Strength of porous material at 0-porosity
t_S	Lifetime (to failure initiation)
t_{CAT}	Lifetime (to catastrophic failure)

Concrete

HCP	Hardened Cement Paste
$g = g(t)$	Degree of hydration
c_{TOT}	Total porosity of HCP
c_{CAP}	Capillary porosity of HCP
W/C	Water/cement ratio (by weight)
A/C	Aggregate(Cement ratio (by weight)
$\phi = \phi(t)$	Creep parameter
$E^{EFF} = E^{EFF}(t)$	Effective Young's modulus ($E/(1+\phi)$)
$\phi^{1000} = \phi(1000)$	Creep parameter at t = 1000 days
$\lambda = \lambda(t)$	Shrinkage
$\lambda^{1000} = \lambda(1000)$	Shrinkage at t = 1000 days

Abbreviations

CSA	Composites spheres assemblage
H/S	Hashin-Shtrikman's stiffness bounds
P/H	Paul-Hansen's stiffness bounds
MOE-MOR	Modulus of elasticity - modulus of rupture

REGNEØVELSER - OPLÆG

I dette afsnit lægges der op til en række regneøvelser i Materialemekanik. Formuleringerner er bevidst holdt meget løse, nærmest stikordsagtige - og nogle steder ret ufuldstændige. Det er meningen, at indholdet af de endelige øvelser aftales med de studerende. Muligheden foreligger, at en øvelse kan "forfremmes" til at være grundlaget i den afløsningsopgave, der kræves udført i forbindelse med kursets afslutning.

1. Composite stiffness and eigenstrain/stress

- Beton består af HCP og sten (inkl. sand). HCP har E_S = 25000 MPa. Stenene har E_P = 60000 MPa. Bestem grænserne for betons stivhed (E) som funktion af stenindhold, og bestem Budiansky's tilnærmede stivhedsløsning. Løsningerne ønskes i grafisk form. Kommenter specielt stivhederne for normal beton ($c \approx 0.75$) og for mørtel ($c \approx 0.5$).

- Betragt en beton med c = 0.75 under termisk påvirkning. Bestem betonens varmeudvidelse (λ) samt spændinger i sten og HCP. Anvend Budiansky's udtryk for betonstivhed. Leg med forskellige varmeudvidelseskoefficienter (λ_P,λ_S).

- Programmer en graf, der giver den vandrette simple middelværdi af P/H-grænserne. Der er en spændende sammenhæng mellem denne graf og Budiansky's løsning. De to grafer tegnes i det samme koordinatsystem.

- Når du har gjort det, så vis matematisk at de to grafer er exact sammenfaldende.

Vink til sidste spørgsmål:

Fra P/H−grænserne fås

$$c_{\varnothing} = \frac{e - 1}{n - 1} \quad ; \quad c_L = \frac{n(1 - 1/e)}{n - 1} \tag{6.1}$$

bestem $c = \tfrac{1}{2}(c_{\varnothing} + c_L)$ *og afbild* $e = f(c)$

Relevante formler:

HASHIN−SHTRIKMAN's stivhedsgrænser

$$n\frac{2 + c(n - 1)}{2n - c(n - 1)} \le \frac{E}{E_S} \le \frac{n + 1 + c(n - 1)}{n + 1 - c(n - 1)} \quad ; \quad \left(n = \frac{E_P}{E_S}\right) \tag{6.2}$$

BUDIANSKY's tilnærmelse af akkurat stivhed

$$e = \frac{E}{E_S} \approx \frac{1}{2}\left[b + \sqrt{b^2 + 4n}\right] \quad med \quad b = (1 - n)(1 - 2c)$$

$$\lambda = \lambda_S + \Delta\lambda \frac{1/e - 1}{1/n - 1} \quad ; \quad (\Delta\lambda = \lambda_P - \lambda_S) \tag{6.3}$$

$$\sigma_P = -K_S \Delta\lambda \frac{c(1/n - 1) - (1/e - 1)}{c(1/n - 1)^2} \quad ; \quad \sigma_S = -\frac{c}{1 - c}\sigma_P \tag{6.4}$$

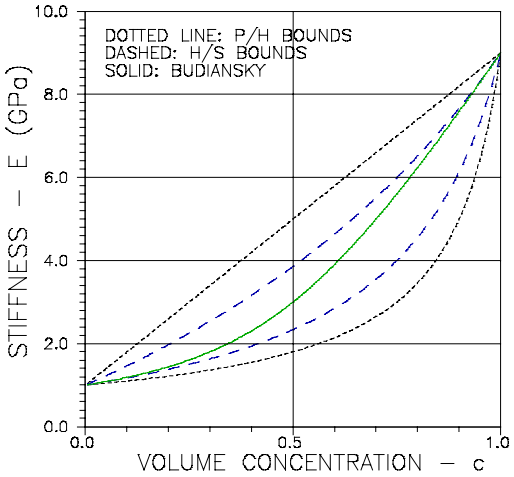

Figure 6.1. *Stiffness bounds and Budiansky's approximation.*

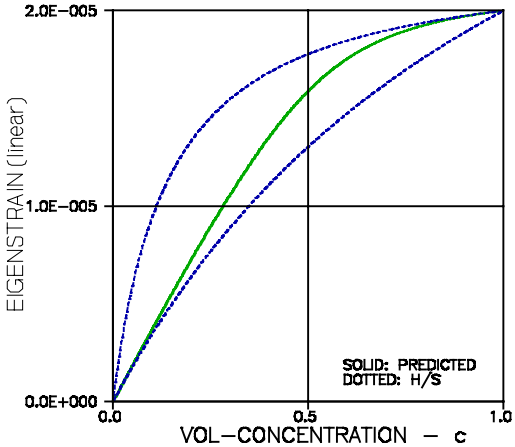

Figure 6.2. *Thermal eigenstrain/°C of spherical powder composite. (E_P,E_S) = (15,1)*10² MPa. (λ_P,λ_S) = (2*10⁻⁵, 0)/°C.*

2. Revnet system (kritisk spændingsintensitetsfaktor)

- Genkald "galgeøvelsen". Opstil program til beregning af spændingsintensitets faktorer.

- Antag, I har en plade af konstant tykkelse med en revnedensitet på ρ = 1 pr 2b*2b = 0.25/b², hvor 2b er revnernes centerafstand. Revnerne har alle en halvlængde l. Bestem pladens styrke som funktion af revnedensitten. Materialet vælger I selv.

Relevante formler

Lagen: *tykkelse t*, *bredde*: 2*b*, *revnelængde*: 2*l*
Brudlast: P_{CR}, $\sigma_{CR} = P_{CR}/(2tb)$

$$K_{CR} = F\sigma_{CR}\sqrt{\pi l} \quad with \quad F = \frac{1}{\sqrt{1 - (l/b)^2}} \tag{6.5}$$

$$\sigma_{CR} = \frac{K_{CR}}{F\sqrt{\pi l}} \quad with \quad \frac{1}{F} = \sqrt{1 - \rho(2l)^2} \quad ; \quad \rho_{CR} = \frac{1}{4l^2} \tag{6.6}$$

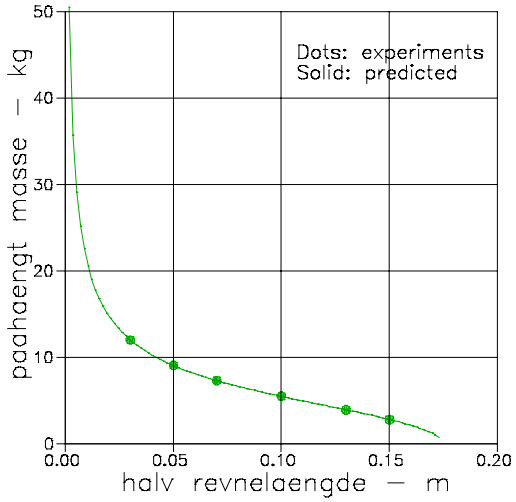

Figure 6.3. *Den påhængte masses afhængighed af revnelængde.*

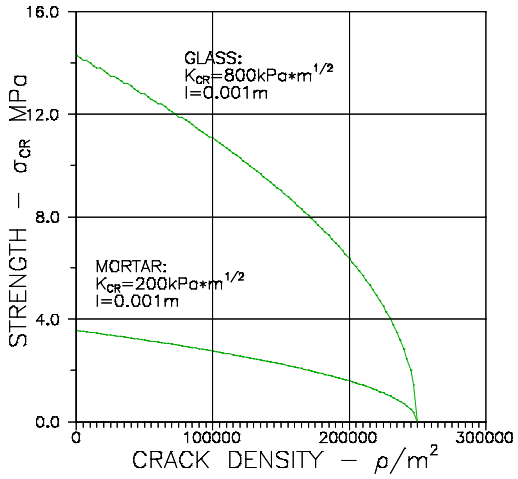

Figure 6.4. *Multi-cracked mortar and glass*

3. Krybning i træ

- Et bøjningsforsøg med træ har givet følgende krybningdresultater. Bestem træets krybningsfunktion beskrevet ved det eksponentielle krybningsudtryk.

t(døgn)	E*c(T)	t(døgn)	E*C(t)
5	1.1	1000	1.6
20	1.2	5000	1.8
50	1.3	8000	1.9
100	1.3	12000	2.1
700	1.5		

TABLE 6.1. Målte krybningsdata.

- Med praktisk relevans kan I lege med programmet. Masser af andre materialer (Polymerer b ≈ 0.45, keramer b ≈ 0.3, gasbeton b ≈ 0.2) opfører sig formelt efter den samme krybningsfunktion som gælder for træ. Fugt nedætter τ dramatisk. Hvordan indvirker dette på kybningen af træ og andre matrialer.

Relevante formler (Afsnit 2.2.4)

$$c = c(t) = \frac{1}{E}\left(1 + \left(\frac{t}{\tau}\right)^{b}\right) \qquad \begin{array}{l} b \text{ er krybningseksponent} \\ \tau \text{ er relaxationstid (el. fordoblingstid)} \end{array} \tag{6.7}$$

$$Y = Y_o + \alpha X \quad med \quad Y = \log_{10}(Ec(t) - 1) \;\; ; \;\; X = \log_{10}(t)$$
$$\Rightarrow \quad b = \alpha = -\frac{Y_o}{X_o} \;\; ; \;\; \tau = 10^{-Y_o/\alpha} = 10^{X_o} \tag{6.8}$$

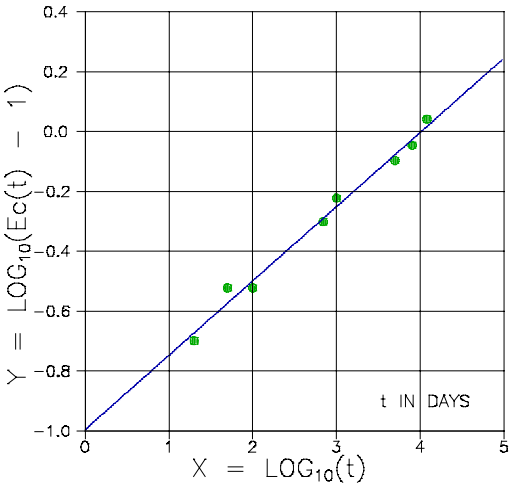

Figure 6.5. *Manipulerede krybningsdata. Lineær regression giver b = 0.248 og τ = 10198 døgn med fit koefficienten r^2 = 0.987*

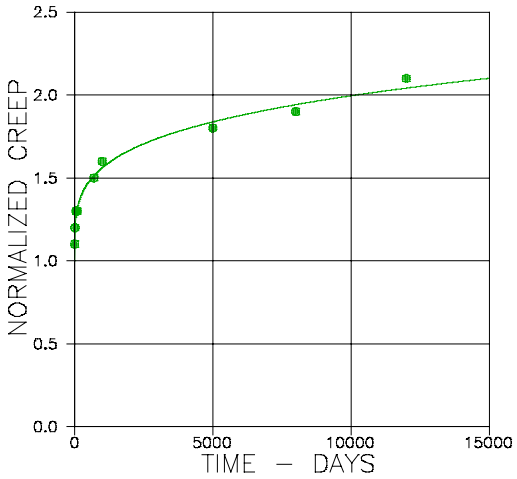

Figure 6.6. *Bedste eksponentielle krybningsbeskrivelse af de givne eksperimentelle data.*

4. Tegls stivhed og styrke - MOE-MOR

Ernst (69) (her fra bkm) har udført stivheds- og styrkeforsøg på 50x50x50 mm terninger af teglmursten. Hans data (og deres beskrivelse) har tidligere været vist i dette notats Sectioner 5.3 (stivhed) henholdsvis 4.4.2 (styrke).

Bestem og optegn MOE-MOR relationen for den undersøgte tegl. Progammér hele proceduren, således, at I kan foretage denne bestemmelse direkte med de eksperimentelle data som in-put.

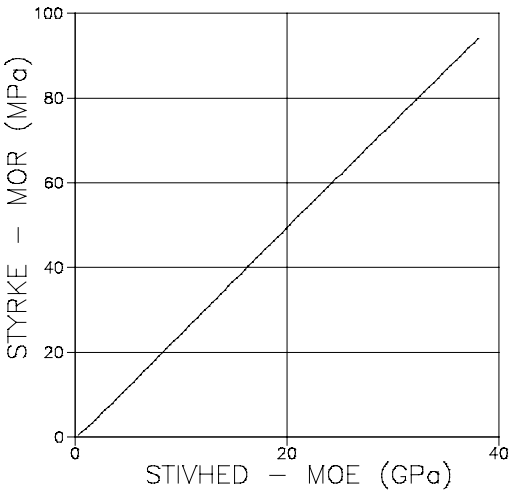

Figure 6.7. *MOE-MOR for den betragtede tegl. E_s = 38 GPa, S_o = 94 MPa.*

FORELÆSNINGSØVELSER

Demo 1: Rheologi og Levetid: Træ

Hensigt

1) At vise tidsafhængig deformation af materiale under konstant last.
2) At illustrere et materiales levetid (under 3 konstante lastniveauer).

Emner og materialer

Der fremstilles 30 små bjælker af knastfrit træ (gran eller fyr). Dimensioner og udskæringsretning (tangentiel-radiær) er vist i Figur 1.1.

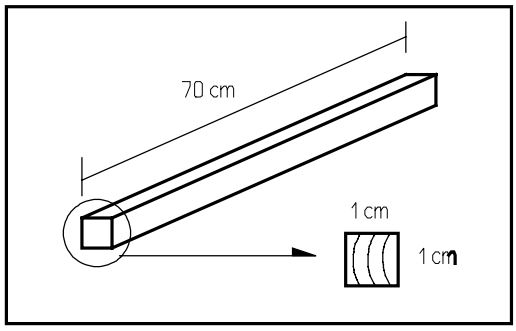

Figur 1.1. Bjælkedimensioner og udskæringsretning.

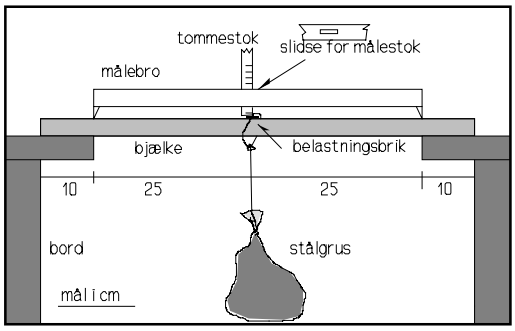

Figur 1.2 Forsøgsopstilling.

Hjælpegrej

Mindst 20 10*10*2 mm aluminiumbrikker (uden skarpe kanter). Kraftigt sejlgarn. 9 kraftige poser (evt. udført af tilbundne stykker fra endeløse slanger): 3 med 10 kg, 3 med 7 kg og 3 med 4 kg stålgrus. De angivne kg-tal er eksempelvise svarende til cirka 30, 50 og 70 % af bjælkernes brudlast. 2 borde. 1 tommestok (med cm). 1 målebro af 15*15 mm firkant-aluminiumrør, 50 cm lang, løftet 1 cm i hver ende med pålimet aluminiumplade, 15*15*25 mm, se Figur 1.2; på midten skal der være en 4 cm lang slidse, hvor tommestokken kan stikkes igennem for måling, se Figur 1.2. 1 tube kontaktlim.

Opstilling og forsgsgang

En bjælke oplægges fra bord til bord som vist i Figur 1.2. Husk at årringene skal stå lodret. En belastningsbrik er på forhånd limet på bjælkemidten med et tyndt lag kontaktlim. - Der foretages en 0-punktsaflæsning af bjælkens (ubelastede) nedbøjning med målebro og tommestok. Der måles til belastningsbrik. - En let pose ophænges forsigtigt med sejlgarn og løkke omkring bjælken (og underlagsbrik). - Der foretages en aflæsning af bjælkens nedbøjning med målebro og

tommestok. Igen måles til brik. - Og sådan fortsættes der, først tre arrangementer med de lette poser, så tre med de mellemtunge, og sidst, tre med de tunge poser. - Forud for ovenstående er bjælkernes brudlast bestemt udfra forsøg på mindst 9 bjælker. Som eksempel antager vi, at disse forsøg giver P_{cr} = 144 N ± 11 % (c.v.)

Målinger

Nedbøjninger og tidspunkter, noteres i en frekvens, der aftales med læreren. "0-aflæsningen" er naturligvis vigtige - såvelsom tidspunkter (så tæt, disse kan skønnes) for sammenbrud af bjælker (levetid).

Resultater og diskussion

Elasticitetsmodul, E, (Ligning 1.2 nedenfor), krybningsfunktion, C(t), og levetid.

På grund af den relativt grove målemetode kan de fundne data kun forventes at give fingerpeg til belysning af de betragtede fænomener. Forsøgsresultaterne skal diskuteres i forelæsningerne i sammenhæng med forelæserens erfaringer fra mere omfattende, "videnskabelige" forsøg - og så teori naturligvis. Bl.a. skal belastningsniveauets (30, 50, 70 %) indflydelse drages ind i diskussionen.

Forhåndsinformation

De opgivne belastninger svarer til ca. 30, 50 og 70 % af korttidsbrudkraften på fex P_{cr} = 144 N ± 11 % (c.v.) svarende til en max trækspænding, σ_{cr}, i bjælkeunderside på

$$\sigma_{CR} = \frac{3}{2}\frac{P_{CR}L}{BH^2} = 108\ MPa \pm 11\% \qquad (1.1)$$

hvor spændvidden, L = 0.5 m, bjælkebredde, B, og -højde, H, begge er 1 cm. "Nedbøjningen" ved brud (100 % belastning) bestemmes ved

$$u_{CR} = \frac{1}{4}\frac{P_{CR}L^3}{EBH^3} \approx 4\ cm \qquad (1.2)$$

hvor elasticitetskoefficienten er skønnet til E ≈ 12000 MPa. Ved 70, 50 og 30 % belastning er u ≈ 3, 2 henholdsvis 1 cm. Formel 1.2 anvendes ellers til bestemmelse af E udfra P og u for de anvendte belastningsniveauer.

Demo 2: Revnemekanik: Glas

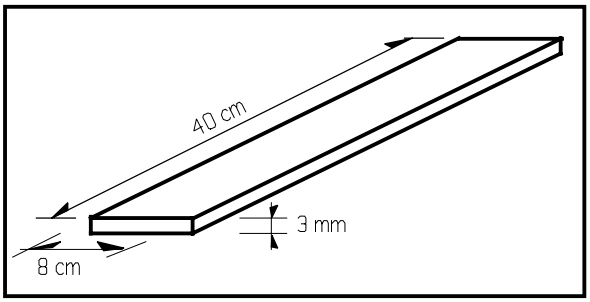

Figur 2.1 Dimensioner af glasbjælker.

Hensigt

At demonstrere meget simpelt, hvordan et materiales styrke reduceres betydeligt blot ved at tilføje en ganske svag revne.

Emner og materialer

Der fremstilles 6 "bjælker" (+ 2 reserver) af 3mm vinduesglas som vist i Figur 2.1.

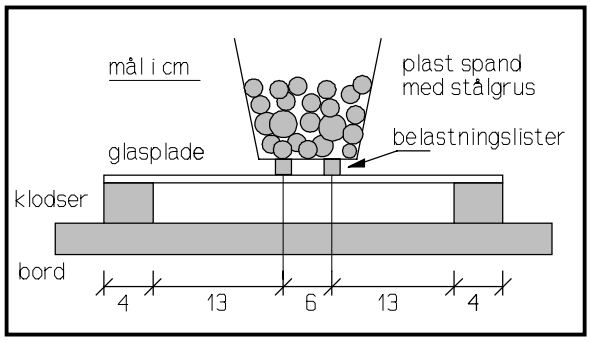

Figur 2.2 Belastningsarrangement

Hjælpegrej

2 understøtningsklodser, 4*4*8 cm. 2 belastningslister, 1*1*8 cm. 1 tom plasticspand, ca. 3 liter. 15 kg stålgrus i en beholder med en kulskovl. nogle almindelige glarmester diamantskærerer. En 15 kg vægt.

Opstilling og forsgsgang

De to "bjælker" anvendes til at øve glarmesterens teknik i at brække glas. Avis nødvendig og en bordkant. Det bemærkes, at snitdybden er af størrelsesordenen 0.05 mm; d.v.s. knap 2 % af glastykkelsen. - Herefter styrkeprøves 2 (uridsede) bjælker som vist i Figur 2.2. Den tomme plastspand placeres omhyggeligt på be-

lastningslisterne og stålgrus drysses forsigtigt i spanden med kulskovlen. Efter brud noteres vægten af spand + stålgrus.

De to sidste bjælker forsynes med en "glarmesterridse" på midten og på tværs af bjælken. Ridsen må ikke føres helt ud til kanten (men tæt på), idet der for en uøvet da nemt vil ske dette, at bjælken brækker allerede inden belastningspåførsel. (Skæringen skal ske på avis). Bjælkerne afprøves på samme måde som de foregående. Ridsen skal ligge i træksiden (undersiden). Vægt af spand + stålgrus noteres.

Resultater og diskussion

Forsøgene viser, at brudkraften på de uridsede glasbjælker er $P_{cr} \approx 90$ N, svarende til et brudmoment på

$$M_{CR} = P_{CR}\frac{0.13}{2} = 5.9\ Nm \tag{2.1}$$

og en max trækbrudspænding

$$\sigma_{CR} = \frac{6M_{CR}}{BH^2} = 50\ MPa \tag{2.2}$$

hvor B = 8 cm og H = 3 mm er bjælkebredde henholdvis –højde. (En styrke på 50 MPa er 1/50 af glasfibres trækstyrke. Dette skyldes, at fibrene er langt tyndere (mindre) og renere end vinduesglas).

De ridsede bjælker har en brudkraft på $P_{cr} \approx 28$ N, svarende til en max trækspænding på $\sigma_{cr} \approx (28/90)*50 = 16$ MPa. Ridsen har altså reduceret styrken til lidt under en 1/3.

Resultaterne belyses i sammenhæng med præsentation af kritiske spændingskoncentrationsfaktorer, K_{cr}. Vinduesglassets K_{cr} kan skønnes ved

$$K_{CR} = 1.1*\sigma_{CR}\sqrt{\pi l} \approx 220\ kPa\sqrt{m} \tag{2.3}$$

hvor $\sigma_{cr} = 16$ MPa og l (ridsedybden) ≈ 0.05 mm. K_{cr}-værdien er af samme størrelse, som gælder for langsgående revner i træ (kløvning).

Demo 3: Revnemekanik: Folier

Hensigt

At belyse, lidt mere detaljeret end i DEMO II, hvordan revner reducerer materialestyrker. Yderligere, at vise forskellen mellem brud i seje og skøre materialer.

Emner og materialer

Der fremstilles 3 duge (+ 2 i reserve), 35*50 cm, af tegne-kalkepapir - og tre duge (+ 3 i reserve), 35*50 cm, af plast (som det LBM bruger i levetidsforsøg på træ som fugtforsegling).

Hjælpegrej

1 sæt, specielt fremstillet gribegrej (incl. løs last-ophængningskrog til udspænding af duge. En ca. 2 m høj ophængningsramme. 5 plast eller stof-poser à 10 kg (stål-grus) tilbundet med sejlgarn afsluttet med løkke til ophængning. 1 tommestok (cm). 1 skalpel. 1 speedmarker. 1 kuglepen. En rulle tape.

Opstilling og forsgsgang

På en plastdugs korte sider anbringes gribesættet. Vær omhyggelig med at dugene gribes med hele den flade, der kan opnås i gribesættet - og at dettes to dele er parallelle. Fløjmøtrikkerne strammes maximalt (med hånden).

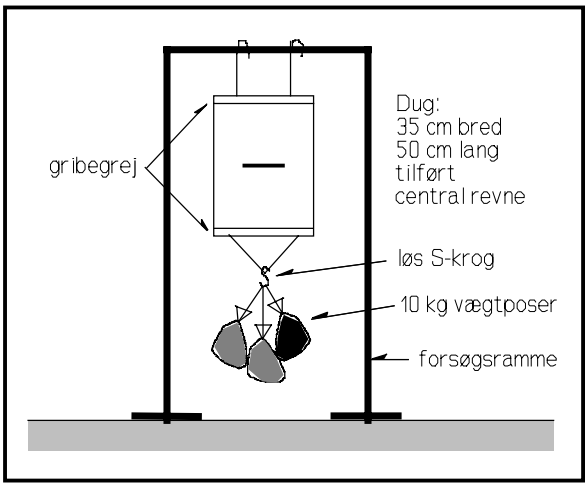

Figur 3.1 Belastningsarrangement

Dugen forsynes på midten (diagonalkrydset) med en svag "vandret" og "lodret" speedmarkermarkering og ophænges som vist i Figur 3.1 med 20 kg masse (2 poser) forsigtigt anbragt på belastningskrogen. - To studerende placerer sig på hver

sin side af dugen - den ene forsynet med en skalpel, den anden med en tommestok. - Der prikkes en lille vandret revne i midten af dugen. Derefter skæres 5 mm af gangen skiftevis til den ene og så til den anden side (stadig vandret). Revnens længde følges hele tiden med tommestokken. - På et tidspunkt er revnen kritisk, dugen går midtover (pas på tæerne). Den kritiske revnelængde og last noteres ned.

De to sidste plastduge afprøves på samme måde, blot nu med 30 henholdsvis 40 kg last. (Hvis der er tid og lyst kan en reservedug afprøves ved 50 kg).

Herefter gentages de beskrevne forsøg på papirduge. Markering af revne sker dog med kuglepen. Særlig omhu skal iagttages ved montering. Papiret går let i stykker ved kanterne; (skulle der komme en mindre revne, kan den repareres med tape).

Resultater og diskussion

Det bemærkes, at der ved revnespidserne i plastdugene foregår en trækhærdning af materialet. Dette kan både ses og mærkes af den, der fører kniven. Det bemærkes også, at man i god tid får en fornemmelse af, at nu bliver situationen farlig, idet der optræder store krybningsdeformationer ved revnespidserne. Det anvendte plast er et såkaldt sejt materiale; (der ved trækhærdning bliver stærkere, men mere skørt. Dette kan faktisk føles med fingrene på den brudte rand af dugen. Trækhærdning bruges ved fremstilling af fibre til kompositmaterialer).

Papirdugene går fuldstændig uvarslet midt over. Der observeres ingen plastiske deformationer som i plasten. Papir er et såkaldt skørt materiale.

Den kritiske spændingsintensitetsfaktor, K_{cr}, for plast og papir kan bestemmes ved

$$K_{CR} = \sigma_{CR}\sqrt{\pi l_{CR}} * \left[1 - \left(\frac{l_{CR}}{b}\right)^2\right]^{-1/2} \qquad (3.1)$$

hvor l_{cr} og b er den halve revnelængde ved brud henholdsvis den halve dugbredde. Brudspændingen er den påhængte kraft (nederste griber incl.) divideret med dugtværsnittet.

Plast: I et forsøg har vi målt den påhængte kraft til P_{cr} = 300 N ved en kritisk revnelængde på $2l_{cr}$ = 16 cm. Vi får

$$\sigma_{CR} = \frac{300}{0.35 * 0.0002} * 10^{-6} = 4.3\ MPa \qquad (3.2)$$

hvilket efter Ligning 3.1 giver

$$K_{CR} = 4.3 * 10^3 \sqrt{\pi * 0.08} * [1 - (0.08/0.175)^2]^{-1/2} = 2400 \; kPa\sqrt{m} \tag{3.3}$$

På lignende måde gav et forsøg med P_{cr} = 200 N og $2l_{cr}$ = 27 cm, K_{cr} = 2900 kPa$\sqrt{}$m.

Papir: I et forsøg har ve målt den påhængte kraft til P_{cr} = 200 N ved en kritisk revnelængde på $2l_{cr}$ = 16 cm. Vi får

$$\sigma_{CR} = \frac{200}{0.35 * 7 * 10^{-5}} * 10^{-6} = 8.2 \; MPa \tag{3.4}$$

hvilket med Ligning 3.1 giver

$$K_{CR} = 8.2 * 10^3 \sqrt{\pi * 0.08} * [1 - (0.08/0.175)^2]^{-1/2} = 4600 \; kPa\sqrt{m} \tag{3.5}$$

En anden papirdug gav $2l_{cr}$ = 13 cm ved P_{cr} = 400 N, svarende til K_{cr} = 8000 kPa$\sqrt{}$m. Middelværdien af disse to målinger er K_{cr} = 6300 kPa$\sqrt{}$m. Spredningen er for stor, hvilket sandsynligvis skyldes fejl på revnelængdemålingen. Vi skal være omhyggelige (og hurtige) med denne måling. Plastrevnerne har en tendens også at "løbe", selvom vi ikke skærer.

LITERATURE

1. Nielsen, L. Fuglsang: ’Composite Materials - Mechanical and physical behavior as influenced by phase geometry’, Dept. Civil. Eng., Technical Report R-051(2003), Technical University of Denmark.

2. *Idem:* ’Numerical analysis of composite materials’, Materialenyt 1.(2001), DSM (Danish Society for Materials Testing and Research).

3. Hammerslev, J.M. in Proc. Cambridge Phil. Soc., 53(1957), 642.

4. Stauffer, D. and Aharony, A.: "Introduction to percolation theory", 2nd ed., Taqylor and Francis, London, 1992.

5. Nielsen, L. Fuglsang: "Stiffness and other physical properties of composites as related to phase geometry and connectivity - Part I: Methods of analysis", 3rd Symposium on Building Physics in the Nordic Countries, Copenhagen, Sept. 13.-15. 1993. Proceedings Vol. 2 (Bjarne Saxhof, editor) Thermal Insulation Laboratory, Technical University Denmark, 1993, pp 725 - 734.

6. Bentz, D.P.: Modelling cement microstructure: "Pixels, particles, and property prediction", Materials and Structures, vol. 32(1999), 187-195.

7. Hill, R.: "Elastic properties of reinforced solids: Some theoretical principles". J. Mech. Phys. Solids, 11(1963), 357 - 372.

8. Nielsen, L. Fuglsang: "Elastic properties of two-phase materials", Mat. Sc. and Eng. Vol 52(1982), 39-62.

9. Paul, B.: "Prediction of elastic constants of multi-phase materials". Trans. of the Metallurgical Soc. of AIME, 218(1960), 36 - 41.

10. Hansen, T.C.: "Creep of concrete: A discussion of some fundamental problems". Bulletin no. 33(1958), Svenska Forskningsinstitutet för Cement och Betong, Tekniska Högskolan, Stockholm".

11. Hashin, Z.: "Elastic moduli of heterogeneous materials". J. Appl. Mech., 29 (1962), 143 - 150.

12. Goodier, J.N.: "Concentration of Stress around Spherical and Cylindrical Inclusions and Flaws", J. Appl. Mech., 55(1933), 39

13. Hashin, Z. and Shtrikman, S.: "Variational approach to the theory of elastic behavior of multi-phase materials". J. Mech. Solids, 11(1963), 127 - 140.

14. Budiansky, B.: On the elastic moduli of some heterogeneous materials". J. Mech. Phys. Solids, 13(1965), 223 - 227.

15. Nielsen. L. Fuglsang: "Mechanics of composite material subjected to eigenstress - With special reference to frost resistance of porous brittle material", Danish Building Research Institute, SBI-Bulletin 96(1993).

16. *Idem:* "Stiffness and other physical properties of composites as related to phase geometry and connectivity - Part II: Quantification of geometry", 3rd Symposium on Building Physics in the Nordic Countries, Copenhagen, Sept. 13.-15. 1993. Proceedings Vol. 2 (Bjarne Saxhof, editor) Thermal Insulation Laboratory, Technical University Denmark, 1993, pp 735 - 743.

17. R.F. Feldman and J.J. Beaudoin: Studies of composites made by impregnation of porous bodies. I. Sulphur impregnant in Portland cement systems", Cem. Concr. Res., 7(1977), 19-30.

18. Fagerlund, G.: "Samband mellan porositet och materials mekaniske egenskaper" (in swedish, "Relations between porosity and mechanical properties of materials"), Div. Build. Technology, Tech. Univ. Lund, Sweden, 1971.

19. Powers, T. C.: "Fundamental aspects of the shrinkage of concrete" (in german), Die Bauwirtschaft, 15(1961), 344-49.

20. Helmuth, R.A. and D.H. Turk: "Elastic moduli of hardened Portland cement and Tricalcium silicate pastes: Effects of porosity", pp. 135-144 in Symposium on structure of Portland cement and concrete. Highw. Res. Bd., Spec. Rept., No. 90, 1966.

21. Murray et al: "The hot pressing of ceramics", in W.D. Kingery: Ceramic Fabrication Processes, J. Wiley & Sons, New York, 1958.

22. Spriggs, R. M., Brissette, L. A., and Vasilos, T.: "Effect of porosity on elastic and shear moduli of polycrystalline magnesium oxide". J. Am. Ceram. Soc., 45(1962), 400.

23. Nielsen, L. Fuglsang: "Elasticity and Damping of Porous Materials and Impregnated Materials", Journ. Am. Ceramic Soc., 67(1984), 93 - 98.

24. *Idem:* "Shrinkage, Swelling, and Stiffness of Composites - Strain and Stress caused by Hygro-thermal action and Solidification or Freezing of Liquid Impregnant", Bygningsstatiske Meddelelser, 62(1991), 47-78.

25. Hansen, E.J. dePlace: "Byggematerialers frostbestandighed - modellering af kritiske vandmætningsgrader", Ph.D. afhandling, SBI rapport 268(1996), Statens Byggeforskningsinstitut, Hørsholm.

26. Nielsen, L. Fuglsang: "Pore size distribution and shrinkage of porous materials - as related to moisture sorption", Report 316(1994), Building Materials Lab., Techn. University of Denmark.

See also "Pore size distribution, moisture distribution, and shrinkage of porous materials - as determined by computer analysis (MATSORP) of measured sorption data", a text note for the Summer School on 'Hydration and Microstructure of High Performance Concrete' held August 16-25, 1999 at the Depart. Struct. Eng. and Materials, DTU, Denmark.

27. Bentz, P.B.: "Modelling drying shrinkage in reconstructed porous materials: Application to porous Vycor glass", Modelling Simul. Mater. Sci. Eng. 6(1998), 211-236.

28. Hashin, Z.: "Assessment of Self Consistent Scheme approximation: Conductivity of particulate composites", J. Compos. Mater. Vol 2(1968), 284.

29. Hashin, Z. and Shtrikman, S.: "A variational approach to the theory of the effective magnetic permeability of multiphase materials", J. Appl. Phys. 33(1962), 3125.

30. Corson, P. B.: "Correlation functions for predicting properties of heterogeneous materials, IV: Effective thermal conductivity of two-phase solids", J. Appl. Phys. (USA) 45(1974), 3180.

31. Stephanow, N. J.: "Electrical conductivity of alloys", Z. anorg. u. allgem. Chem. 78(1912), 1.

32. Jensen, O. Mejlhede: "Chloride ingress in cement paste and mortar measured by Electron Probe Micro Analysis", Report ??(1998), Dept. Struct. Eng. and Materials, Tech. Univ. Denmark.

33. Bentz, D.P., Garboczi, E.J., Haecker, C.J., and Mejlhede, O.M.: "Effects of cement particle size distribution on performance properties of Portland cement based materials", Cement and Concrete Research, 29(1999), 1663-1671.

34. Garboczi, E.J. and Bentz, D.P.: "Computer simulation of the diffusivity of cement based materials", J. Mat. Sci. 27(1992), 2083-2092.

35. Nielsen, L. Fuglsang: "Rheologishe Eigenschaften für isotrope linear-viscoelastische Kompositmaterialien", Cement and Concrete Research, 3(1973), 751-766.

36. *Idem:* "Effects of Creep in Uncracked Composite Structures of Steel and Concrete", Bygningsstatiske Meddelelser, 38(1967), 65.

37. *Idem:* "Kriechen und Relaxations des Betons", Beton- und Stahlbetonbau, 11(1970), 272-275.

38. *Idem:* "On the Prediction of Creep Functions for Concrete", in "Fundamental Research on Creep and Shrinkage of Concrete" (ed. F. Wittmann), Martinus Nijhoff Publishers, The Hague 1982, 279 - 289.

39. *Idem:* "The improved Dischinger method as related to other methods and practical applicability", pp 169 - 191 in "Design for Creep and Shrinkage in Concrete Structures", Special Publication SP-76(1982), American Concrete Institute.

40. CEB-FIP: "Model code for concrete structures", Comité Euro-International du Béton, Paris, 1978.

41. Nielsen, L. Fuglsang: "The improved Dischinger method as related to other methods and practical applicability", pp 169 - 191 in "Design for Creep and Shrinkage in Concrete Structures", Special Publication SP-76(1982), American Concrete Institute.

42. *Idem:* "Power Law Creep as related to Relaxation, Elasticity, Damping, Rheological Spectra and Creep Recovery - With Special Reference to Wood". IUFRO-Engineering Group Conference 1984. Xalapa, Mexico. Proc. Techn. Univ. Denmark, Build. Mat. Lab., Copenhagen 1984, 181-204.

43. Nielsen, A.: "Rheology of building materials", thesis, Statens Institut för Byggnadsforskning, Stockholm, Document D6(1972).

44. Flügge, W.: "Viscoelasticity", Blaisdell Publ. Comp., London 1967

45. Lee, E.H.: "Stress analysis in viscoelastic bodies". Quarterly of Appl. Mathematics, 13(1955), 183.

46. Nielsen, L. Fuglsang: "Interne Spannungen sowie Schwind- und Temperaturdeformationen des Betons", Cement and Concrete Research, 4(1974), 31 - 44.

47. *Idem:* "Constitutive equations for concrete", Bygningsstatiske Meddelelser, 45(1974), 65.

48. Nielsen, Knud E.C.: "Aggregate stresses in concrete", Thesis, Proceedings 41(1971), Swedish Cement and Concrete Research Institute, Royal Institute of Technology, Stockholm.

49. Nielsen, L. Fuglsang: "ComCon (version 1.0) - Software for Composite analysis of concrete (Creep, relaxation, eigenstrain/stress, loss of prestress): Underlaying theory and documentation", www.bkm.dtu.dk, Report I-21, Dept. Struct. Eng. and Materials, Tech. Univ. Denmark, 1999.

50. Mullit, Paw: "ComCon (version 1.0) - Software for Composite analysis of concrete (Creep, relaxation, eigenstrain/stress, loss of prestress): User Manual", www.bkm.dtu.dk, Report I-22, Dept. Struct. Eng. and Materials, Tech. Univ. Denmark, 1999.

51. Griffith, A.A., 'The phenomenon of rupture and flow in solids'. Trans. Royal Soc. of London, 221(1920), 163.

52. Dugdale, D.S., 'Yielding of steel sheets containing slits'. J. Mech. and Phys. of Solids, 8(1960), 100 - 104.

53. Nielsen, L. Fuglsang, 'Revnebevægelse i lineær-viskoelastiske materialer', (in danish with extensive english summary, Crack propagation in linear viscoelastic materials), Byg-ningsstatiske Meddelelser, 49(1978), 1-45.

54. *Idem*, 'Lifetime of wood as related to strength distribution' in (J. Bodig, ed) 'Reliabiliy-based design of engineered wood structures', Kluwer Academic Publishers, London, 1992.

55. *Idem*, 'Fatigue and residual strength of wood - subjected to static and variable load', Holz als Roh- u. Werkstoff, in press.

56. Murakami, Y. (ed): "Stress intensity factors handbook", Vols. I and II, Pergamon Press, New York, 1987.

57. Paris, P.C. and Sih, G.C.: "Stress analysis of cracks"; in Fracture Toughness Testing and Its Application. American Society for Testing and Materials, Baltimore, MD, 1965.

58. Tada, H., Paris, P.C., and Irwin, G.R.: "The Stress Analysis of Cracks Handbook", Del Research Corp., Hellertown, PA, 1973.

59. Nielsen, L. Fuglsang: "Materialemekanik II" (Material Mechanics II), Building Materials Laboratory, Tech. Univ. Denmark, tech. rep. 189(1988), 175 pp.

60. *Idem:* "Strength and stiffness of porous materials". Journ. Am. Ceramic Soc. 73(1990), 2684-2689.

61. *Idem:* "Strength of porous material - simple systems and densified systems", Mate-rials and Structures, november 1998.

62. Balshin, M.Y.: "Relation of mechanical properties of powder metals and their porosity and the ultimate properties of porous metal-ceramic materials". Dokl Akad Nauk SSSR 67/5/(1949).

63. Hasselman, D.P.H.: "Relation between effects of porosity on strength and on Young's modulus of elasticity of polycrystalline materials", *J. Am. Ceram. Soc.*, 46(1963), 564 - 565.

64. Ryshkewitch, E.: "Compression Strength of Porous Sintered Alumina and Zirconia". Journ. Am. Ceram. Soc., 36(1953), 65 - 68.

65. Duckworth, W.: "Discussion of Ryshkewitch Paper". J. Am. Ceram. Soc. 36(1953), 68. (Ryshkewitch, E.: "Compression Strength of Porous Sintered Alumina and Zirconia". J. Am. Ceram. Soc. 36(1953), 65 - 68).

66. J.J. Beaudoin and R.F. Feldman: "A study of mechanical properties of autoclaved Calcium silicate systems", Cem. Concr. Res., 5(1975), 103-118.

67. R.F. Feldman and J.J. Beaudoin: Studies of composites made by impregnation of porous bodies. I. Sulphur impregnant inPortland cemnt systems", Cem. Concr. Res., 7(1977), 19-30.

68. Rössler, H. og I. Odler: " Investigations on the relationship between porosity, structure and strength of hydrated Portland cement paste - I: Effect of porosity", Cem. Concr. Res., 15(1985), 320 - 330.

69. Hansen, E. dePlace and Schmidt, L.: "Sammenhæng mellem porøsitet og elasticitetsmodul, samt porøsitet og styrke for teglsten", (in danish, Stiffness and strength of bricks as related to porosity), A students report in Material mechanics (Course 6110), Spring 1988, Build. Mat. Lab., Techn. Univ. Denmark.

70. Nielsen, L. Fuglsang, 'DVM-analysis of wood', Appendix A in Borg Madsen: 'Structural Behavior of Timber', Timber Engineering Ltd., North Vancouver, B.C., Canada 1992.

71. Wood, L.W.: "Relation of strength of wood to duration of stress". U.S. Forest Products Laboratory, Madison, Wisc., USA, Report No. R-1916(1951).

72. Krebs, H.J.: "The influence of moisture content on the longterm mechanical properties of wood" (in danish). Thesis, Build. Mat. Lab., Tech. Univ. Denmark, 1984.

73. Corson, P. B.: "Correlation functions for predicting properties of heterogeneous materials, IV: Effective thermal conductivity of two-phase solids", J. Appl. Phys. (USA) 45(1974), 3180.

74. Larsen, E.S. and Nielsen, C.B.: "Decay of bricks due to salt". Materials and Structures, 23(1990), 16 - 25.

75. Nielsen, L. Fuglsang: "On the Prediction of Rheological Parameters for Concrete", Nordic Conference on Deformations in Concrete Structures, Copenhagen, march 1980. Proc. DIALOG 1/80(1980), 81, Danish Engineering Academy, Dept. Civ. Eng., Lyngby, Denmark

76. *Idem:* "Strength developments in hardened cement paste - Examination of some empirical equations", Materials and Structures, 26(1993), 255-260.

77. Powers, T.C.: "Physical properties of cement paste", Proc. Fourth Int. Symp. on the Chemistry of Cement, Washington, D.C.,1960, US Dept. of Commerce, National Bureau of Standards, Monograph 2(1962), no. 43.

78. Powers, T.C. and T.L. Brownyard: "Studies of the physical properties of hardened cement paste", ACI Journ., Proc. 41(1946-47), 101, 249, 469, 549, 669, 845, 865, 933, 971, (Chicago, Portland Cement Ass., Res. Dept. Bulletin 22(1948))

79. Hansen, P. Freiesleben: "Hærdeteknologi-1, Portland cement" og "Hærdeteknologi-2, Dekrementmetoden", Bkf-centralen, 1978.

80. Spange, H. and Pedersen, E.S.: "Early age properties of selected concrete", in "High Performance Concrete - The Contractors Technology, HETEK", Report 59(1997), Ministry of Transport, Road Directorate, Denmark.

81. Lokhorst, S.J. and van Breugel, K.: "Simulation of the effect of geometrical changes

of the microstructure on the deformational behavior of hardening concrete", Cement and Concrete Res., vol. 27(1997), 1465 - 1479.

82. Flood, E.A.: "Adsorption potentials, adsorbent self-potentials and thermodynamic equilibria". In "Solid surfaces and the gas-solid interface", American Chemical Soc., Washington, Advances in Chemistry Series No 33(1961), 249.